

AN ANALYTICAL THEORY OF MOIST CONVECTION

by

CHRISTOPHER STEPHEN BRETHERTON

B.S., California Institute of Technology
(1980)

SUBMITTED TO THE DEPARTMENT OF MATHEMATICS
IN PARTIAL FULFILLMENT OF THE REQUIREMENTS
FOR THE DEGREE OF

DOCTOR OF PHILOSOPHY

at the

MASSACHUSETTS INSTITUTE OF TECHNOLOGY
December, 1984

© Christopher Stephen Bretherton, 1984

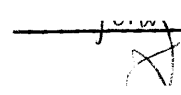
The author hereby grants to M.I.T. permission to reproduce and to
distribute copies of this thesis document in whole or in part.

Signature of Author



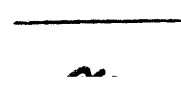
Department of Mathematics
September 13, 1984

Certified by



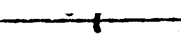
Kerry A. Emanuel
Thesis Supervisor

Certified by



Chairman, Applied Mathematics Committee
David J. Benney

Accepted by



Arthur P. Mattuck
Chairman, Department of Mathematics

MASSACHUSETTS INSTITUTE
OF TECHNOLOGY

FEB 20 1985

ARCHIVE

AN ANALYTICAL THEORY OF MOIST CONVECTION

by

CHRISTOPHER STEPHEN BRETHERTON

Submitted to the Department of Mathematics on September 12, 1984
in partial fulfillment of the requirements for the Degree of
Doctor of Philosophy

ABSTRACT

I formulate a thermodynamically accurate model of two-dimensional non-precipitating moist convection in a shallow conditionally unstable layer of air between two conducting plates which exactly saturate the air between them. In this model, the buoyancy is a piecewise linear function of a single thermodynamic variable, the liquid buoyancy, which combines linearly when air parcels are mixed and is proportional in saturated air to the amount of suspended liquid water.

I first examine the stability of infinitesimal perturbations from static equilibrium. Isolated updrafts with vertical cloud boundaries grow fastest; the subsidence around them decays exponentially in a horizontal radius which is the minimum of three length scales determined by eddy mixing, rotation, and gravity wave propagation. Multiple updraft clouds can also grow but are unstable. Variational methods show that no growing oscillatory or travelling wave solutions are possible. In three dimensions, cylindrical updrafts grow even faster, but the rest of the theory is analogous.

I then do an asymptotic nonlinear analysis of a field of widely spaced clouds when the latent heating is barely sufficient to allow a cloud to grow. The effects of a weak mean vertical motion induced by horizontal temperature variations is included. A complex amplitude expansion leads to equations for the slowly varying strength and position of each cloud. If uniformly spaced clouds of equal amplitude are closer than a critical distance they are subject to a subharmonic instability. Every second cloud is suppressed. A strict upper bound on the spacing exists only in a mean upward motion, but for clouds more than twice the critical distance apart, a sufficiently large finite amplitude perturbation produces a stable new cloud. Gradual spatial modulations of the cloud spacing diffuse away and cannot lead to mesoscale organization. The observed inhomogeneity of cloud fields is due to strongly supercritical, time dependent convection. My theory suggests that two scales, the Rossby and wave-propagation radii, characterize mesoscale and cloud-scale organization respectively.

Thesis Supervisor: Dr. Kerry A. Emanuel
Title: Assistant Professor of Meteorology

ACKNOWLEDGEMENT

I would like to thank Dr. Kerry Emanuel for his unfailing good cheer and for the physical insights that he lent to this work, Dr. William V. R. Malkus for leading me into the excitements of nonlinear stability theory as a language of inquiry, and Marge Zabierek for putting it all in print.

Pertinax - Robert Frost

Let chaos storm!

Let cloud shapes swarm!

I wait for form.

TABLE OF CONTENTS

	<u>Page</u>
CHAPTER 1. Introduction	6
CHAPTER 2. A Mathematical Model of Moist Convection	24
2.1 Introduction.	24
2.2 The Buoyancy in Shallow Nonprecipitating Convection.	26
2.3 The Equations of Motion	32
CHAPTER 3. The "Linear Dynamics of Moist Convection in an Exactly Saturated Atmosphere	39
3.1 Introduction.	39
3.2 The Simplest Case	41
3.3 Cylindrically Symmetric Moist Convection.	56
3.4 Multiple Updraft Solutions.	63
3.5 The Effects of Variable Viscosity	70
3.6 Moist Convection with Rotation.	79
3.7 The Stability of Separable Eigenmodes	86
3.8 A Variational Principle and the Nonexistence of Oscillatory Modes	95
3.9 A Summary of "Linear" Moist Convection.	102
CHAPTER 4. The Interaction of Weakly Nonlinear Clouds in Mean Vertical Motion.	103
4.1 Introduction.	103
4.2 An Overview of the Asymptotic Expansion	104
4.3 Derivation of the Amplitude Equations	114
4.4 The Amplitude Equations and Cloud Spacing	133
4.5 Collective Disturbances of a Cloud Field.	149
4.6 Summary	153
CHAPTER 5. Conclusion	155
5.1 A Synopsis.	155
5.2 Limitations	160
5.3 Some Extensions	162
5.4 Some Mesoscale Convective Phenomena	164
APPENDICES	
I. Some Thermodynamics	169
II. The Mean Fields in the Absence of Convection.	175
III. Product Formulas.	179
IV. Inverting the "Linear" Operator	181
V. The $O(\mu^{3/2})$ Inhomogeneous Solutions	191
VI. Numerical Values of the Coefficients.	205
VII. The Buoyancy Flux from a Uniform Field of Clouds.	206
BIBLIOGRAPHY	208

CHAPTER 1

Introduction

Among the most ubiquitous sights of the sky the world over are cumulus clouds, a manifestation of atmospheric convection. An understanding of the dynamics of moist convective circulations has proved elusive, however. They range enormously in scale and organization from scattered fair-weather cumuli to squall lines to "supercell" thunderstorms to hurricanes. What unites them is that their principal source of energy is latent heating due to the condensation of water vapor from humid air rising from near the ground.

There are four principal complications not present in Rayleigh-Bénard convection. Firstly, the interplay of latent heating and compressibility is fundamental to moist convection and is the reason a good laboratory analogue to the process has not been found. To release latent heat, an air parcel must cool by adiabatic expansion. This heating must more than counteract the usually stable entropy stratification to allow convection to continue--the mechanism explored in this work. In fact, much of the energy of a hurricane may be derived from the heating of air by warm ocean water as it spirals into the low-pressure core and tries to cool by adiabatic expansion. Since deep convection may extend over two pressure scale heights, it cannot accurately even be assumed to be almost incompressible. Secondly, rain can fall out of a cloud, either evaporating below cloudbase or

reaching the ground. Air parcels in the cloud can thus increase their buoyancy while cooling the drier air below, resulting in tilted up-drafts and wavelike propagation of clouds. Thirdly, vertical wind shear tends to organize linear dry convection in rolls along the mean shear vector [Asai, 1971]. However, precipitating clouds can organize so as to tilt into the shear so that the right amount of cross-roll shear can substantially strengthen the convection [Seitter and Kuo, 1983]. Fourthly, convection in the atmosphere is not bounded between flat conducting plates. It is penetrative and heat and moisture transfer from the lower boundary may be quite complex. These four effects combine to produce the wealth of phenomena that is seen.

Analytical Studies

I will concentrate on obtaining an understanding of the effects of latent heating alone and ignore the dynamical effects of precipitation and shear. Despite twenty-five years of numerical and analytic studies there has been no clear understanding of how a field of convective clouds evolves, of what determines the spacing and clustering of clouds and thus the average upward heat flux, and whether collective instabilities of the cloud field could lead to wave-CISK, a self-exciting, nearly vertically propagating gravity wave. I will now review some of what has been learned theoretically.

The peculiar nature of moist convection was explored in an elegant paper by Bjerknes (1938). When the atmosphere is stable to dry overturning, but enough latent heat is released in the ascent of

a moist parcel to keep it buoyant relative to undisturbed dry air at the same level, it is called "conditionally unstable." However, to compensate for the upward movement of cloudy air there must be subsidence of dry air. Bjerknes pointed out that part of the latent heating is matched by the adiabatic warming of air outside the cloud, so it cannot be converted into kinetic energy and stifles the convection unless the subsidence rate is small. By considering a horizontal slice through the atmosphere, assuming the motion in the clouds is uniform and upward while the clear air outside is uniformly descending, he derived a critical ratio of cloud area m' to clear area m which could not be exceeded for convection to occur and expressed the belief that "...it is likely that a system with relatively small m'/m will dominate, that is a system with appreciable upward motion in narrow cloud towers and slow downward motion in the wide cloudless spaces."

The next step was made by Haque (1952), who was interested in the development of hurricanes. He imagined that a hurricane arises from the convection of a localized area of unstable air embedded in stably stratified air and asked how broad a wavelength of convection could be sustained. Using an inviscid hydrostatic linear stability theory for convection between two plates he found that the maximum wavelength was about 150 km (about a Rossby deformation radius), in broad agreement with hurricane radii; however, he did not explain why such an instability should not prefer the much faster growing short wavelengths.

In a seminal paper, Lilly (1960) realized that if the unstable air in Haque's model is identified with rising cloudy air and the stable air with descending dry air, one obtains a simple model of moist convection in which the stability of the atmosphere depends on the sign of the vertical motion, an ad-hoc but broadly correct parametrization. He extended the model to a uniformly spaced field of clouds and showed that in accordance with Bjerknes' prediction, infinitely spaced but infinitely narrow clouds grow the fastest. He also compared cylindrical clouds to slab-symmetric (two-dimensional) clouds and showed that if the dry air was sufficiently stable, cylindrical clouds grew substantially faster. Lastly, he computed the first nonlinear corrections to all the fields. The vertical velocity and thus the cloud boundary remain unchanged. The average temperature in the upper half of the cloud increases, presumably stabilizing the convection, but if the growth rate is so small as to be comparable to the Coriolis parameter f , the pressure minimum at the center of the cloud is deepened. He did not address the nonlinear equilibration of the cloud, and his use of the hydrostatic approximation even in narrow intense updrafts was somewhat inaccurate.

Kuo (1961, 1965) extended Lilly's model to include the effects of mixing by adding an eddy diffusivity and dropping the hydrostatic assumption, and calculated the marginally stable mode. However, he did not realize there is a matching condition on the horizontal temperature gradient and was left with an underdetermined system. Using a variational method to resolve the ambiguity, he was led to the conclusion that clouds grow faster the further they are apart.

Unsatisfied with this result he used coarser trial functions for which the marginal latent heating was minimized at a finite wavelength, a conclusion corroborated by a flawed finite amplitude stability criterion. The new feature of his results was a scale selection for the marginal cloudwidth--clouds have a width comparable to the domain height. Just as important, his model served as a guide for later work.

Yamasaki (1972, 1974) corrected and elaborated Kuo's work, making the peculiar assumption that the eddy diffusivity works only in the horizontal direction. Numerically solving the linear stability problem, he found that Lilly's conclusions hold for the viscous model as well--i.e. that cylindrical clouds appear to grow faster and that isolated clouds grow fastest. He considered a nonlinear finite difference numerical model of the equations and found steady nonlinear solutions with a similar character to the linear modes. He studied the interaction between clouds and concluded that clouds suppress each other even faster nonlinearly than linearly, but the width of his computation domain, only two cloud heights, was inadequate.

Kitade (1972) treated the effects of a mean vertical motion (created by large scale weather systems and the average global circulation, for instance). Unfortunately, he did not realize the limitations of Kuo's work. Further, he considered a wide region between two plates in which vertical motion is induced by pumping fluid in through the lower halves of the lateral boundaries and removing it in their top halves and looked for a marginally stable cloud assumed to form in the center of the domain. In the absence of convection this forcing does not produce a uniform vertical motion;

instead the vertical motion is localized to regions within a domain height of the lateral boundaries, so clouds will first form near the domain edges. He used an improper variational formulation to pick out a solution to the inhomogeneous problem which minimizes the amount of latent heating necessary to trigger convection, even though such a forced solution exists even in the absence of latent heating. Many of his solutions had more than one region of upward motion, yet only one region in which latent heating was accounted for. Kitade's results indicated upward motion enhanced convection, but were not definitive.

Asai and Nagasuji (1977,1982) continued Yamasaki's numerical investigations, using a wider domain and in their second paper a correct formulation of the thermodynamics of nonprecipitating convection. They found steady state cloud fields in which all clouds were of approximately equal strength and spacing but did not explore the dependence of the spacing on such parameters as the eddy viscosity and the amount of latent heating; all their numerical experiments used a fairly high value of the eddy viscosity ($100 \text{ m}^2/\text{s}$) which leads to a Rayleigh number based on the latent heating of only about seven times the marginal value. They found with their choice of parameters that the spacing is not unique but is most likely to coincide with the spacing which minimizes the total gravitational potential energy and is less than that which would maximize the total heat flux. Since latent heating, which raises the potential energy, plays such an important role it is difficult to understand why this should be true in general, and the issue has remained clouded.

In contrast stands the "mutual protection hypothesis" of Randall

and Huffman (1980), who claim that even nonprecipitating clouds will not tend to be evenly spaced, because each cloud creates in its neighborhood relatively favorable conditions for the development of succeeding clouds. Their argument depends crucially on the time-dependence of each cloud. After a cloud begins to decay it leaves behind a moist region surrounded by a dry region of air adiabatically warmed by subsidence. The temperature anomalies rapidly propagate away as gravity waves but the moistening remains, creating favorable conditions for the growth of more clouds in the neighborhood of the old cloud. They showed that a very idealized model of a cloud field in which this hypothesis is implicit leads to clumping of clouds into ever larger groups surrounded by large regions of clear subsiding air. This idea has received some support from a recent numerical simulation of Delden and Oerlemans (1982) described below.

Lastly, Shirer and Dutton (1979) looked at a Lorenz-type model of moist convection, with mixed success. They assumed condensation occurred wherever the motion was upward. They allowed only a single sinusoidal mode in the horizontal, which cannot adequately describe the different physics inside and outside a cloud. Their equations were identical to a truncated model of dry convection with an effective stability equal to the average of the dry and cloudy values, because in this model latent heating is positive in the updrafts and zero in the downdrafts, so it has a nonzero average at all heights where clouds can occur. Shirer (1982) generalized the model by allowing condensation only above a certain critical height, biasing the horizontally uniform component of latent heating toward the upper half of

the domain. This vertical asymmetry causes the bifurcation of convection from the rest state to become transcritical, and Shirer claimed it leads to subcritical finite amplitude steady convection. However, he did not properly account for the fact that the uniform heating is always positive, regardless of the sign of the amplitude of the sinusoidal mode. This should change the bifurcation structure so as to make finite amplitude convection always supercritical. Physically, the latent heating of the upper half of the domain stabilizes the stratification. Regardless, Shirer's model seems more appropriate to boundary layer convection in which clouds are restricted to the very top of the domain and latent heat release is not the fundamental driving force. His investigations (Shirer, 1980) of convection in shear are quite valuable if thought of in such terms.

In summary, linear moist convection theories in which condensation is assumed to occur simultaneously with upward motion predict that clouds should be infinitely spaced and have a width roughly equal to the depth of convection. Further, unlike for dry convection, a three-dimensional planform is linearly preferred. Numerical investigations into the nonlinear regime show that steady clouds can coexist in a wide enough domain, and that their spacing tends to become uniform but is not uniquely determined and tends to decrease in the presence of mean vertical motion. Nobody has tried to rationalize this spacing or understood these results in a more thermodynamically appropriate model. It is also not clear how to fit the clumping hypothesis together into the same framework, or whether wavelike modes might also be possible to

excite in a horizontally infinite domain. A physical understanding of these points can perhaps be pivoted on a mathematical understanding of the bifurcation structure of simple models of moist convection.

Numerical Modelling

Cumulus convection has been the subject of frequent numerical modelling efforts. Although most of them have been slanted toward comparison with real observations rather than a systematic understanding of the factors governing cloud evolution, I will concentrate on those studies which lend some insight into these factors.

Ogura (1963) first incorporated the effects of latent heating into a numerical model which I will describe in some detail as it formed the basis of the more sophisticated models which followed. He considered nonprecipitating convection in a 3 km by 3 km computational domain between two perfectly conducting stress-free boundaries which maintained constant levels of relative humidity, and parameterized turbulent mixing processes with a constant but small ($40 \text{ m}^2/\text{s}$) eddy viscosity. As in the atmosphere, the degree of conditional instability decreased strongly with height. The stratification of dry air was independent of height, but because the cooler air at higher altitudes can hold much less water vapor, cloudy air parcels release less latent heat as they rise higher in the atmosphere. Thus conditional instability usually gives rise to penetrative convection. He looked at the growth of a bubble of warm air which initiated a cloud in a conditionally unstable atmosphere. The bubble grew into a buoyant vortex

ring which rose as a cloud to the top of the domain and then decayed due to cool, dry inflow. The integration was stopped when the circulation collapsed into a gravity wave-like oscillation; no steady convective circulation could be maintained, probably because of the low eddy viscosity. The time it took for the plume to rise through the layer was much shorter than the time in which diffusion could replace the moisture which it took with it. He compared slab-symmetric (two-dimensional) clouds to cylindrically symmetric clouds and noted that the slab-symmetric clouds had significantly larger compensating downdrafts around their updraft cores. Unlike in Lilly's model there were regions of downward motion within the cloud and the downdraft maxima were close to the cloud edge. His clouds were quite narrow compared to their height due to the lack of an effective mixing mechanism, and subsidence outside the cloud appeared to be restricted to within a cloud height of its edge.

Murray (1970) and Soong and Ogura (1973) did further numerical experiments aimed primarily at understanding the differences between slab-symmetric and cylindrical clouds. Murray found that for a basic state corresponding to a summer Florida sounding, a cylindrical cloud grew much larger than its two-dimensional counterpart before collapsing and growing again in the same place. He did not look at other basic states, however, and used a larger grid spacing of 200 m which could only poorly resolve cloud features often one or two gridpoints wide. Soong and Ogura used a Smagorinsky-type turbulent diffusivity proportional to the mean shear and added simple precipitation physics. With a different mean profile they again found that cylindrical

clouds grew faster and achieved larger amplitudes before decaying, although the differences were not nearly as spectacular as in Murray's study, probably because Murray's basic state was only barely conditionally unstable. They attributed these differences to the fact that the buoyant acceleration of air at the cloud center was opposed by a pressure gradient which was larger in two dimensions. More fundamentally, there is more room for subsidence to take place around the perimeter of a cylindrical cloud. Air need not be forced to descend and warm as rapidly, so the vertical pressure gradient which forces this return flow (but which retards the updraft) can be smaller.

Hill (1974) first numerically examined the evolution of a field of clouds in a two-dimensional domain 5km by 16km wide as the ground was randomly heated, again starting with a realistic morning sounding. Until the convective boundary layer grew deep enough so that its top saturated, rolls of aspect ratio one dominated, but once clouds began to form and grow vertically in the conditionally unstable stratification, the larger circulations grew at the expense of those less vigorous, and the aspect ratio widened until only two cells were left in the domain, at which point rain began to fall out of the larger cell, evaporating in the air beneath. The cooled air induced the formation of other clouds as it spread outward along the ground. Hill's primary objective was simulation, and indeed his model quite accurately portrayed the cloudtop heights and the rise of cloudbase as dry air was mixed into the boundary layer observed by Plank (1969). It left open what determined the cloud spacing and whether, if the heating had been less intense, a statistically steady cloud field

would have developed and whether clumping of clouds could have begun before rain started.

Yau and Michaud (1982) extended Hill's work to three dimensions. They studied convection in a strongly sheared environment, so long two-dimensional rolls (cloud streets) tended to dominate. Within the streets cloud towers formed; the preference of nonprecipitating moist convection for three-dimensional circulations seemed again to manifest itself. Again they were mainly interested in modelling, so they did not consider the effect of varying the shear on the planform.

Delden and Oerlemans (1982), however, were more interested in cloud clumping. They used a 4 km by 60 km domain and went back to a constant, rather small eddy diffusivity of $25 \text{ m}^2/\text{s}$ (except for water vapor, which they only allowed to diffuse horizontally). Maintaining the top of their domain at a fixed temperature and imposing a constant heat flux through the bottom boundary, they found that after two hours, clouds began to clump even though no precipitation was allowed. Initially, circulations became broader and broader until only a few long-lasting clouds were left in the domain. After about two hours a transition to a pulsating form of convection began in which each cloud lasted briefly, but spawned two neighbors a fixed distance away before decaying. Clusters of such clouds dominated the remaining three hours of simulation, lending support to the Randall-Huffman clumping mechanism. The simulation leaves room for criticism. The grid spacing of 200m was rather large to deal with such a slowly damped model. The eddy diffusion was applied to inappropriate thermodynamic variables such as the temperature and water vapor instead of

quantities which are not created or destroyed in the process of mixing, such as the total water mixing ratio. It remains unclear from their work whether clumping was induced by evaporatively cooled downdrafts or moistening. However, it raises the possibility of an interesting new mechanism for mesoscale organization of convection.

Observations of Nonprecipitating Cumuli

Although there have been many observational studies of cumulus convection, few of them have addressed the interaction between clouds in an unsheared environment, and because of the lack of specific theoretical predictions, the data available are not easily compared with theory.

Riehl and Malkus (1964) were among the first to look at cumulus organization over the oceans. They found that cloud rows predominate; the spacing of clouds within each row was much less than the row spacing. A pure roll-like structure was almost never observed; each row was made of discrete units. Two modes of organization occurred. When convection did not penetrate the inversion which typically capped the moist boundary layer, the rows aligned along the mean wind in this layer ("parallel organization"), typically spaced proportional to and little more than a boundary layer depth apart. If the inversion weakened and the depth of cloud increased, so did the aspect ratio. I quote a remarkable example of a "subharmonic" instability of these cloud rows observed while approaching a region of large scale upward motion in the trough of an easterly wave:

"...at the halfway point [of the flight] evenly sized rows at 4-km normal intervals were found. One hour (370 km) later, it appeared that every fourth cloud was being built up at the expense of the intervening three. Rows of cumuli 4 km apart were still measured, but every 16 km a much more developed row was found, in which the larger clouds were close to congestus. By the time the aircraft had reached a location about 300 km east of the trough, the major lines had become 24-26 km apart and the minor ones intervening had been suppressed almost to the vanishing point."

In situations permitting deeper convection in which there was significant wind shear above the boundary layer a "crosswind mode" of rows of tall cumulonimbus clouds occurred lined up with this shear (but across the low-level winds) and spaced much more widely (30-80 km); often the two patterns were superposed. The aspect ratio of this mode, in which cloud towers extended through most of the depth of convection was large (between two and six). In regions of light winds little organization of the cloud field was present; wind shear was the dominant patterning force. Cloudiness and cloud field structure depended substantially on the large scale upper-level flow, but did not change gradually; instead, many mesoscale regions with abrupt transitions were observed.

Using aerial photography, Plank (1969) looked at boundary layer convection over Florida when there was little mean shear, mainly to determine the statistical distribution of cloud sizes at various times in the day. Cloud spacing grew in the morning, and as convection deepened and coagulated into larger cells, rain began. To this point no organization was observed. Groups of larger clouds surrounded by tremendous numbers of tiny clouds often characterized the afternoon cloud field, in which the size and spacing of the larger clouds often

increased a factor of ten from their early morning values. Since the boundary layer thickness increased steadily through the day and was not measured, it is difficult to calculate the aspect ratio of convection except to say that it clearly increased by a factor of two to four. Any clumping of nonprecipitating clouds did not occur fast enough to be noticeable before rain came into play. The fractional cloud cover was almost always small (10-30%) except just after noon, when it rose to near one half.

Lopez (1976) used airborne radar to study cloud populations east of the Caribbean Sea. Small radar echos ($< 100 \text{ km}^2$) corresponding to nonprecipitating clouds almost all grew and dissipated independently, lasting less than ten minutes. Although they often were clustered they rarely merged or arose from a splitting of a preexisting echo. A statistical analysis by Cho (1978) showed that in regions of homogeneous weak convection the cloud distribution was consistent with the notion that each cloud does not feel the effects of any other. The fractional cloud cover was quite small (3-10%) except in regions of intense precipitation; correspondingly, the distance between a cloud and its nearest neighbor had a distribution very skewed toward small spacings, but was on the average quite large (13.6 km) compared to the boundary layer depth. There was typically little low-level wind, and linear organization was only seen in large (precipitating) echoes, but the degree of mesoscale variation was again remarkable.

There has also been much interest in a process which has been thought to be primarily convective--"mesoscale cellular convection" (MCC). Satellite pictures show that large areas of ocean are often

covered by either polygonal lattices of cloud separated by clear air (open MCC) or wide blobs of cloud surrounded by clear air (closed MCC). These patterns occur at the top of convecting boundary layers over the ocean topped by strong inversions produced by synoptic scale subsidence (Agee and Dowell, 1973). Although the striking resemblance to Bénard cells has led many investigators to the conclusion that this is a quintessential example of mesoscale organization in moist convection, I will discuss in chapter five why there is probably more to it.

The primary conclusions that one can draw from these observations are as follows. If the cloud depth is a large fraction of the layer depth, the spacing between clouds or cloud clusters is large (30-80 km), so that the aspect ratio is large. Clouds organize into evenly spaced rows in a vertical wind shear, but seem more-or-less randomly spaced in light winds until precipitation begins, when clumping, merging and splitting of clouds occur. Even in light winds strong mesoscale (100-300 km) variations in the cloud field occur. Mesoscale cellular convection is another regular form of organization. To understand any of these processes it is important to explore completely the more basic problem of unsheared nonprecipitating convection, despite the apparent randomness of the cloud field that appears to result from it, because it forms a conceptual template of moist convection onto which physical effects can be added.

The Aims of this Work

In chapter two I formulate a model of moist convection based on accurate thermodynamics while retaining the conceptual simplicity of an eddy viscosity. The temperature and relative humidity are specified at two plates. If the basic state is exactly saturated with water vapor, "linear" equations identical to those of Kuo's model obtain, but in a different variable.

In chapter three I reproduce (except now with vertical diffusion) analytically the results of Yamasaki (1972) for those "linear" equations. I find exponentially growing separable solutions with stationary vertical cloud boundaries. The subsidence around each cloud decays on a characteristic length which I calculate and physically interpret as the minimum of a three length scales based on the eddy viscosity, the earth's rotation, and the growth rate. I consider a crude model of the effect of reduced turbulent mixing in the stable air outside the cloud. I also show that these separable solutions to the equations are stable and that no growing wavelike or oscillatory modes exist.

In chapter four I derive a set of nonlinear equations for the updraft strengths and positions of a field of clouds when isolated clouds are barely unstable. The equations capture all the dynamics of Asai and Nagasuji's simulations and predict a minimum stable cloud spacing for weakly nonlinear convection. Their general form is quite robust to changes in the boundary conditions or mean state, and their

only stable equilibria seem to be uniformly spaced steady clouds of equal strength.

In chapter five I point to the future. Simplified amplitude equations may be able to help in the understanding of time-dependent convection, precipitating convection, wave-CISK, and clumping. In the end, it is our analytical understanding of idealized models of convection and their bifurcation structure that allows us to properly interpret more realistic simulations and understand the effects of moist convection on larger scale weather systems and climate.

CHAPTER 2

A Mathematical Model of Moist Convection2.1 Introduction

Moist convection in the atmosphere is thermodynamically and dynamically complicated. All three phases of water participate in turbulent motions, often extending through the entire troposphere in which water droplets, snowflakes, or hail may all move at various rates relative to the air around them. In this chapter I will construct the equations for an idealized model which allows one to understand the simplest of these effects.

The first thermodynamic assumption is a shallow layer approximation. Boundary layer convection typically has a depth of 1-2 km, much smaller than the pressure and potential temperature scale heights. Deep full-troposphere convection can penetrate up to two scale heights; nevertheless, numerical models of such convection such as those of Seitter and Kuo (1983) show there is little qualitative change in the character of convection due to the density falloff.

The second thermodynamic assumption, that any water which condenses forms into liquid water droplets whose fall speeds are small compared to typical advective velocities, restricts this model to clouds out of which no rain is falling, such as often occur in the marine boundary layer. In more violent convective systems rain can

play an important role and lead to wavelike disturbances such as tropical squall lines which do not form in this model.

The dynamical assumptions are more unrealistic, although they could be realized in a laboratory experiment. The convecting air is confined between two rigid plates which act as stress-free boundaries at which the temperature and water content of the air are prescribed. Turbulence is modelled in the simplest possible way using a large eddy diffusivity.

In the atmosphere the constraints are often quite different. Moist convection is usually confined by a cap of very stably stratified dry air, so it is penetrative and may entrain air from above. The convection usually extends to the surface, which if it is ocean, may act as a source of air of the almost-constant sea-surface temperature which is nearly saturated with water vapor (so that the water content is fixed). However, if the surface is land, its temperature can rapidly change (due to shadow or rain) in response to the convection, and it transfers water to the air much less efficiently. Finally, I have deliberately ignored the generation and organization of turbulence by the convection by treating it as isotropic diffusion. Turbulence within a convective cloud is much stronger than outside it (an effect modelled primitively in section 3.5) and may lead to evaporatively cooled downdrafts driven by downward mixing of air from above the cloud which can much modify the fluxes of heat and water that this simple model predicts. However, an eddy viscosity gives us a benchmark model which is easily comprehensible, yet allows mixing to occur.

In this chapter I'll derive the equations for the model. Using the thermodynamic assumptions. I derive in section 2.2 a simple new representation of the buoyancy of an air parcel in terms of two quantities that are conserved following it in the absence of mixing. In section 2.3 I will write down the equations which incorporate the dynamical assumptions as well.

2.2 The Buoyancy in Shallow Nonprecipitating Convection

If motions in a fluid are slow compared to its sound speed, as are convective motions in the atmosphere, and occur in a layer shallow to the density and entropy scale heights, then the Boussinesq approximation holds [Spiegel and Veronis, 1962]. The variations in the density of the fluid which lead to its convection enter only into the vertical momentum equation as a vertical acceleration called the buoyancy,

$$(2.2.1) \quad B = - \frac{g}{\rho_0} (\rho - \rho_0(z)) ,$$

which is proportional to the deviation of the density $\rho(x,y,z)$ from an arbitrary reference density $\rho_a(z)$ normalized by a mean density ρ_0 which I take to be ρ_a evaluated at a mean height z_0 . An atmospheric air parcel contains both air and water in any of its phases. I will identify properties of this mixture which do not change as it responds adiabatically to pressure changes and express B as a function of these "invariants."

One such invariant is the mass ratio "r" of water in all phases to dry air. The total mass of water carried along by a mass of air remains unchanged if, as I assume, no rain falls out or in. I partition this mass ratio into the mass mixing ratios of water vapor q_v and liquid water q_l . I assume no frozen water is present, so

$$(2.2.2) \quad r = q_v + q_l .$$

Notice r is "linearly mixing"; if a mass of air m_1 with $r = r_1$ is mixed with a mass m_2 of air with $r = r_2$, it follows from the conservation of mass for water that

$$(2.2.3) \quad r_{\text{mixture}} = \frac{m_1 r_1 + m_2 r_2}{m_1 + m_2} .$$

In adiabatic motions, the entropy S per unit mass of dry air is also invariant. In appendix (I) I derive from S an approximately invariant, approximately linearly mixing quantity $\theta_{v\ell}$, the liquid water virtual potential temperature. It is the virtual temperature a parcel would have if lowered reversibly to a reference pressure p_{ref} , usually taken as 1000mb, at which it is unsaturated. In terms of the more familiar potential temperature θ , the virtual temperature θ_v is

$$(2.2.4a) \quad \theta_v = \theta + \epsilon q_v \theta_o ,$$

$$(2.2.4b) \quad \epsilon = .608 = \frac{R_v}{R_d} - 1 .$$

and

$$(2.2.5a) \quad \theta_{v\ell} = \theta_v - \gamma q_\ell = \theta + \epsilon q_v \theta_o - \gamma q_\ell ,$$

$$(2.2.5b) \quad \gamma \equiv \frac{L_{vo} \theta_{vo}}{C_{\rho do} T_o} ,$$

in a shallow layer around a reference level z_o at which typical values of thermodynamic quantities are denoted by a subscript "o".

Define a reference state which is completely dry and lies along an adiabat

$$(2.2.6a) \quad \theta_a(z) = \theta_o ,$$

$$(2.2.6b) \quad q_{va}(z) = 0 .$$

Relative to this state, the buoyancy of an air parcel is (see appendix I again)

$$(2.2.7) \quad B = g \left\{ \frac{\theta_v - \theta_o}{\theta_o} - q_\ell \right\} .$$

Neither q_ℓ nor θ_v is an invariant, so I will next express the buoyancy in terms of the two invariants $\theta_{v\ell}$ and r .

In a cloud, small liquid water droplets evaporate in milliseconds if the ambient air is not saturated and form equally fast on existing condensation nuclei if it supersaturates. Therefore, if the saturation mixing ratio is $q^*(\rho, T)$

$$(2.2.8) \quad q_\ell = \begin{cases} 0 & , \quad r \leq q^*(p,T) \\ r - q^*(p,T) & , \quad r > q^*(p,T) \end{cases} .$$

In the unsaturated air it is now easy to relate the buoyancy to the invariants, since when $q_\ell = 0$, $\theta_v = \theta_{v\ell}$,

$$(2.2.9) \quad B = B_u \equiv g \left\{ \frac{\theta_{v\ell} - \theta_o}{\theta_o} \right\} , \quad r < q^*(p,T) .$$

If the air is saturated matters are more complicated, since q_ℓ must be calculated from knowledge of $q^*(p,T)$, so q^* must be written in terms of $\theta_{v\ell}$ and r alone. In the shallow-layer approximation q^* can be linearized about the reference pressure and temperature:

$$(2.2.10) \quad q^*(p,T) = q^* + (p - p_o) \left. \frac{\partial q^*}{\partial p} \right|_0 + (T - T_o) \left. \frac{\partial q^*}{\partial T} \right|_0$$

In the Boussinesq approximation,

$$(2.2.11) \quad \frac{p - p_o(z)}{p_o} \ll \frac{T - T_a(z)}{T_o} \approx \frac{\theta - \theta_a(z)}{\theta_o} ,$$

so

$$p - p_o \approx p_a(z) - p_o \approx (z - z_o) \left. \frac{\partial p_a}{\partial z} \right|_0 ,$$

$$T - T_o = T - T_a(z) + T_a(z) - T_o$$

$$= \frac{T_o}{\theta_o} (\theta - \theta_a(z)) + (z - z_o) \left. \frac{\partial T_a}{\partial z} \right|_0 ,$$

$$\begin{aligned}
(2.2.12a) \quad q^*(p,T) &= q_o^* + (z - z_o) \left[\frac{\partial p_o}{\partial z} \bigg|_0 \frac{\partial q^*}{\partial p} \bigg|_0 + \frac{\partial T_o}{\partial z} \frac{\partial q^*}{\partial T} \bigg|_0 \right] \\
&\quad + \frac{T_o}{\theta_o} \frac{\partial q^*}{\partial T} \bigg|_0 (\theta_v - \theta_{vo}) \\
&= q_o^* - \alpha(z - z_o) + \beta(\theta - \theta_s),
\end{aligned}$$

where, noting the coefficient of $(z - z_o)$ is the total derivative of q^* along an adiabat,

$$(2.2.12b) \quad \alpha = - \frac{dq^*}{dz} \bigg|_a ,$$

$$(2.2.12c) \quad \beta = \frac{T_o}{\theta_o} \frac{\partial q^*}{\partial T} \bigg|_0 .$$

I now have q^* in terms of θ . Since (2.2.5a) can be solved for θ in terms of θ_{vl} , r and q^* , (2.2.5a) and (2.2.12a) can be simultaneously solved for q^* and θ in terms of θ_{vl} and r :

$$(2.2.13a) \quad q^* - q_o^* = \frac{-\alpha(z - z_o) + \beta(\theta_{vl} - \theta_{vo}) + \beta\gamma(r - q_o^*)}{1 + \beta(\gamma + \epsilon\theta_o)} ,$$

$$(2.2.13b) \quad \theta - \theta_o^* = \frac{\alpha(\gamma + \epsilon\theta_o)(z - z_o) + (\theta_{vl} - \theta_{vo}) + \gamma(r - q_o^*)}{1 + \beta(\gamma + \epsilon\theta_o)} .$$

Finally, these may be substituted into (2.2.7) to obtain the saturated buoyancy

$$\begin{aligned}
(2.2.14) \quad B = B_s &\equiv g \left\{ \frac{\theta_{vl} + \gamma q_l - \theta_{vo}}{\theta_o} - (r - q^*) \right\} \\
&= g \left\{ \frac{\theta_{vl} - \theta_o}{\theta_o} + \left(\frac{\gamma}{\theta_o} - 1 \right) (r - q^*) \right\} \\
&= B_u + B_l,
\end{aligned}$$

where the liquid buoyancy is

$$\begin{aligned}
(2.2.15) \quad B_l &= g \left(\frac{\gamma}{\theta_o} - 1 \right) (r - q^*), \\
&= g \left(\frac{\gamma}{\theta_o} - 1 \right) \left\{ \frac{\alpha(z - z_o) - \beta(\theta_{vl} - \theta_{vo}) + (1 + \beta\epsilon\theta_o)(r - q_o^*)}{1 + \beta(\gamma + \epsilon\theta_o)} \right\}
\end{aligned}$$

B_l is directly proportional to the difference between the mixing ratio and its saturated value; inside a cloud B_l is proportional to the amount of liquid water q_l .

It is convenient to use B_u and B_l as the thermodynamic variables. Defining

$$(2.2.16) \quad \Gamma \equiv \frac{g\alpha}{1 + \beta(\gamma + \epsilon\theta_o)} \left(\frac{\gamma}{\theta_o} - 1 \right),$$

it follows from (2.2.9) and (2.2.15) that B_u and $B_l - \Gamma z$ are linearly mixing and adiabatically invariant, and that the buoyancy can elegantly be written

$$(2.2.17) \quad B = \begin{cases} B_u & , \quad B_l \leq 0 \\ B_u + B_l & , \quad B_l > 0 \end{cases}$$

In shallow, nonprecipitating convection, the effect of moisture is to increase the buoyancy inside a cloud in proportion to the amount of liquid water present, due to the latent heat release from the condensation of that water.

2.3 The Equations of Motion

I can now state the governing equations. The momentum and the thermodynamic invariants are all assumed to diffuse at the rate ν (which can be taken as the molecular diffusivity of a fluid of Prandtl number one or can be interpreted as an eddy viscosity). If I make the Boussinesq approximation in a frame rotating at an angular velocity $\underline{\omega}$,

$$(2.3.1) \quad \nabla \cdot \underline{u} = 0 ,$$

$$(2.3.2) \quad \frac{D\underline{u}}{Dt} = -\nabla p + B\hat{k} + \nu \nabla^2 \underline{u} - 2\underline{\omega} \times \underline{u} ,$$

$$(2.3.3) \quad \frac{DB_u}{Dt} = \nu \nabla^2 B_u ,$$

$$(2.3.4) \quad \frac{DB_\ell}{Dt} = \Gamma w + \nu \nabla^2 B_\ell .$$

D/Dt is a substantial derivative and p is the pressure divided by the mean fluid density. In section 3.5, I will explore the consequences of taking ν to be larger inside the cloud than outside, an ad hoc model of the turbulent mixing.

The boundary conditions are applied at two rigid, stress-free plates at which the temperature and water mixing ratio are specified (figure 2.1):

$$(2.3.5) \quad w = u_z = v_z = 0 ,$$

$$(2.3.6) \quad B_{u,\ell}(x,y,0) = B_{u_0,\ell_0}(x,y),$$

$$(2.3.7) \quad B_{u,\ell}(x,y,h) = B_{u_h,\ell_h}(x,y) \quad \text{at } z = 0, h .$$

It is convenient to non-dimensionalize the equation using h/π as a length scale and $h^2/\pi^2\nu$ as a timescale. The nondimensional versions of (2.3.1)-(2.3.7) are identical to their original counterparts with (from here on, dimensional quantities are starred)

$$(2.3.8) \quad v^* \leftarrow 1 ,$$

$$(2.3.9) \quad \Gamma^* \leftarrow \frac{h^4}{\nu^2 \pi^4} \cdot \Gamma \quad (\text{for nondimensionalization})$$

$$(2.3.10) \quad \underline{\omega}^* \leftarrow \frac{\omega h^2}{\nu \pi^2} .$$

These equations cover all situations treated in this work. However, for two-dimensional flow between two nonrotating plates, each exactly saturated at a fixed temperature, the nondimensional equations simplify somewhat. Define a streamfunction $\tilde{\psi}$ such that

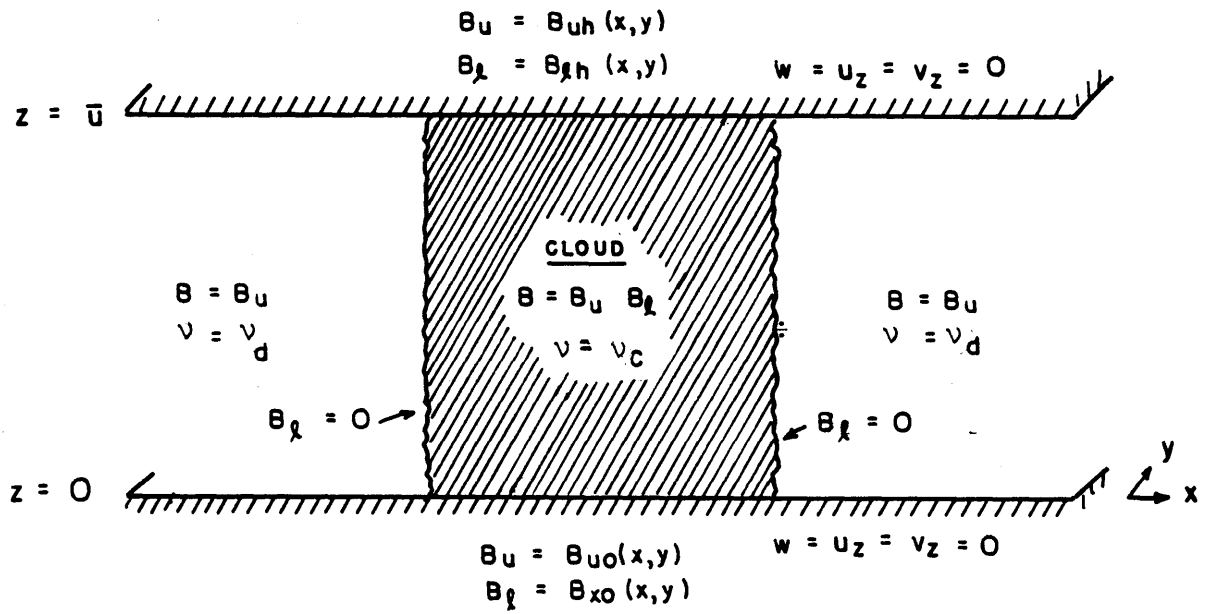


Figure 2.1

A diagram of my model of moist convection and a typical clous which forms when both boundaries are exactly saturated with water vapor.

$$(2.3.11) \quad \tilde{w} = \tilde{\psi}_x, \quad \tilde{u} = -\tilde{\psi}_z .$$

Let B_{uo} and B_{uh} be the unsaturated buoyancy of the fluid in contact with the bottom and top plates. Then the nondimensional buoyancy frequency N_d of the fluid in its state of rest is

$$(2.3.12) \quad N_d^2 = (B_{uh} - B_{uo})/\pi .$$

Let \tilde{B}_u be the deviation of the unsaturated buoyancy from its value \bar{B}_u in the state of no motion,

$$(2.3.13) \quad \bar{B}_u(z) = B_{uo} + N_d^2 z ,$$

and similarly for \tilde{B}_ℓ . Since both plates are exactly saturated, $B_{\ell o} = B_{uo} = 0$, so

$$(2.3.14) \quad \bar{B}_\ell(z) = 0 .$$

The boundary conditions (2.3.6) - (2.3.8) imply

$$(2.3.15) \quad \tilde{\psi} = \tilde{\psi}_{zz} = 0 ,$$

$$(2.3.16) \quad \tilde{B}_u = \tilde{B}_\ell = 0 \quad \text{at } z = 0, \pi .$$

For a growing disturbance, \tilde{B}_u and \tilde{B}_ρ are related because they are advected and diffused identically. From the nondimensional versions of (2.3.2) and (2.3.3), if I define

$$(2.3.17) \quad \tilde{\phi} = \frac{\tilde{B}_\rho}{\Gamma} + \frac{\tilde{B}_u}{N_d^2},$$

then

$$(2.3.18) \quad \tilde{\phi} = 0 \quad \text{at } 0, \pi,$$

$$(2.3.19) \quad \frac{D\tilde{\phi}}{Dt} = \nu \nabla^2 \tilde{\phi}.$$

Since $\tilde{\phi}$ decays through diffusion it cannot grow on the average.

Let an average $\langle \rangle$ of a function \tilde{f} be defined as

$$(2.3.20) \quad \langle \tilde{f} \rangle = \lim_{L \rightarrow \infty} \frac{1}{4\pi L^2} \int_0^\pi dz \int_{-L}^L dx \int_{-L}^L dy \tilde{f}(x, y, z).$$

Then

$$\langle \phi \frac{D\tilde{\phi}}{Dt} \rangle = \frac{D}{Dt} \langle \frac{1}{2} \tilde{\phi}^2 \rangle + \langle \nabla \cdot \left(\underline{u} \frac{\tilde{\phi}^2}{2} \right) \rangle = \langle \tilde{\phi} \cdot \nu \nabla^2 \tilde{\phi} \rangle = -\langle \nu [\nabla \tilde{\phi}]^2 \rangle,$$

so

$$(2.3.21) \quad \frac{d}{dt} \langle \frac{1}{2} \tilde{\phi}^2 \rangle = -\langle \nu (\nabla \tilde{\phi})^2 \rangle \leq -\nu \langle \tilde{\phi}_z^2 \rangle \leq -\nu \langle \tilde{\phi}^2 \rangle.$$

The second inequality follows from an expansion of $\tilde{\phi}$ in a Fourier sine series $\tilde{\phi} = \sum_{n=1}^{\infty} \hat{\phi}_n \sin nz$. $\langle \tilde{\phi}^2 \rangle$ decays exponentially fast to zero no matter how much convection occurs, so it is consistent to set $\tilde{\phi}$ to its $t \rightarrow \infty$ limit, when perturbations \tilde{B}_ρ and \tilde{B}_u are in phase:

$$(2.3.22) \quad \tilde{\phi} \equiv 0, \quad \tilde{B}_u = -\frac{N_d^2}{\Gamma} \tilde{B}_\ell.$$

Having done this, I can write the buoyancy perturbation in terms of \tilde{B}_ℓ alone. From (2.2.17) and (2.3.22),

$$(2.3.23) \quad \tilde{B} = -\frac{N^2}{\Gamma} \tilde{B}_\ell,$$

where

$$(2.3.24) \quad N^2 = \begin{cases} N_d^2, & \tilde{B}_\ell < 0, \\ -N_c^2 \equiv \Gamma - N_d^2, & \tilde{B}_\ell > 0. \end{cases}$$

depends on whether the parcel is saturated. If the dry buoyancy stratification N_d^2 is small enough so that $\Gamma > N_d^2$, $N^2 < 0$ inside the cloud and parcels there can extract energy from the mean state by buoyant overturning.

The remaining equations (2.3.2) and (2.3.4) can be written in terms of $\tilde{\psi}$ and \tilde{B}_ℓ :

$$(2.3.25) \quad \left(\frac{D}{Dt} - \nabla^2\right) \nabla^2 \tilde{\psi} = \tilde{B}_x,$$

$$(2.3.26) \quad \left(\frac{D}{Dt} - \nabla^2\right) \tilde{B}_\ell = \Gamma \tilde{\psi}_x.$$

These equations possess both the advective nonlinearity and a new nonlinearity resulting from the different form of \tilde{B} inside and outside clouds. The latter has the peculiar feature that \tilde{B} is linear in \tilde{B}_ℓ if all one does is to multiply \tilde{B}_ℓ by a positive

scalar, and introduces a free boundary (the cloud edge) which must be calculated as part of the solution, across which the fields must be matched.

From (2.3.23), \tilde{B}_x has a discontinuity at the cloud boundary which must be matched by a discontinuity in the highest derivative of $\tilde{\psi}$ normal to the cloud boundary in (2.3.25). All lower derivatives of $\tilde{\psi}$, however, can be continuous, so $\tilde{\psi}$ and its first three x derivatives are continuous. Expanding (2.3.26),

$$(2.3.27) \quad \left(\frac{\partial}{\partial t} - \nabla^2\right)\tilde{B}_\ell = (\Gamma - \tilde{B}_{\ell z})\tilde{\psi}_x - \tilde{B}_{\ell x}\tilde{\psi}_z ;$$

the right hand side can be differentiated twice in x and still have no discontinuous $\tilde{\psi}$ derivatives, so the highest derivative of \tilde{B}_ℓ , $\nabla^2\tilde{B}_\ell$ is continuously twice differentiable. Thus

$$(2.3.28) \quad \left. \begin{array}{l} \tilde{\psi}, \tilde{\psi}_x, \tilde{\psi}_{xx}, \tilde{\psi}_{xxx} \\ \tilde{B}_\ell, \tilde{B}_{\ell x}, \tilde{B}_{\ell xx}, \tilde{B}_{\ell xxx}, \tilde{B}_{\ell xxxx} \end{array} \right\} \text{are continuous across } \tilde{B}_\ell = 0 .$$

The free boundary significantly alters the mathematical structure of the equations. This reflects itself in quite different physics from those of dry convection, as I show in the next two chapters.

CHAPTER 3

The "Linear" Dynamics of Moist Convection in an
Exactly Saturated Atmosphere

3.1 Introduction

The Boussinesq equations (2.3.12-14) are nonlinear even for small amplitude disturbances because the buoyancy is a different function of the "liquid water buoyancy" B_ℓ depending on whether an air parcel is inside or outside a cloud. In this limit, solutions with different cloud boundaries still cannot be superposed to obtain another solution.

However, there are some important solutions which can be found analytically. These solutions are exponentially growing clouds with boundaries which are stationary and vertical; because of this geometry they are separable, and mathematically can be found by matching at the unknown cloud boundary the solutions of sixth-order ordinary differential equations for the horizontal structure inside and outside the cloud. This entails solving two nonlinear equations for two parameters, the cloud width and growth rate, given a cloud spacing. The most unstable modes in a conditionally unstable atmosphere are single cloudy updrafts surrounded by an infinite expanse of dry, descending air. The subsidence decays exponentially away from the cloud in a "frictional deformation radius"

$$R_{fr}^* = N^* h^*{}^3 / \pi^3 v_d^*$$

unless the eddy viscosity away v_d^* away from the cloud is so small that either the Rossby deformation radius due to the vertical component $f^*/2$ of the earth's rotation,

$$R_{rot}^* \equiv N^* h^* / f^* \pi,$$

or the "transient deformation radius" due to the finite speed $N^* h^*$ of which information about changes in the convection propagates away from the cloud,

$$R_t^* = N^* h^* / \Omega^* \pi,$$

where Ω^* is the growtrate of the convective mode, is smaller.

One might expect that since there is an asymmetry between up and downgoing motions, concentrated updrafts surrounded by broad hexagonal regions of descent would be favored. In fact the limit of such a planform as clouds become widely spaced, a circular updraft surrounded by an infinite region of descent, is substantially more unstable than the two-dimensional circulations so far considered.

Lastly, what is not seen? First, I find that clouds with several updrafts and saturated downdrafts can grow; however they are unstable to modification of their cloud boundaries which lead to development of single-updraft clouds. Simulations seem to show that convective clusters of clouds interspersed with unsaturated downdrafts also are not seen. Second, I will show, using a variational approach, that growing wavelike convection is impossible in the model, as is any form

of periodic oscillation in the geometry of the convection. Lastly, I apply the variational principle to show that the modes with vertical cloud boundaries are stable to "nonseparable" perturbations which wrinkle the cloud-edge. Thus, there are no modes with almost, but not quite vertical cloud boundaries which grow faster than the separable modes.

In conclusion, it seems highly probable that any small initial perturbation will evolve into a set of widely spaced stationary cloudy updrafts with vertical cloud boundaries. In three dimensions these updrafts will be nearly cylindrical. In chapter four, I'll look at how these updrafts interact with each other, and the effect of non-linearity and a mean forced vertical motion on the resulting field of convection.

3.2 The Simplest Case

In this section I do the simplest problem, in which rotation is neglected, the motion is two-dimensional, and the eddy viscosity is the same inside and outside the cloud, in the "linear" limit in which fluid velocities are infinitesimal.

The picture which emerges is that updrafts prefer to be widely spaced but have a width approximately equal to the domain height surrounded by a region of subsidence concentrated within a "frictional deformation radius" of the cloud. This subsidence extends into the edges of the cloud, where it is driven by evaporative cooling.

From (2.3.23)-(2.3.26), the equations are

$$(3.2.1) \quad (\partial_t - \nabla^2) \nabla^2 \tilde{\psi} = \tilde{B}_x ,$$

$$(3.2.2) \quad (\partial_t - \nabla^2) \tilde{B}_\ell = \Gamma \tilde{\psi}_x ,$$

$$(3.2.3) \quad \tilde{B} = -\frac{N^2}{\Gamma} \tilde{B}_\ell ,$$

$$(3.2.4) \quad N^2 = \begin{cases} N_d^2, & \tilde{B}_\ell < 0 , \\ -N_c^2, & \tilde{B}_\ell > 0 . \end{cases}$$

Conditional instability occurs when $N_d^2 > 0$ but $-N_c^2 < 0$. The boundary conditions, from (2.3.15)-(2.3.16), are

$$(3.2.5) \quad \tilde{\psi} = \tilde{\psi}_{zz} = \tilde{B}_\ell = 0 \quad \text{at } z = 0, \pi .$$

To easily match across the cloud boundary it is convenient to define a "liquid water potential" \tilde{L} such that

$$(3.2.6) \quad \frac{\partial \tilde{L}}{\partial x} = \tilde{B}_\ell(x, z, t) .$$

and use it as the principal dependent variable. Integrate (3.2.2) once with respect to x , and appropriately choose the integration constant inherent in the definition of \tilde{L} to find

$$(3.2.7) \quad \tilde{\psi} = \frac{1}{\Gamma} (\partial_t - \nabla^2) \tilde{L} .$$

Use this to eliminate ψ from (3.2.1) and obtain an equation for \tilde{L} alone,

$$(3.2.8) \quad (\partial_t - \nabla^2)^2 \nabla^2 \tilde{L} = -N^2 \tilde{L}_{xx} .$$

The boundary conditions can be derived from (3.2.5) and (3.2.7),

$$(3.2.9) \quad \tilde{L} = \tilde{L}_{zz} = \tilde{L}_{zzzz} = 0 \quad \text{on } z = 0, \pi .$$

A special class of separable solutions with sinusoidal vertical structure exist in which the cloud boundaries are vertical. The most unstable of these have the structure

$$(3.2.10) \quad \tilde{L} = \hat{L}(x, t) \sin z ,$$

and obey a horizontal structure equation

$$(3.2.11) \quad (\partial_t + 1 - \partial_x^2)^2 (\partial_x^2 - 1) \hat{L} = -N^2 \hat{L}_{xx} .$$

At the cloud boundary, $\tilde{B}_x \propto -N^2 \hat{L}_{xx}$ changes discontinuously in response to the discontinuous change in N^2 there. The matching conditions (2.3.28) imply the first five derivatives of \hat{L} are continuous. Since $\tilde{\psi}$ is continuous, (3.2.7) shows \hat{L} itself is also continuous:

$$(3.2.12) \quad \hat{L}, \hat{L}_x, \hat{L}_{xx}, \hat{L}_{xxx}, \hat{L}_{xxxx}, \hat{L}_{xxxxx} \text{ continuous at } \hat{L}_x = 0 .$$

In fact, an even more special class of solutions (which I call eigenmodes) have stationary, vertical cloud boundaries and grow exponentially with time:

$$(3.2.13) \quad \tilde{L} = L(x) \sin z \cdot e^{\Omega t} .$$

They obey the sixth order ODE

$$(3.2.14) \quad \left(\Omega + 1 - \frac{d^2}{dx^2}\right)^2 \left(\frac{d^2}{dx^2} - 1\right)L = -N^2 L_{xx} .$$

I seek solutions with clouds of width "a" spaced periodically with wavelength λ . If the x-origin is taken to be at the center of the cloud then we may assume \tilde{B}_ρ is symmetrical about $x = 0$, so $L(x)$ is antisymmetrical about $x = 0$. Let $g(x, \rho)$ satisfy

$$(3.2.15) \quad \frac{d^2 g}{dx^2} = \rho^2 g .$$

Then g will satisfy (3.2.14) in the cloudy air if ρ satisfies the characteristic polynomial.

$$(3.2.16) \quad p_c(\rho) = (\Omega + 1 - \rho^2)^2(\rho^2 - 1) - N_c^2 \rho^2 = 0 ,$$

and in the clear air if

$$(3.2.17) \quad p_d(\rho) = (\Omega + 1 - \rho^2)^2(\rho^2 - 1) + N_d^2 \rho^2 = 0 .$$

Physically, the first root corresponds to a vertical shearing of the fluid which decays exponentially with x on a viscous lengthscale. If conditional convection occurs with growth rate Ω , then purely moist convection must be even more unstable for some range of wavenumbers. The edges of this band are the two pairs of "convective" modes of (3.2.16) which are sinusoidal,

$$(3.2.18) \quad \rho = \pm \begin{cases} \rho_{c1} = r_{c1}, & \text{(viscous)} \\ \rho_{c2} = ir_{c2}, & \text{(convective)} \\ \rho_{c3} = ir_{c3}. \end{cases}$$

In the clear air the modes are a pair of viscously damped modes with complex ρ and a gravity wave response in which an exponentially decaying temperature perturbation drives horizontal motions as far as viscosity will allow:

$$(3.2.19) \quad \rho = \pm \begin{cases} \rho = r_{d1}, & \text{(gravity wave)} \\ \rho = r_{d2} + ir_{d3}, & \text{(viscous)} \\ \rho = r_{d2} - ir_{d3}. \end{cases}$$

I construct a solution L in the cloudy air which obeys the condition of antisymmetry at $x = 0$, and a solution in the dry air obeying antisymmetry at $x = \lambda/2$. The fundamental solutions g which do this can be written

$$(3.2.20) \quad g(x, \rho) = \begin{cases} g_c(x, \rho) = i \frac{1}{\rho} \sin i_{\rho x} = \frac{1}{\rho} \sinh \rho x, \\ g_d(x, \rho) = \begin{cases} \frac{1}{\rho} \sinh \rho(x - \frac{\lambda}{2}), & \lambda < \infty \\ -\frac{1}{\rho} \exp\{-\rho(x - \frac{a}{2})\}. & \lambda = \infty \end{cases} \end{cases}$$

so the most general real L is

$$(3.2.21) \quad L = \begin{cases} b_{c1}g_c(x, \rho_{c1}) + b_{c2}g_c(x, \rho_{c2}) + b_{c3}g_c(x, \rho_{c3}) & 0 < x < \frac{a}{2}, \\ b_{d1}g_d(x, \rho_{d1}) + b_{d2}g_c(x, \rho_{d2}) + b_{d3}g_c(x, \rho_{d3}) & \frac{a}{2} < x < \frac{\lambda}{2}, \end{cases}$$

where the b_{ci} and b_{di} are real constants (except b_{d2} and b_{d3} , which are complex conjugates) to be determined by the matching conditions (3.2.12), which give a matrix equation

$$(3.2.22a) \quad M[b_{d1} \ b_{d2} \ b_{d3} \ -b_{c1} \ -b_{c2} \ -b_{c3}]^T = 0, \quad ,$$

$$(3.2.22b) \quad M = \begin{bmatrix} g_{d1} & g_{d2} & g_{d3} & g_{c1} & g_{c2} & g_{c3} \\ f_{d1} & f_{d2} & f_{d3} & f_{c1} & f_{c2} & f_{c3} \\ \rho_{d1}^2 g_{d1} & \rho_{d2}^2 g_{d2} & \rho_{d3}^2 g_{d3} & \rho_{c1}^2 g_{c1} & \rho_{c2}^2 g_{c2} & \rho_{c3}^2 g_{c3} \\ \rho_{d1}^2 f_{d1} & \rho_{d2}^2 f_{d2} & \rho_{d3}^2 f_{d3} & \rho_{c1}^2 f_{c1} & \rho_{c2}^2 f_{c2} & \rho_{c3}^2 f_{c3} \\ \rho_{d1}^4 g_{d1} & \rho_{d2}^4 g_{d2} & \rho_{d3}^4 g_{d3} & \rho_{c1}^4 g_{c1} & \rho_{c2}^4 g_{c2} & \rho_{c3}^4 g_{c3} \\ \rho_{d1}^4 f_{d1} & \rho_{d2}^4 f_{d2} & \rho_{d3}^4 f_{d3} & \rho_{c1}^4 f_{c1} & \rho_{c2}^4 f_{c2} & \rho_{c3}^4 f_{c3} \end{bmatrix}$$

in which

$$(3.2.23) \quad f(x, \rho) = \frac{\partial g}{\partial x}(x, \rho) = \begin{cases} f_c(x, \rho) = \cos i\rho x = \cosh \rho x & , \\ f_c(x, \rho) = \begin{cases} \cosh \rho(x - \frac{\lambda}{2}) & \lambda < \infty, \\ \exp\{-\rho(x - \frac{a}{2})\} & \lambda = \infty, \end{cases} \end{cases}$$

$$(3.2.24) \quad f, g_{di} = f, g_d(\frac{a}{2}, \rho_{di}),$$

$$(3.2.25) \quad f, g_{ci} = f, g_c(\frac{a}{2}, \rho_{ci}),$$

For a solution to exist and for the resulting cloud boundary to be at $a/2$,

$$(3.2.26) \quad \det M = 0 ,$$

$$(3.2.27) \quad L_x(a/2) = b_{c1} f_{c1} + b_{c2} f_{c2} + b_{c3} f_{c3} = 0 .$$

The two constraints (3.2.26) and (3.3.27) are nonlinear equations for the growth rate Ω and cloudwidth a . To simultaneously solve these equations, I first did a coarse search. For any Ω and a , $\det M$ is computed, and setting $b_{c3} = 1$ the first five rows of (3.2.22a) are solved for the remaining b 's, allowing $L_x(a/2)$ to be computed from (3.2.27). Let

$$(3.2.28) \quad \sigma(\Omega, a) = \begin{array}{l} 1 \dots \det M < 0, \quad L_x(a/2) < 0 \\ 2 \dots \det M < 0, \quad L_x(a/2) > 0 \\ 3 \dots \det M > 0, \quad L_x(a/2) < 0 \\ 4 \dots \det M > 0, \quad L_x(a/2) > 0 \end{array} .$$

A computer-generated map of σ over a reasonable range of Ω and a can be made to arbitrary resolution. A solution is demarcated by the intersection of regions with $\sigma = 1, 2, 3, 4$. After coarsely locating solutions in this way, the values of $\det M$ and $L_x(a/2)$ at three points close to the root give a better guess at the solution using a two-dimensional extension of the "secant method" [Ralston and Rabinowitz, p. 338] which assumes $\det M$ and $L_x(a/2)$ are locally linear functions of Ω and a . The method converges at a faster-than-linear rate to a root pair.

Once a root pair (Ω, a) and the associated constants $\{b_i\}$ are found, \tilde{B}_ℓ and w can easily be found using (3.2.6) and (3.2.7),

$$(3.2.29a) \quad \tilde{B}_\ell = \begin{cases} b_{c1} f_c(x, \rho_{c1}) + b_{c2} f_c(x, \rho_{c2}) + b_{c3} f_c(x, \rho_{c3}) & 0 < x < \frac{a}{2} \\ b_{d1} f_d(x, \rho_{d1}) + b_{d2} f_d(x, \rho_{d2}) + b_{d3} f_d(x, \rho_{d3}) & \frac{a}{2} < x < \frac{\lambda}{2}, \end{cases}$$

$$(3.2.29b) \quad w = \begin{cases} \gamma_{c1} b_{c1} f_c(x, \rho_{c1}) + \gamma_{c2} b_{c2} f_c(x, \rho_{c2}) + \gamma_{c3} b_{c3} f_c(x, \rho_{c3}) & 0 < x < \frac{a}{2} \\ \gamma_{d1} b_{d1} f_d(x, \rho_{d1}) + \gamma_{d2} b_{d2} f_d(x, \rho_{d2}) + \gamma_{d3} b_{d3} f_d(x, \rho_{d3}) & \frac{a}{2} < x < \frac{\lambda}{2}, \end{cases}$$

where

$$(3.2.30) \quad \gamma_{c,di} = (\Omega + 1 - \rho_{c,di}^2) / \Gamma .$$

Shown in figure 3.1 is a typical solution with infinite intercloud spacing and $N_d^2 = N_c^2$ just large enough to make $\Omega = 0$. The cloud width "a" is about equal to the domain height, and the cloud is surrounded by a broad expanse of air which is dry and warm due to its descent through a stable mean stratification. The descent rate drops off exponentially as $\exp(-r_{d1}x)$; for fairly large N_d, r_{d1} is approximately (from 3.2.17)

$$(3.2.31) \quad r_{d1} \approx \frac{\Omega + 1}{N_d} .$$

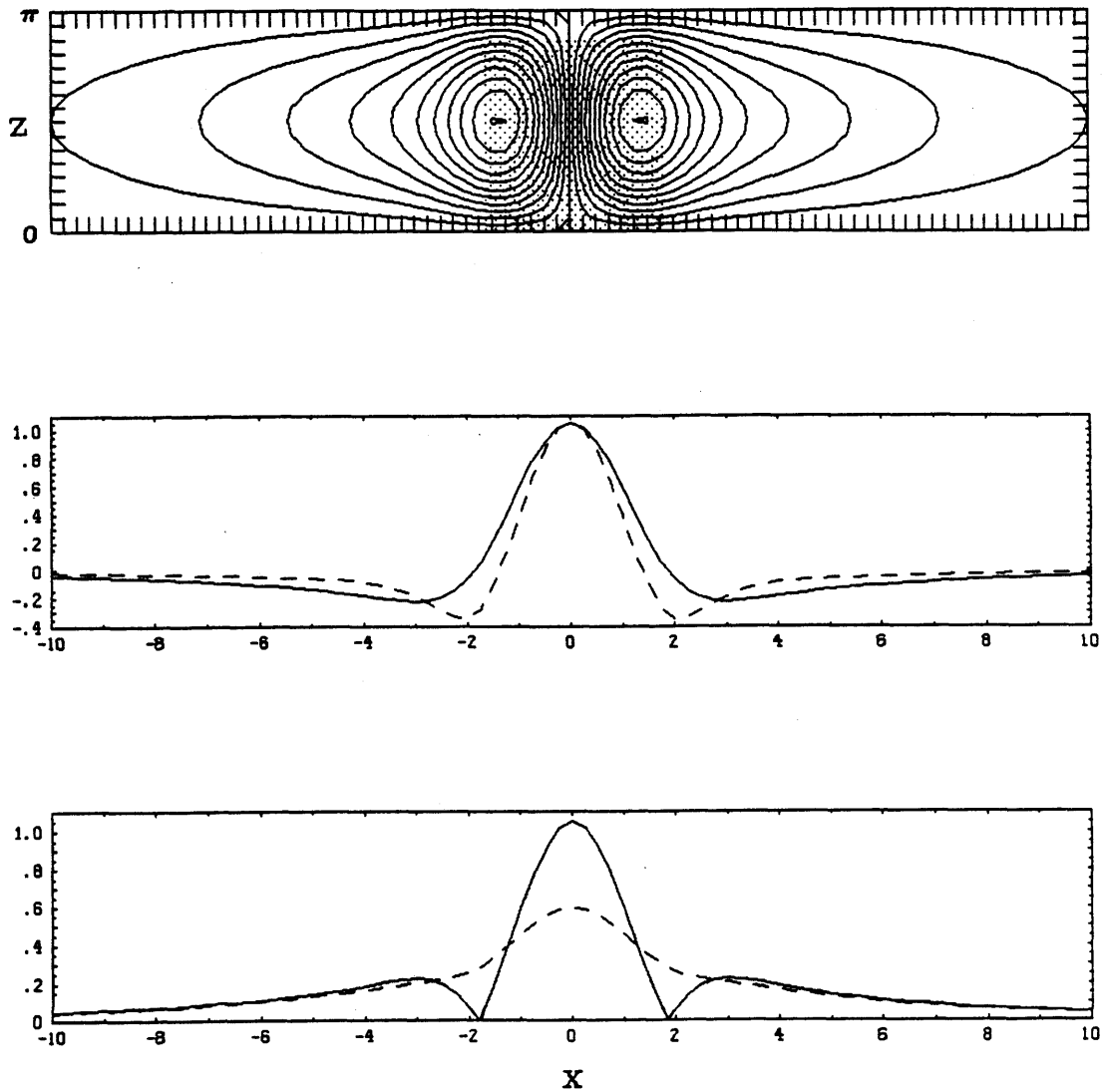


Figure 3.1

The neutral solution with $\lambda = \infty$, $N_c^2 = N_d^2 = 14.23$.

- (a) Streamlines (solid). The cloud is shaded; regions with more liquid are darker.
- (b) Profiles of B_l (solid) and w (dashed) at midheight ($z = \pi/2$). In Kuo's model the solid line would profile w .
- (c) The buoyancy B in my model (solid) and Kuo's model (dashed).

so that the dimensional width of the region of descent is proportional to the "frictional deformation radius" R_{fric}^* , which is the horizontal distance over which a buoyancy perturbation can induce motion while working against friction.

$$(3.2.32) \quad R_{\text{descent}}^* = \frac{h^*}{\pi r_{1d}} \approx \frac{1}{\Omega + 1} R_{\text{fric}}^* ,$$

$$(3.2.33) \quad R_{\text{fric}}^* = N \frac{h^*}{\pi} \cdot \frac{h^{*2}}{v_d^{*2}} = N_d \frac{h^*}{\pi} .$$

Since N_c must be at least 3-4 and typically $N_d^2 \gtrsim N_c^2$ in the atmosphere, the region of descent is wider than the region of ascent.

Near the edge of the cloud a strong downdraft develops since the air is coldest there. This cold air forms from diffusive mixing of moist air from inside the cloud with dry air outside the cloud. The mixture cools by evaporation of the liquid water in the cloudy air until it is no longer saturated, forming cold air around the cloud boundary.

It is interesting to compare this eigenfunction to the model proposed by Kuo (1961), a variant of which was correctly solved by Yamasaki (1972) (he curiously assumed the vertical eddy viscosity to be zero, probably by analogy with large-scale flows in which eddies have a much larger characteristic lengthscale horizontally than vertically because differential vertical motion is inhibited by the earth's rotation, leading to a much larger effective diffusivity in the horizontal). In Kuo's model, air contained between two plates feels an effective stratification N^2 which depends on the sign of

the vertical motion. In my notation, he would take the stratification as

$$(3.2.34) \quad N^2(w) = \frac{d\bar{B}}{dz} = \begin{cases} N_d^2 & w < 0, \\ -N_c^2 & w > 0, \end{cases}$$

and propose the equations analogous to (3.2.1-2) of my model

$$(3.2.35) \quad \partial_t \nabla^2 \tilde{\psi} = \tilde{B}_x + \nabla^4 \tilde{\psi},$$

$$(3.2.36) \quad \partial_t \tilde{B} = -N^2 \psi_x + \nabla^2 \tilde{B},$$

$$(3.2.37) \quad \tilde{\psi} = \tilde{\psi}_{zz} = \tilde{B} = 0 \quad \text{at } z = 0, \pi.$$

Solving these for $\tilde{\psi}$,

$$(3.2.38) \quad (\partial_t - \nabla^2)^2 \nabla^2 \tilde{\psi} = -N^2 \tilde{\psi}_{xx},$$

$$(3.2.39) \quad \tilde{\psi} = \tilde{\psi}_{zz} = \tilde{\psi}_{zzzz} = 0.$$

(3.2.38) indicates that the discontinuity of N^2 where $\tilde{\psi}_x = 0$ is matched by a jump in $\nabla^2 \tilde{\psi}$, but all lower derivatives of $\tilde{\psi}$ are continuous across the cloud boundary,

$$(3.2.40) \quad \psi, \psi_x, \dots, \psi_{xxxxx} \text{ continuous at the cloud boundary } \psi_x = 0.$$

This problem is identical to the one I considered, except the stream-function replaces the liquid water potential L . However, the solution

is clearly different, as is seen from figure 3.1. Now the region of upward motion by definition extends to the cloud edge; the evaporative downdraft at the cloud edge is missed. Further, the buoyancy distribution is very different. From (3.2.35) the buoyancy can be expressed in terms of ψ , choosing an integration constant $\tilde{B} = 0$ at the cloud edge.

$$(3.2.41a) \quad \tilde{B}(x) = B(x) \sin z e^{\Omega t}$$

$$(3.2.41b) \quad B(x) = \begin{cases} b_{c1} \gamma_{c1} \left(\frac{\rho_{c1}^2 - 1}{\rho_{c1}^2} \right) [f_c(x, \rho_{c1}) - f_{c1}] + b_{c2} \gamma_{c2} \left(\frac{\rho_{c2}^2 - 1}{\rho_{c2}^2} \right) [f_c(x, \rho_{c2}) - f_{c2}] + \\ \quad + b_{c3} \gamma_{c3} \left(\frac{\rho_{c3}^2 - 1}{\rho_{c3}^2} \right) [f_c(x, \rho_{c3}) - f_{c3}] & 0 < x < \frac{a}{2} \\ b_{d1} \gamma_{d1} \left(\frac{\rho_{d1}^2 - 1}{d1} \right) [f_d(x, \rho_{d1}) - f_{d1}] + \\ \quad + \operatorname{Re} \left[\gamma_{d2} \left(\frac{\rho_{d2}^2 - 1}{d2} \right) (b_{d2} + i b_{d3}) (f_d(x, \rho_{d2}) - f_{d2}) \right] & \frac{a}{2} < x < \frac{\lambda}{2} ; \end{cases}$$

$B(x)$ is the curve of long dashes in figure 3.1, and is drastically different than the buoyancy $-\frac{N^2}{T} B_\ell$ of my theory. Instead, the entire region around the cloud is buoyant; there is no cold air at the cloud edge. This is because positive buoyancy is being generated everywhere since $N^2(w) \cdot w > 0$ always, and diffusion smears out the local minimum of generation where $w = 0$ (the cloud edge). This wide peak in buoyancy naturally leads to a wider updraft (the solid line in the figure) than in my model (the dashed line).

One might think that the Kuo model is a good physical representation

of a cloud from which all liquid water falls as rain. In an exactly saturated atmosphere with no mixing this is initially indeed so. But a parcel rising through the cloud sheds all of its liquid water so that it becomes distinctly sub-saturated as it descends in the return circulation. When it once again begins to rise, it clearly will not saturate at all unless it picks up moisture in the course of its circulation, and no latent heating, ergo no change in N^2 , will occur as the parcel rises. Thus the Kuo hypothesis is not consistent with any form of cloud physics, but merely reflects the reasonable intuition that rising air is cloudy.

In either model, if the growthrate Ω and cloud width "a" are plotted as functions of the intercloud spacing λ (figure 3.2a), one sees that the infinite wavelength mode grows the fastest, but all modes with $\lambda \geq 2N_c = 2R_{fr}$ have very similar structure. As the intercloud spacing increases, the cloud width expands slightly to a limiting value. The critical value of N_c^2 depends only weakly on N_d^2 (figure 3.2b), and when $N_c^2 = N_d^2$, the critical value $N_{co}^2 = 14.23$ is about twice that needed to induce moist convection in a cloudy atmosphere of stratification $-N_c^2$ (which is $27/4$). At larger N_c^2 (figure 3.3) the clouds narrow down, reflecting the narrower preferred scale of pure moist convection, and secondary modes corresponding to clouds with several updrafts appear, albeit with lower growthrates. These I will discuss in section 3.4.

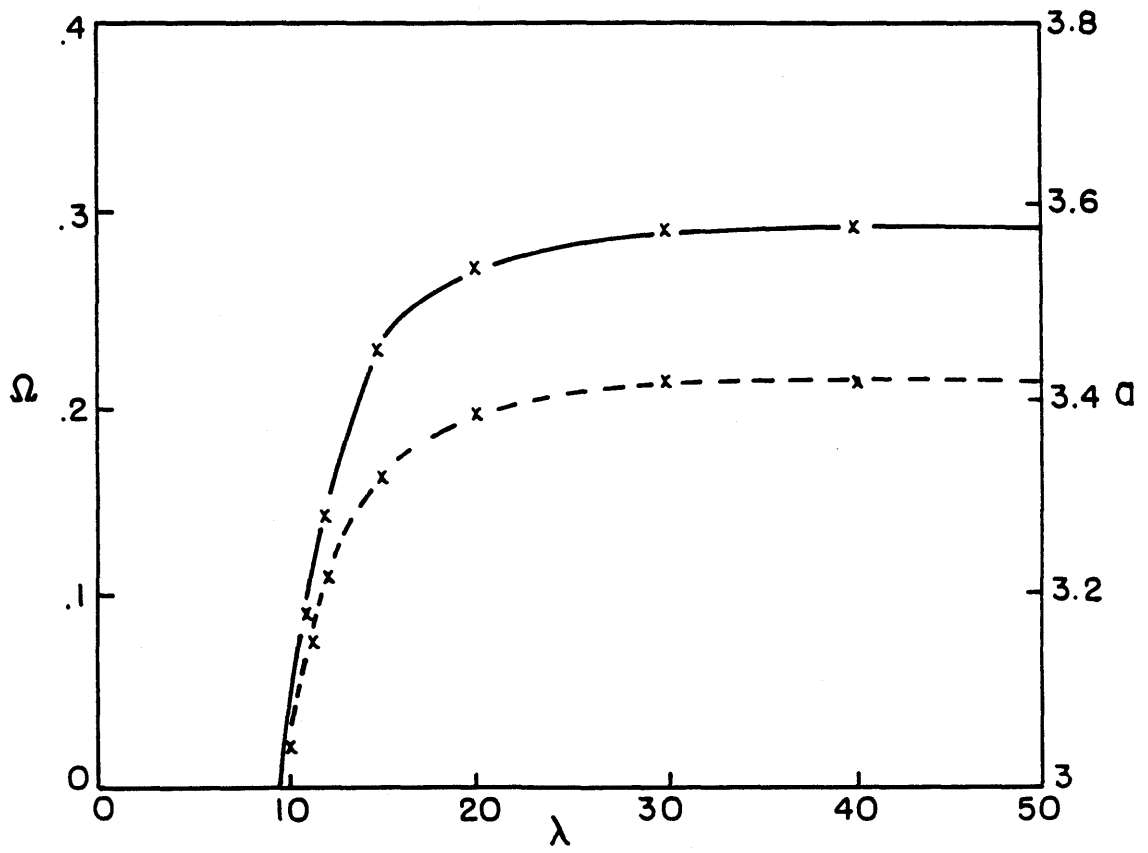


Figure 3.2a

Growthrate Ω (solid) and cloudwidth a (dashed) as a function of
 cloud spacing λ ($N_d^2 = N_c^2 = 20$)

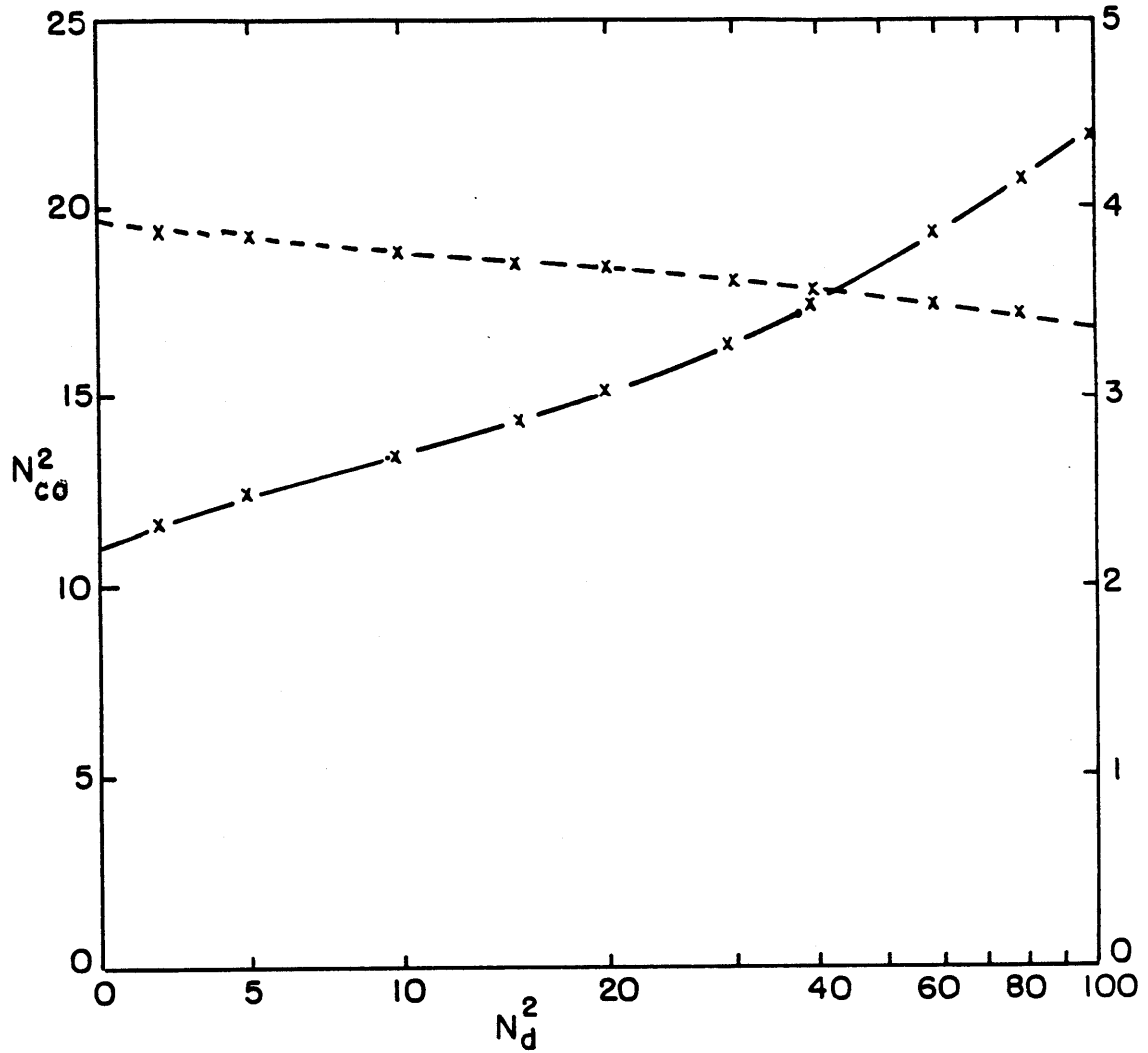


Figure 3.2b

The dependence of the marginal cloud Rayleigh number (solid) and the cloudwidth a_c (dashed) on N_d^2

3.3 Cylindrically Symmetric Moist Convection

Since there is a strong asymmetry between up and downward motions in moist convection, one might expect a cylindrical cloud, which has more room for downwelling around its perimeter, to have different stability properties from a "line" cloud such as discussed in section 3.2. In fact, I will show that a cylindrical cloud surrounded by an infinite expanse of clear air is distinctly more unstable than its two-dimensional analogue due to the slower downward velocities required in the stable dry air. This conclusion was reached also by Lilly (1960), Yamasaki (1972) in his modification of Kuo's model, as well as by numerous numerical studies such as those of Murray (1970) and Soong and Ogura (1973).

For three dimensional moist convection the "linearized" equations of motion in a nonrotating reference frame are (from 2.3.1-4, 2.3.24),

$$(3.3.1a) \quad (\partial_t - \nabla^2)\tilde{u} = -\tilde{p}_x ,$$

$$(3.3.1b) \quad (\partial_t - \nabla^2)\tilde{v} = -\tilde{p}_y ,$$

$$(3.3.1c) \quad (\partial_t - \nabla^2)\tilde{w} = -\tilde{p}_z + \tilde{B} ,$$

$$(3.3.1d) \quad (\partial_t - \nabla^2)\tilde{B}_\ell = \Gamma\tilde{w} ,$$

$$(3.3.1e) \quad \tilde{u}_x + \tilde{v}_y + \tilde{w}_z = 0 .$$

Using $\frac{\partial}{\partial x}$ (3.3.1a) + $\frac{\partial}{\partial y}$ (3.3.1b) and continuity, u and v can be eliminated:

$$(3.3.1f) \quad (\partial_t - \nabla^2)(-\tilde{w}_z) = -(\tilde{p}_{xx} + \tilde{p}_{yy}) .$$

To eliminate \tilde{p} , take $[\frac{\partial^2}{\partial x^2} + \frac{\partial^2}{\partial y^2}](3.3.1c) - \frac{\partial}{\partial z}$ (3.3.1f),

$$(3.3.1g) \quad (\partial_t - \nabla^2)\nabla^2\tilde{w} = \tilde{B}_{xx} + \tilde{B}_{yy} .$$

Using (3.3.1d) to eliminate w and remembering $\tilde{B} = -\frac{N^2}{T}\tilde{B}_\ell$,

$$(3.3.1h) \quad (\partial_t - \nabla^2)^2\nabla^2\tilde{B}_\ell = -N^2(\partial_x^2 + \partial_y^2)\tilde{B}_\ell .$$

For cylindrically symmetrical convection the liquid water potential L defined such that

$$(3.3.2) \quad \tilde{B}_\ell = \frac{1}{r} \frac{\partial L(r)}{\partial r} \cdot \sin z \cdot e^{\Omega t}$$

is introduced. Define

$$(3.3.3) \quad \Delta = r \frac{\partial}{\partial r} \frac{1}{r} \frac{\partial}{\partial r} .$$

Since

$$(3.3.4) \quad \nabla^2 \frac{1}{r} \frac{\partial F}{\partial r} = \left[\frac{\partial^2}{\partial z^2} + \frac{1}{r} \frac{\partial}{\partial r} r \frac{\partial}{\partial r} \right] \frac{1}{r} \frac{dF}{dr} \sin z = \frac{1}{r} \frac{d}{dr} [\Delta - 1] F ,$$

(3.3.1h) can be multiplied by r and integrated to obtain

$$(3.3.5) \quad (\Omega + 1 - \Delta)^2 (\Delta - 1)L = -N^2 \Delta L .$$

To solve (3.3.5) we first find eigenfunctions of Δ . The related problem

$$(3.3.6) \quad \frac{1}{r} \frac{d}{dr} r \frac{df}{dr} = \rho^2 f(r, \rho) ,$$

has solutions

$$(3.3.7) \quad f(r, \rho) = \begin{cases} J_0(i\rho r) & \text{regular as } r \rightarrow 0, \\ K_0(\rho r) & \text{regular as } r \rightarrow \infty. \end{cases}$$

Let $g(r, \rho)$ be defined by

$$(3.3.8) \quad f(r, \rho) = \frac{1}{r} \frac{dg}{dr} .$$

Clearly, g solves

$$(3.3.9) \quad \frac{1}{r} \frac{d}{dr} \left[r \frac{d}{dr} \frac{1}{r} \frac{dg}{dr} \right] = \frac{1}{r} \frac{d}{dr} [\rho^2 g] .$$

Multiplying by r and integrating it is clear $g(r, \rho)$ is the desired eigenfunction:

$$(3.3.10) \quad \Delta g = \rho^2 g .$$

Using the recursion relations (derived from [9.1.27] and [9.6.26] of Abramowitz and Stegun (1964))

$$(3.3.11a) \quad J_0 = \frac{1}{z} \frac{d}{dz} [zJ_1] ,$$

$$(3.3.11b) \quad K_0 = -\frac{1}{z} \frac{d}{dz} [zK_1] ,$$

$$(3.3.11c) \quad \frac{dJ_0}{dz} = -J_1 ,$$

$$(3.3.11d) \quad \frac{dK_0}{dz} = -K_1 ,$$

one sees that (7) and (8) imply

$$(3.3.12) \quad g(r, \rho) = \begin{cases} g_c(r, \rho) \equiv \frac{r}{\rho} J_1(i\rho r) & \text{regular as } r \rightarrow 0, \\ g_d(r, \rho) \equiv -\frac{r}{\rho} K_1(\rho r) & \text{regular as } r \rightarrow \infty. \end{cases}$$

From this point on the analysis parallels section (3.2). The most general solution regular at $r = 0$ and as $r \rightarrow \infty$ for a cloud of diameter "a" is, as before

$$(3.3.13) \quad L = \begin{cases} b_{1c} g_c(r, \rho_{1c}) + b_{2c} g_c(r, \rho_{2c}) + b_{3c} g_c(r, \rho_{3c}) & r < \frac{a}{2} , \\ b_{1d} g_d(r, \rho_{1d}) + b_{2d} g_d(r, \rho_{2d}) + b_{3d} g_d(r, \rho_{3d}) & r > \frac{a}{2} . \end{cases}$$

The solution must be matched across the cloud boundary $r = \frac{a}{2}$, where $N^2 \Delta L = N^2 r \frac{dB_l}{dr}$ has a discontinuity due to the jump in N^2 , which must be compensated by a discontinuity only in the highest derivative $\frac{d^6 L}{dr^6}$ on the left side of (3.3.5). Thus

$$(3.3.14) \quad L, \frac{1}{r} \frac{dL}{dr}, \Delta L, \frac{1}{r} \frac{d}{dr} \Delta L, \Delta^2 L, \frac{1}{r} \frac{d}{dr} \Delta^2 L \quad \text{are continuous} \\ \text{across } r = \frac{a}{2} .$$

These conditions lead to equations identical to (3.2.22)–(3.2.27) except for the new definitions of f and g . The vertical velocity and liquid buoyancy can be found, using (3.3.6) and (3.3.8), to satisfy the same equations as (3.2.29)–(3.2.30) with x replaced by r . But the new functional forms have a sizeable influence on the growth rate of the solutions (figure 3.3); the three dimensional modes become unstable at 30% lower values of N_c^2 for $N_c^2 = N_d^2$.

A look at the eigenfunction (figure 3.4) shows why this is so. For a given peak updraft speed, the downdraft speeds are uniformly smaller in the circular cloud since the whole annular region around the cloud can absorb the return flow. The fluid moves slower and warms less due to adiabatic compression, so the rate of work $-\tilde{w}\tilde{B}$ (excluding pressure work, which averages to zero along any closed steady parcel trajectory) which must be done on the stably stratified fluid to force it back down into the updraft is less in the circular case, allowing the buoyancy from latent heating to more efficiently cause kinetic energy growth.

Although it would be complex to prove, it is plausible to assume that a cylindrical updraft surrounded by an infinite expanse of drier downwelling air is the most unstable three-dimensional eigenmode. However, for simplicity I will continue to work in two dimensions. The features and equations of the theory I will develop could be carried over naturally (but with tedious algebra) to such three-dimensional modes without qualitative change.

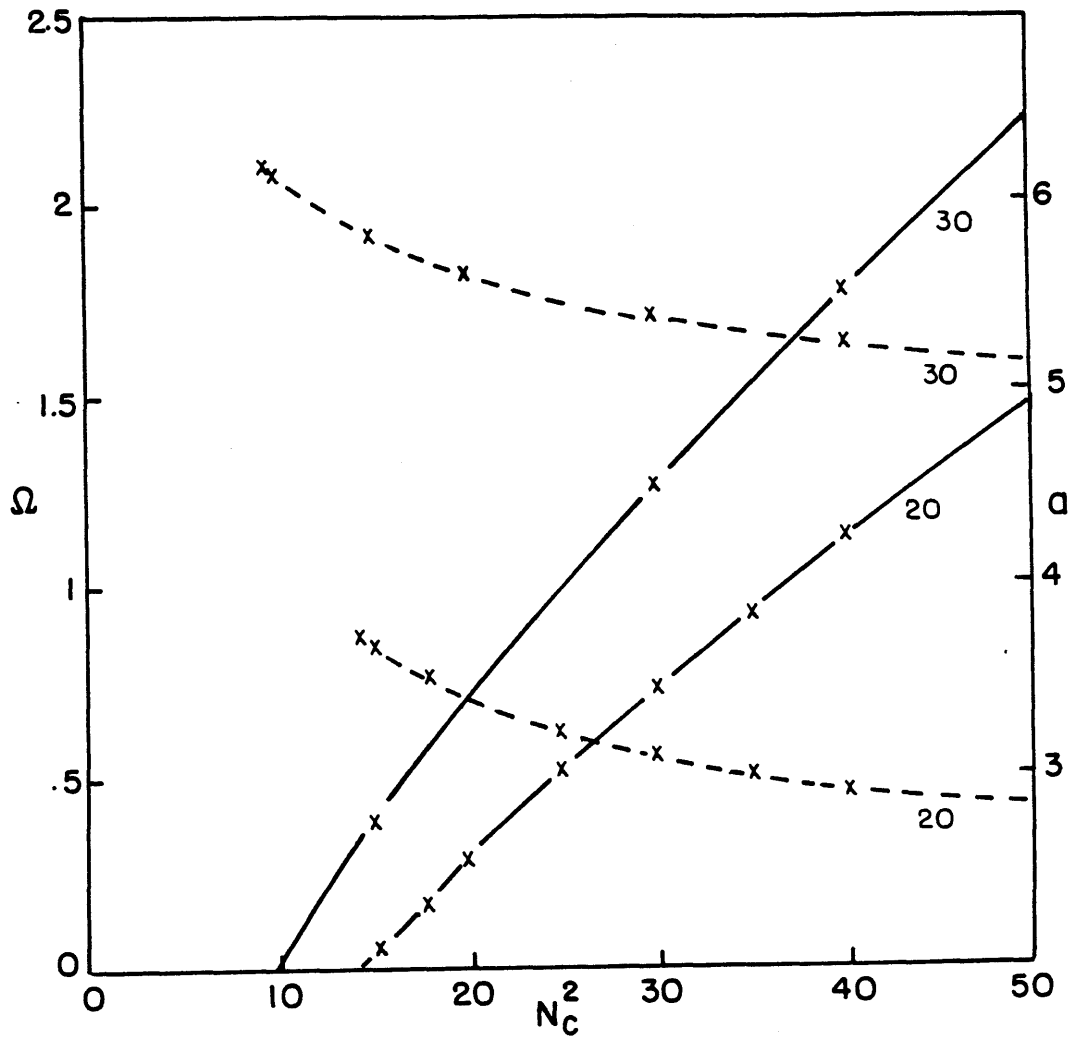


Figure 3.3

Growth rate (solid) and cloudwidth (dashed) when $N_c^2 = N_d^2$ as a function of N_c^2 for slab-symmetric (2D) and cylindrically symmetric (3D) clouds with infinite intercloud spacing.

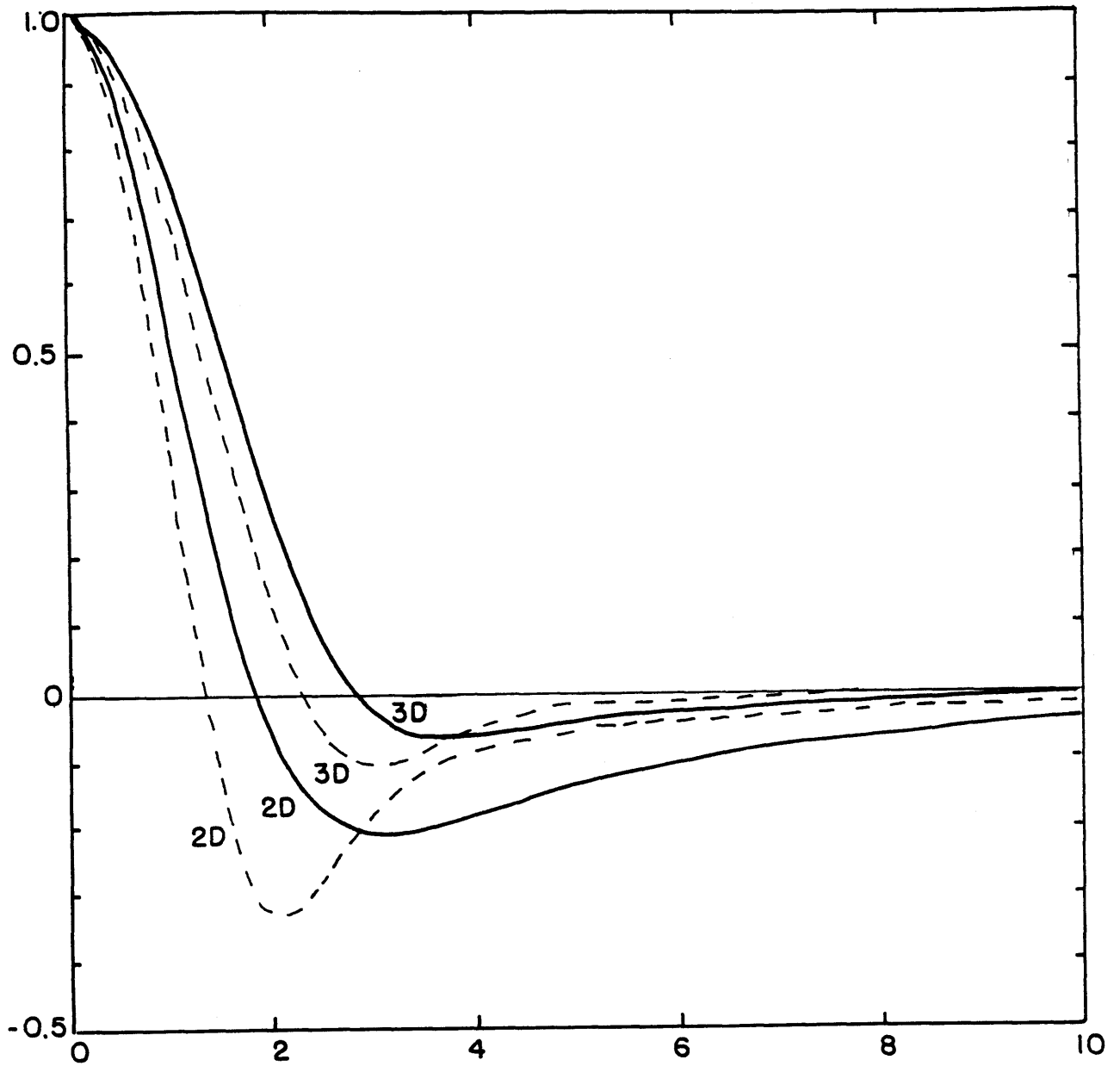


Figure 3.4

A comparison of B_l (solid) and ω (dashed) in the 2D and 3D eigenmodes when the cloud spacing is infinite

3.4 Multiple Updraft Solutions

Cumulus clouds are often observed to have a more complex pattern of updrafts and downdrafts than the solutions so far presented. One reason for this, cloudtop entrainment instability, was first proposed by Squires (1958). Unsaturated air above a cloud is mixed into cloudy air, evaporating some of its liquid water and cooling the mixture. If the air above the cloud is not too warm, the mixed parcel is denser than the cloudtop air and sinks. The densest mixture occurs when enough unsaturated air has been mixed in to just evaporate all the liquid water, so one might expect just saturated plumes to descend from cloudtop. If they entrain enough moist air to compensate for the evaporation of liquid water by adiabatic warming, they can remain dense and sink deep into the cloud. A model of this process based on self-similar plumes was proposed by Emanuel (1981).

In my theory, the physics of condensation, a crude version of turbulent mixing, and a source of cold, just-saturated air at "cloudtop" ($z = \pi$) are present, so one might ask whether the equations of section (3.2) admit solutions with analogous downdrafts. Indeed they can; there are growing eigensolutions with an arbitrary number of updrafts separated by such plumes. However, these solutions grow slower than single updraft eigenmodes, and even within the "linear" theory they are unstable to perturbations which alter the cloud boundaries and lead to the growth of single-updraft modes. Therefore, they are not selected while the "linear" dynamics predominate.

An identical procedure to that used to find the single updraft

solution recovers these modes. A three-updraft example is shown in figure 3.5. Each downdraft remains slightly saturated, fed by diffusion of water from the adjacent updrafts. The average motion on the cloud remains upward, condensing the liquid water necessary to sustain cloud, and outside the cloud the motions are little different from the single updraft mode. I could find no eigenmodes in which a cloud was split by unsaturated downdrafts.

The greater the number of updrafts, the more sluggishly the mode grows (figure 3.6). Since the equation (3.2.8) is nonlinear, it is also sensible to ask about the stability of its eigenmodes. It is remarkably simple to determine when an eigenmode is unstable to perturbations of the same vertical structure as it, for such perturbations leave the solution separable in z and obey an equation closely related to the equation for the eigenmode itself.

Consider a separable eigensolution \tilde{L}_0 of (3.2.14) with cloud width a_0 and growthrate Ω_0 with an infinitesimal perturbation $\epsilon\tilde{L}_1$ of the same vertical structure

$$(3.4.1a) \quad \tilde{L}(x, z, t) = A\{L_0(x)e^{\Omega_0 t} + \epsilon\hat{L}_1(x, t)\} \sin z ,$$

where A is chosen so there is no mean \hat{L}_1 , i.e.

$$(3.4.1b) \quad \int_{-\infty}^{\infty} \hat{L}_1(x, t) dx = 0 .$$

Let N_0 be the effective buoyancy frequency associated with this mode,

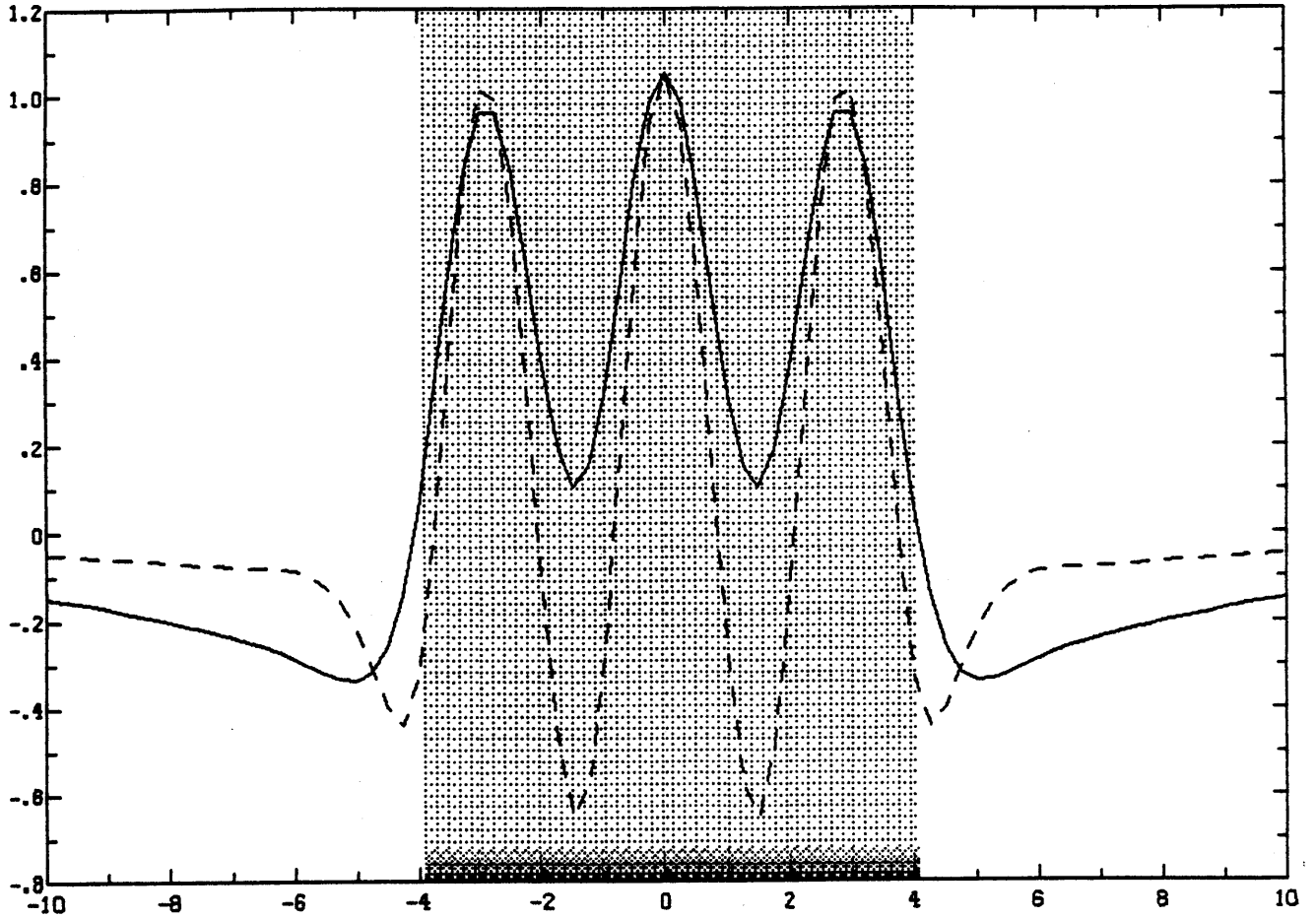


Figure 3.5

A three updraft eigenmode of infinite wavelength with $\Omega = .046$, $a = 8.12$.
 Ordinates at which cloud is present are shaded, B_l is solid, and ω is
 dashed. It is unstable to eigenperturbations of growthrates $\Omega_1 = 2.15$
 and $\Omega_2 = 1.48$.

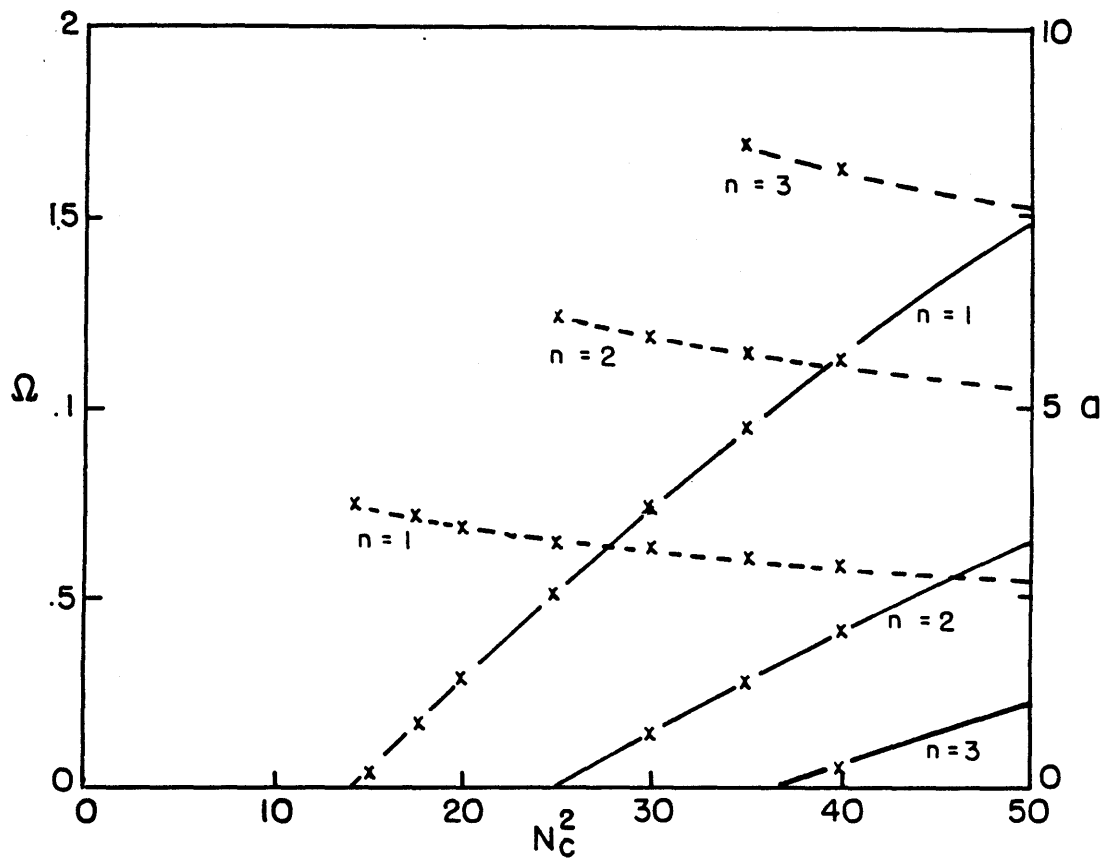


Figure 3.6

Growth rates (solid) and cloudwidths (dashed) for n-updraft modes,

$$n = 1, 2, 3, \text{ when } N_c^2 = N_d^2$$

$$(3.4.2a) \quad N_0^2 = \begin{cases} -N_c^2, & |x| < a_0/2, \\ N_d^2, & |x| > a_0/2, \end{cases}$$

where for simplicity I consider the case of infinite cloud separation, although this is not important to the argument. In section 3.7 I will show (see (3.7.8) and (3.7.12)) that

$$(3.4.2b) \quad (\partial_t + 1 - \partial_x^2)^2 (\partial_x^2 - 1) \hat{L}_1 = -N_0^2 \hat{L}_{1xx},$$

$$(3.4.2c) \quad \hat{L}_1, \hat{L}_{1x}, \hat{L}_{1xx}, \hat{L}_{1xxx}, \hat{L}_{1xxxx} \text{ are continuous across } x = \pm a_0/2,$$

$$(3.4.2d) \quad \hat{L}_{1xxxxx} \Big|_c^d = \Gamma \hat{L}_{1x}(\pm a_0/2, t).$$

($f|_c^d$ denotes the jump in f from the "cloudy" side of $\pm a_0/2$ to the "dry" side.)

If I define a first integral $\hat{\ell}$ of \hat{L}_1 ,

$$(3.4.3) \quad d\hat{\ell}_1/dx = \hat{L}_1(x, t),$$

and integrate (3.4.2b), I obtain (using (3.4.1b))

$$(3.4.4a) \quad (\partial_t + 1 - \partial_x^2)^2 (\partial_x^2 - 1) \hat{\ell}_1 = -N_0^2 \hat{\ell}_{1xx}, \quad \hat{\ell}(\pm \infty) \rightarrow 0.$$

The matching conditions (3.4.2c) and (3.4.2d) become:

(3.4.4b) $\hat{\ell}_{1x}, \hat{\ell}_{1xx}, \hat{\ell}_{1xxx}, \hat{\ell}_{1xxxx}, \hat{\ell}_{1xxxxx}, \hat{\ell}_1$ are continuous
across $x = \pm a_0/2$.

This is identical to the original equation (3.2.11) for \tilde{L}_0 except the cloud boundaries are fixed at $\pm a_0/2$ and can be solved in exactly the same way for "eigenperturbations"

$$(3.4.5) \quad \hat{\ell}_1(x,t) = \ell_1(x)e^{\Omega_1 t} ,$$

by just solving (3.2.27) for Ω_1 ,

$$(3.4.6) \quad \det M = 0 ,$$

with "a" fixed equal to a_0 . Since $\hat{L}_{1x} = \hat{B}_{\ell 1}(a_0/2, t)$ need not be zero, the cloud boundary begins to move.

For an n-updraft eigenmode, numerically one finds there are n-1 eigenperturbations with growthrates $\Omega_1 > \Omega_0$ to which the eigenmode is unstable, and numerical simulations of "separable" clouds evolving according to (3.2.11) show all such perturbations lead in the end to the formation of a single-updraft cloud. Although multiple-updraft modes can exist in this "linear" model, they will not be observed until it breaks down.

The single updraft still has perturbations with $\Omega_1 = \Omega_0$, its own growthrate, with

$$(3.4.7) \quad \hat{\ell}_1(x,t) = c_1 L_0(x)e^{\Omega_0 t}$$

$$(3.4.8) \quad \tilde{L}(x,z,t) = (L_0(x) + \epsilon c_1 \frac{dL_0}{dx}) e^{\Omega_0 t} \sin z$$

$$L_0(x + \epsilon c_1) e^{\Omega_0 t} \sin z ,$$

but these clearly represent translations of the eigenmode, not instabilities of it, and it is stable (for single-updraft modes of finite cloud spacing, stable to perturbations of the same wavelength) to perturbations with the same vertical structure as the eigenmode.

3.5 The Effects of Variable Viscosity

Cumulus convection in the atmosphere is turbulent. I have chosen for simplicity to model it as a laminar process in which the effective Rayleigh number is lowered by an increased eddy mixing.

Because kinetic energy can be created only within clouds, motions there (as I showed already) are more intense and turbulent. If an eddy diffusivity is associated with the unsteady part of the flow, then it should be much larger within the clouds.

In this section, I sidestep the problem of how this turbulence is generated and concentrate on the effects of its spatial inhomogeneity. A simple ad hoc model is to replace the constant eddy diffusivity ν by

$$\nu = \begin{cases} \nu_d^* \\ \nu_c^* \end{cases}, \text{ or after nondimensionalizing, } \begin{cases} \tau, \tilde{B}_\ell < 0, \\ 1, \tilde{B}_\ell > 0, \end{cases}$$

$$\tau = \frac{\nu_d^*}{\nu_c^*}.$$

Convection is destabilized at small τ due to the increased frictional deformation radius $R_{fr}^* \propto \nu_d^{*-1}$, which allows subsidence to spread out over a wider area and reduces the downward motion against the stable stratification. However, an interesting feature of the solution is a sharp viscous boundary layer which forms just outside the cloud edge.

From (2.3.24)-(2.3.28) the "linearized" vorticity and buoyancy equations are

$$(3.5.3a) \quad \left. \begin{aligned} (\partial_t - \nabla^2) \nabla^2 \tilde{\psi} &= \frac{N_c^2}{\Gamma} \tilde{B}_{\ell x} \\ (\partial_t - \nabla^2) \tilde{B}_{\ell} &= \Gamma \psi_x \end{aligned} \right\} \tilde{B}_{\ell} > 0 ,$$

$$(3.5.3c) \quad \left. \begin{aligned} (\partial_t - \tau \nabla^2) \nabla^2 \tilde{\psi} &= -\frac{N_d^2}{\Gamma} \tilde{B}_{\ell x} \\ (\partial_t - \tau \nabla^2) \tilde{B}_{\ell} &= \Gamma \psi_x \end{aligned} \right\} \tilde{B}_{\ell} < 0 .$$

I will seek eigenfunction solutions with stationary vertical cloud boundaries

$$(3.5.4) \quad \tilde{B}_{\ell}(x, z, t) = \frac{dL(x)}{dx} e^{\Omega t} \sin z ,$$

and eliminate ψ from the equations by integrating (3.5.3b) and (3.5.3d) and choosing integration constants such that

$$(3.5.5a) \quad \left. \begin{aligned} \psi &= \frac{1}{\Gamma} \left(\Omega + 1 - \frac{d^2}{dx^2} \right) L, \\ (\Omega + 1 - \frac{d^2}{dx^2})^2 \left(\frac{d^2}{dx^2} - 1 \right) L &= N_0^2 \frac{d^2 L}{dx^2}, \end{aligned} \right\} \tilde{B}_{\ell} > 0 \quad (x < a/2),$$

$$(3.5.5c) \quad \left. \begin{aligned} \psi &= \frac{1}{\Gamma} \left(\Omega + \tau \left[1 - \frac{d^2}{dx^2} \right] \right) L, \\ (\Omega + \tau \left[1 - \frac{d^2}{dx^2} \right])^2 \left(\frac{d^2}{dx^2} - 1 \right) L &= -N_d^2 \frac{d^2 L}{dx^2}, \end{aligned} \right\} \tilde{B}_{\ell} < 0 \quad (x > a/2).$$

The matching conditions are somewhat subtle. Let $f|_c^d$ denote the jump in a quantity f from the cloudy to the unsaturated ("dry")

air. The viscous stresses instantly remove any discontinuity in \underline{u} or \tilde{B}_ℓ ,

$$(3.5.6) \quad \tilde{u} \Big|_c^d = \tilde{w} \Big|_c^d = \tilde{B}_\ell \Big|_c^d = 0 .$$

Consider a pillbox of unit depth in y , infinitesimal thickness and height Δz centered on the vertical cloud boundary. Since there can be no net force on the pillbox,

$$(3.5.7a) \quad F_x \Big|_c^d = \Delta z \cdot \sigma_{xx} \Big|_c^d = 0 ,$$

$$(3.5.7b) \quad F_z \Big|_c^d = \Delta z \cdot \sigma_{xz} \Big|_c^d = 0 .$$

where $[\sigma_{ij}]$ is the stress tensor, in nondimensional form

$$(3.5.7c) \quad \sigma_{ij} = -p\delta_{ij} + \nu \left(\frac{\partial v_i}{\partial x_j} + \frac{\partial v_j}{\partial x_i} \right) ;$$

Consequently

$$(3.5.8a) \quad \sigma_{xx} \Big|_c^d = [-\tilde{p} + 2\nu\tilde{v}_x] \Big|_c^d = 0 ,$$

$$(3.5.8b) \quad \sigma_{xz} \Big|_c^d = \nu[\tilde{v}_z + \tilde{w}_x] \Big|_c^d = 0 .$$

The first condition involves the pressure change across the interface. To relate this to velocity changes, differentiate (3.5.8a) with respect to z and use mass conservation,

$$(3.5.9) \quad \tilde{p}_z \Big|_c^d = 2\nu\tilde{v}_{xz} \Big|_c^d = -2\nu\tilde{w}_{zz} \Big|_c^d .$$

Substitute this into the vertical momentum equation on both sides, remembering $\tilde{B} = 0$ on both sides of the interface,

$$(3.5.10) \quad (\partial_t - \nu\nabla^2)\tilde{w} \Big|_c^d = -\tilde{p}_z \Big|_c^d + \tilde{B} \Big|_c^d = 2\nu\tilde{w}_{zz} \Big|_c^d ,$$

$$(\partial_t - \nu[\partial_x^2 + 3\partial_z^2])\tilde{w} \Big|_c^d = 0 .$$

The last condition is that \tilde{B}_ℓ not accumulate in the pillbox. Its viscous flux must balance:

$$(3.5.11) \quad \nu\tilde{B}_{\ell x} \Big|_c^d = 0 .$$

The equations (3.5.6), (3.5.8b), (3.5.10), (3.5.11) generate six matching conditions on $L(x)$:

$$(3.5.12a) \quad \frac{1}{\Gamma}[\Omega + \nu(1 - \frac{d^2}{dx^2})]L \Big|_c^d = 0 ,$$

$$(3.5.12b) \quad \frac{1}{\Gamma}[\Omega + \nu(1 - \frac{d^2}{dx^2})]L_x \Big|_c^d = 0 ,$$

$$(3.5.12c) \quad L_x \Big|_c^d = 0 ,$$

$$(3.5.12d) \quad \frac{1}{\Gamma}\nu(\frac{d^2}{dx^2} + 1)[\Omega + \nu(1 - \frac{d^2}{dx^2})]L_x \Big|_c^d = 0 ,$$

$$(3.5.12e) \quad \frac{1}{\Gamma}[\Omega + \nu(3 - \frac{d^2}{dx^2})][\Omega + \nu(1 - \frac{d^2}{dx^2})]L_x \Big|_c^d = 0 ,$$

$$(3.5.12f) \quad \nu L_{xx} \Big|_c^d = 0 .$$

When $\tau = 1$ these conditions reduce to those used in section (3.2) and the solution proceeds similarly. The characteristic polynomial in the dry air is now

$$(3.5.8) \quad p_d(\pi) = [\Omega + \tau(1 - \rho^2)]^2[\rho^2 - 1] + N_d^2 \rho^2 = 0 ,$$

so its roots $\pm\rho_{d1}$, $\pm\rho_{d2}$, $\pm\rho_{d3}$ are altered. In particular, the root ρ_1 associated with the thermally driven eigenmode of (3.5.8) is much decreased to

$$(3.5.9) \quad \rho_1 \approx \frac{\Omega + \tau}{N_d}$$

because with less diffusion a heat source can induce convergence from a much wider region. L still has the form (3.2.21) but the matrix matching L between the dry and cloudy regions is altered to

(3.5.10a)

$$\begin{array}{l}
 \text{M} = \left[\begin{array}{cccccc}
 \gamma_{d1} g_{d1} & \gamma_{d2} g_{d2} & \gamma_{d3} g_{d3} & \gamma_{c1} g_{c1} & \gamma_{c2} g_{c2} & \gamma_{c3} g_{c3} \\
 \gamma_{d1} f_{d1} & \gamma_{d2} f_{d2} & \gamma_{d3} f_{d3} & \gamma_{c1} f_{c1} & \gamma_{c2} f_{c2} & \gamma_{c3} f_{c3} \\
 f_{d1} & f_{d2} & f_{d3} & f_{c1} & f_{c2} & f_{c3} \\
 \tau(\rho_{d1}^2 + 1)\gamma_{d1} g_{d1} & \tau(\rho_{d2}^2 + 1)\gamma_{d2} g_{d2} & \tau(\rho_{d3}^2 + 1)\gamma_{d3} g_{d3} & (\rho_{c1}^2 + 1)\gamma_{c1} g_{c1} & (\rho_{c2}^2 + 1)\gamma_{c2} g_{c2} & (\rho_{c3}^2 + 1)\gamma_{c3} g_{c3} \\
 \gamma_{d1}(\gamma_{d1} + 2\tau)f_{d1} & \gamma_{d2}(\gamma_{d2} + 2\tau)f_{d2} & \gamma_{d3}(\gamma_{d3} + 2\tau)f_{d3} & \gamma_{c1}(\gamma_{c1} + 2)f_{c1} & \gamma_{c2}(\gamma_{c2} + 2)f_{c2} & \gamma_{c3}(\gamma_{c3} + 2)f_{c3} \\
 \tau\rho_{d1}^2 g_{d1} & \tau\rho_{d2}^2 g_{d2} & \tau\rho_{d3}^2 g_{d3} & \rho_{c1}^2 g_{c1} & \rho_{c2}^2 g_{c2} & \rho_{c3}^2 g_{c3}
 \end{array} \right]
 \end{array}$$

where

$$\gamma_{ci} = [\Omega + (1 - \rho_{ci}^2)] / \Gamma$$

(3.5.10b)

$$\gamma_{di} = [\Omega + \tau(1 - \rho_{di}^2)] / \Gamma$$

One may now solve (3.5.26) and (3.2.27) exactly as before with this new matching matrix. In figure 3.7 the growthrate and cloudwidth are plotted as functions of τ for $N_d^2 = N_c^2 = 15$. As τ is lowered the growthrate increases and the cloud spreads out somewhat. A glance at how the eigenfunction $w(x)$ changes with τ (figure 3.8) shows the more even descent at low τ . However, a viscous boundary layer of thickness $O(\tau^{1/2})$ forms just outside the cloud. Just inside this boundary layer at the cloud edge descent still occurs due to evaporative cooling. Inside the cloud, the eigenfunction is changed almost imperceptibly.

Clearly, then, the most important effect of lowering the turbulent diffusivity of the dry air is to give each cloud a much wider region of influence,

$$R_{\text{descent}}^* = \begin{cases} R_{\text{fric}}^* = \frac{N_d^* h^3}{\pi v^*}, & \Omega \leq \tau \quad (\Omega^* \leq \frac{\pi^2 v_d^*}{h^2}) \\ R_t^* = \frac{N^* h^2}{\pi \Omega^*}, & \Omega \geq \tau \quad (\Omega^* \geq \frac{\pi^2 v_d^*}{h^2}), \end{cases}$$

(from (3.5.9)), while leaving its internal structure nearly unaltered. It is quite possible, if v_d^* is small, that the region of downwelling around a growing cloud is not limited by its frictional deformation radius, but by the distance R_t^* , which is the distance internal gravity waves, which have speed $N_d^2 h^* / \pi$, can propagate in an e-folding time for the convection. In the next section, I'll show that rotation can also influence the radius of downwelling.

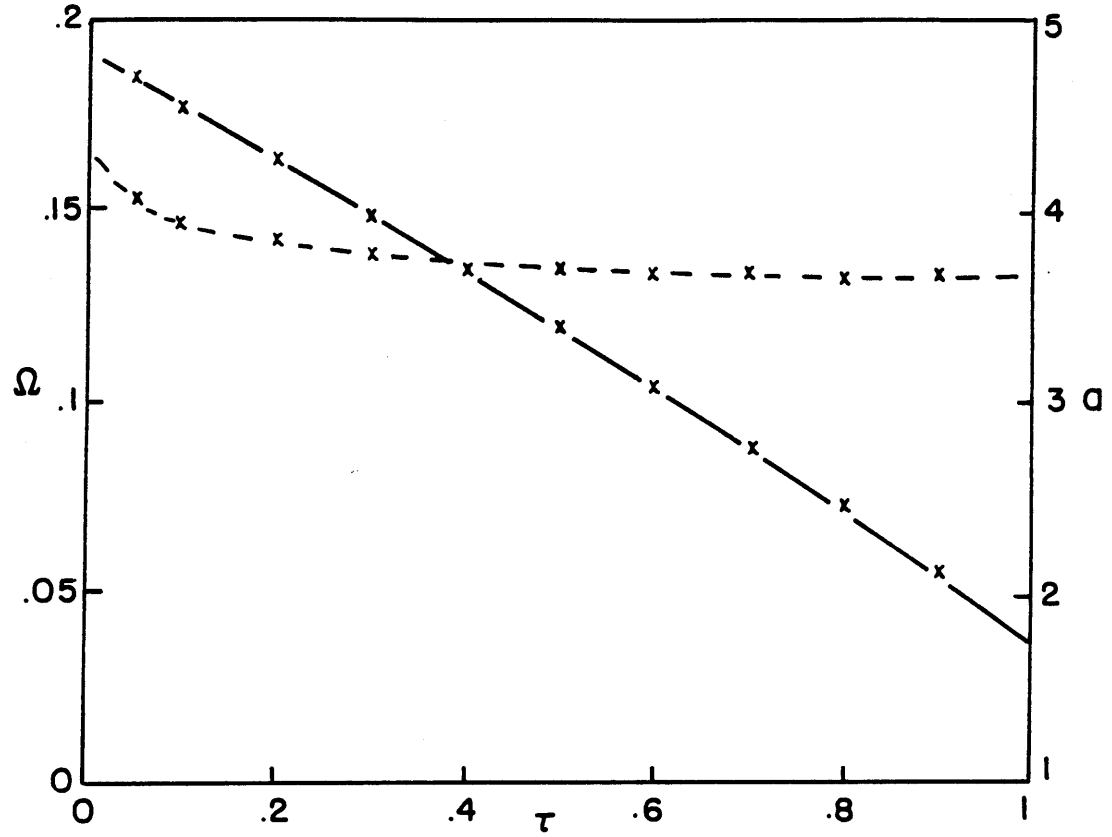


Figure 3.7

The growthrate Ω (solid) and cloudwidth a (dashed) as a function of the viscosity ratio τ when $N_c^2 = N_d^2 = 15$

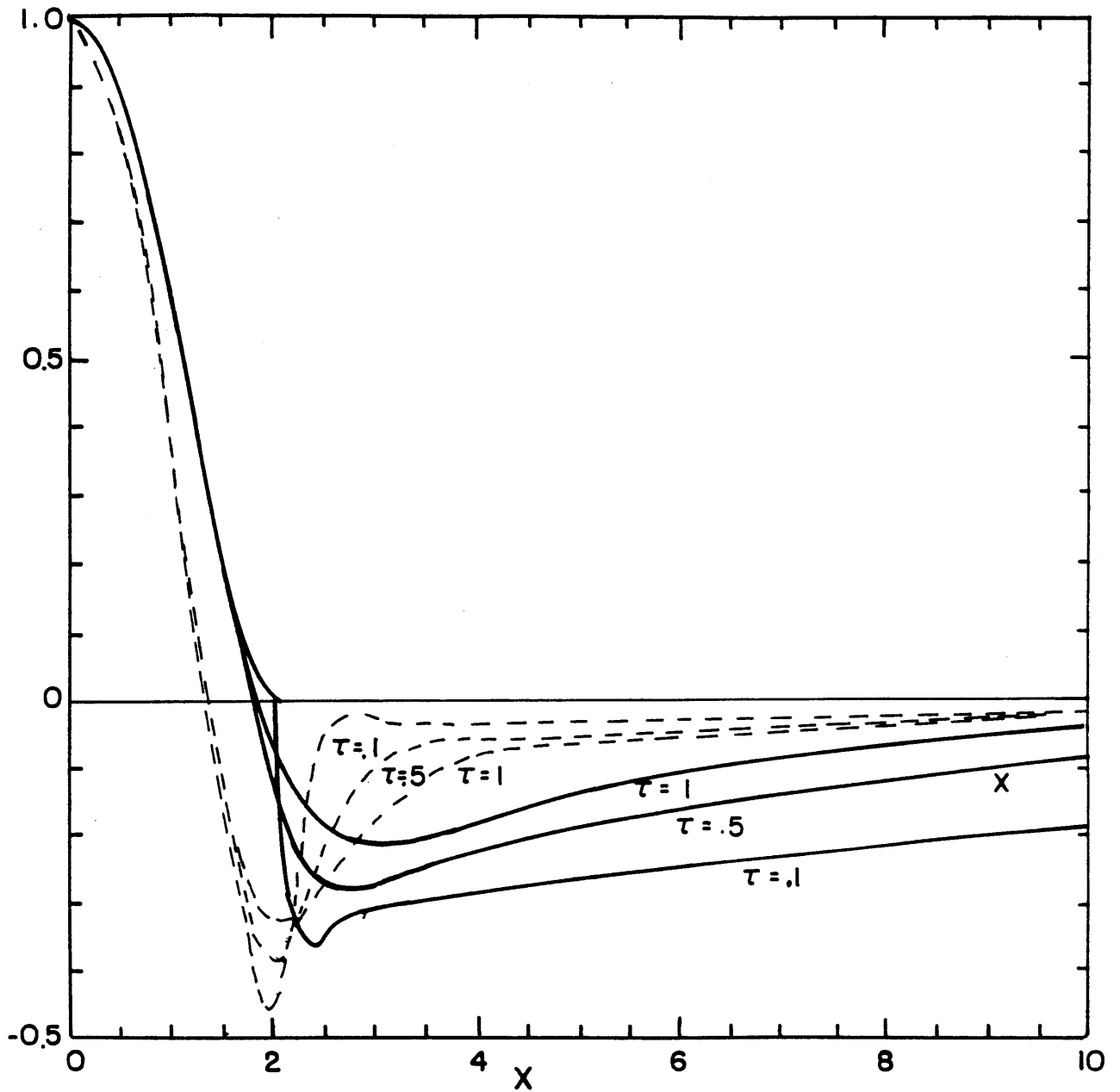


Figure 3.8

B_l (solid) and ω (dashed) for a range of viscosity ratios when $N_c^2 = N_d^2 = 15$.

3.6 Moist Convection with Rotation

In the earth's atmosphere, an air parcel typically moves through a convective cloud in a few minutes, over which time the earth's rotation has a negligible effect. Why worry about it, then?

Downwelling air is moving much more slowly and over a much wider expanse, especially if the clear air viscosity is small so the frictional deformation radius is large. It's possible for the earth's rotation to modify the flow of this air. In particular, one may ask: Can this make a finite intercloud spacing most unstable? I will show infinite cloud spacing is still preferred, but if the frictional deformation radius is larger than the Rossby radius

$$(3.6.1) \quad R_{\text{rot}}^* = N_d^* h^* / f^* \pi$$

the downwelling occurs primarily within a Rossby radius of the updraft.

In the region in which rotation might be important, motions are slow and almost horizontal and therefore are affected primarily by the vertical component ω_z^* of the earth's rotation $\underline{\omega}^*$, so to simplify the equations I ignore the horizontal component of rotation, which would just lead to a slight tilting of $O(\omega^*/N^*)$ of the updraft into the rotation axis; but would make the equations nonseparable.

Consider two-dimensional convection in a frame rotating with

$$\underline{\omega}^* = \omega_z^* \hat{k}$$

$$(3.6.2) \quad f^* = 2\omega_z^*, \quad (\text{nondimensionally, } f = f^* h^{*2} / \pi^2 v_c^*),$$

and assume $\nu_c = \nu_d$. Even though a large clear air viscosity decreases the lengthscale of convection and thus the effectiveness of rotation, by considering artificially large values of "f" we may qualitatively deduce its effects.

Absorbing the centrifugal acceleration into the gravitational acceleration and thus redefining the "vertical" axis slightly, one obtains nondimensionalized "linear" (i.e., no advective terms) equations (3.2.1)-(3.2.2) with Coriolis accelerations added for perturbations from an exactly saturated atmosphere, with the addition of an equation for the velocity along a roll $\tilde{v}(x,z)$:

$$(3.6.3a) \quad (\partial_t - \nabla^2)\nabla^2\tilde{\psi} = \tilde{B}_x - f\tilde{v}_z ,$$

$$(3.6.3b) \quad (\partial_t - \nabla^2)\tilde{B}_\ell = \Gamma\tilde{\psi}_x ,$$

$$(3.6.3c) \quad (\partial_t - \nabla^2)\tilde{v}_z = f\tilde{\psi}_{zz} ,$$

$$(3.6.3d) \quad \tilde{u}_z = \tilde{v}_z = \tilde{w} = \tilde{B}_\ell = 0 \quad \text{at } z = 0, \pi .$$

There are separable solutions with

$$(3.6.4) \quad \tilde{F}(x,z,t) = F(x) \cdot e^{\Omega t} \sin z ,$$

$$B_\ell(x) = dL/dx .$$

Integrating (3.6.3b) and noting $\tilde{\psi}_{zz} = -\tilde{\psi}$ in (3.6.3a),

$$(3.6.5a) \quad \left(\Omega + 1 - \frac{d^2}{dx^2}\right)L = \Gamma\psi \quad ,$$

$$(3.6.5b) \quad \left(\Omega + 1 - \frac{d^2}{dx^2}\right)v_z = -f\psi \quad ,$$

$$(3.6.5c) \quad \left(\Omega + 1 - \frac{d^2}{dx^2}\right)\left(\frac{v_z}{f} + \frac{L}{\Gamma}\right) = 0 \quad .$$

For a growing solution, as discussed in section 2.3, equations (2.3.19)-(2.3.25), I must take

$$(3.6.6) \quad v_z = -fL/\Gamma \quad ,$$

which, when used with (3.6.5a) in (3.6.3a) produces a sixth order equation for $L(x)$ alone:

$$(3.6.7) \quad \left(\Omega + 1 - \frac{d^2}{dx^2}\right)^2 \left(\frac{d^2}{dx^2} - 1\right)L = -N^2 L_{xx} + f^2 L \quad ,$$

that is almost identical to the equation (3.2.14) derived in the absence of rotation. Since $L(x)$ is continuous across cloud edges, so is v_z . Consequently, the matching conditions remain the same as (3.2.12),

$$(3.6.8) \quad L, L_x, L_{xx}, \dots, L_{xxxxx} \quad \text{are continuous across} \quad L_x = 0,$$

and one proceeds exactly as in section (3.2) except that the characteristic polynomials are altered to

$$(3.6.9a) \quad p_c(\rho) = (\Omega + 1 - \rho^2)^2(\rho^2 - 1) - N_c^2 \rho^2 + f^2 = 0$$

$$(3.6.9b) \quad p_d(\rho) = (\Omega + 1 - \rho^2)^2(\rho^2 - 1) + N_d^2 \rho^2 + f^2 = 0 .$$

Solving (3.2.26) and (3.2.27) with these new characteristic polynomials for $N_d^2 = N_c^2$, I found the critical N_c^2 needed to trigger convection as a function of the nondimensionalized rotation f (figure 3.9); the small f ($\lesssim 1/10$) typical of the atmosphere raise the critical N_c^2 only $O(f^2)$. Plotting the growthrate as a function of the intercloud spacing λ , (figure 3.10), I found the maximum growthrate occurred at infinite λ and the growthrate decreased substantially when $\lambda \lesssim 4 \min [R_{\text{fric}}^*, R_{\text{rot}}^*]$.

To understand this, examine the root ρ_{d1} of $p_d(\rho)$ which determines the decay scale in the clear air of the thermal perturbations due to the cloud. Assuming

$$(3.6.10) \quad N_d \gg 1, f,$$

(3.6.9b) can be solved assuming $\rho_{d1} \ll 1$ to obtain

$$(3.6.11) \quad \rho_{d1} = \sqrt{(\Omega + 1)^2 + f^2} / N_d ,$$

which implies a dimensional decay scale

$$(3.6.12) \quad R_d^* = h / \rho_{d1} \pi = N_d^* h / \left\{ (\Omega^* + \frac{\pi^2 v_d^*}{h^2})^2 + f^{*2} \right\}^{1/2} \pi .$$

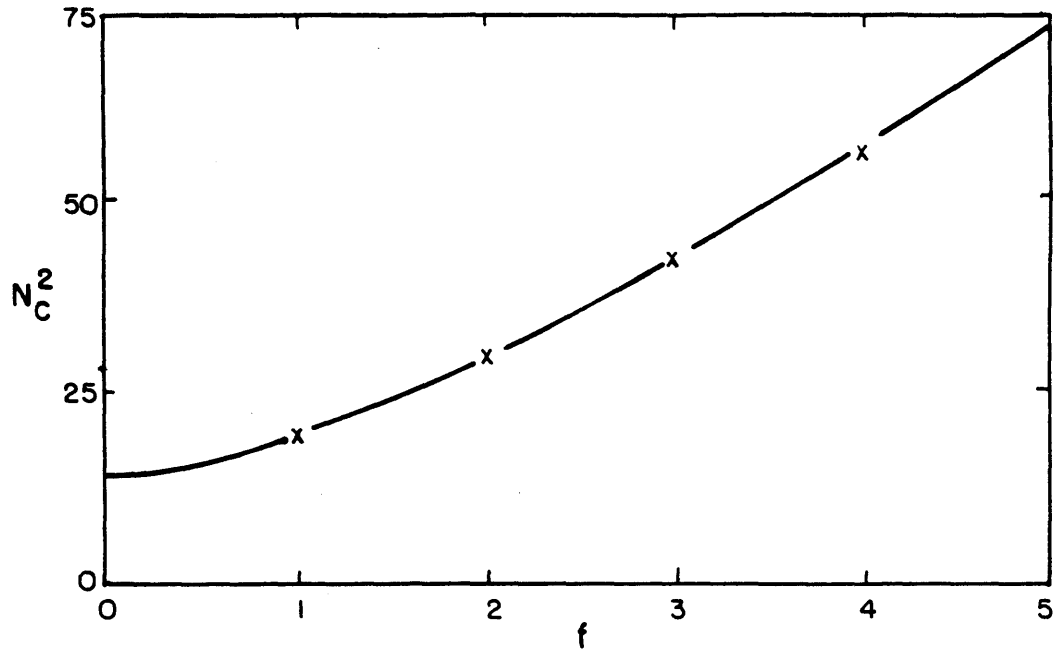


Figure 3.9

The critical N_c^2 needed to trigger convection in the presence of nondimensional rotation f about the vertical when $N_c^2 = N_d^2$.

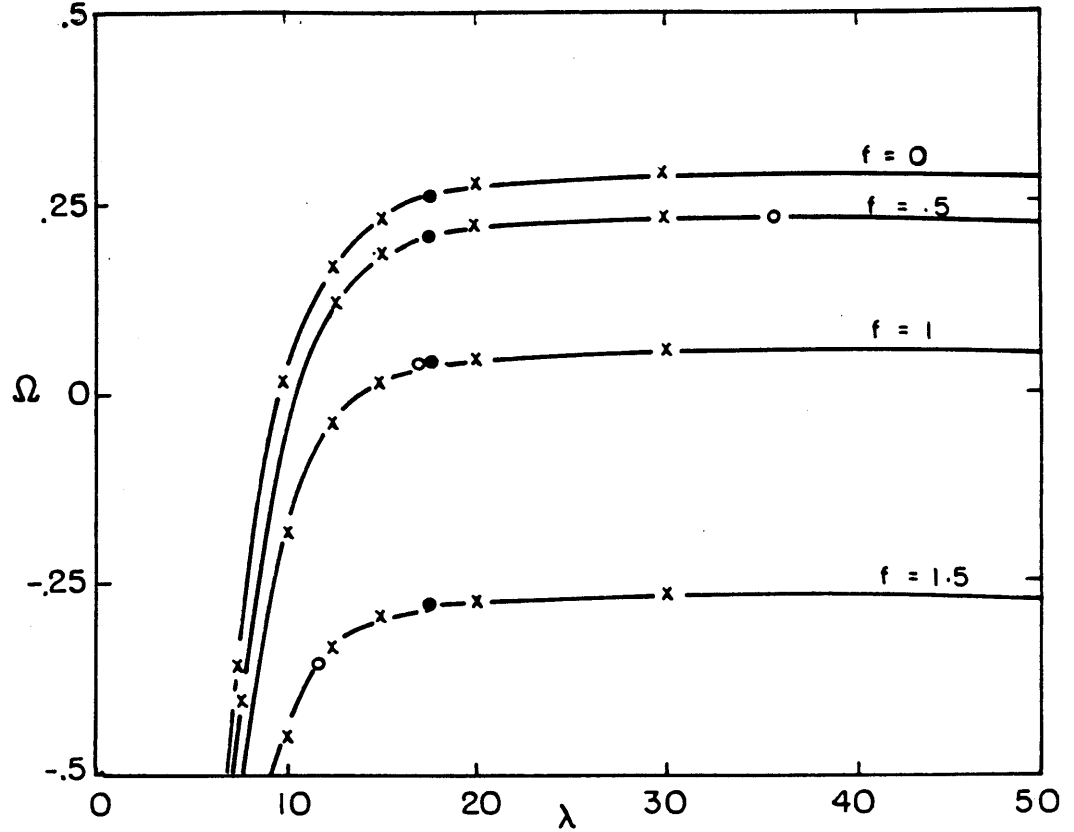


Figure 3.10

The growthrate Ω as a function of the intercloud spacing for $N_c^2 = N_d^2 = 20$ in the presence of varying levels of rotation. The open circle on each line is at $\lambda = 4N_d/f$, proportional to the Rossby radius, while the black circles are at $\lambda = 4N_d$, proportional to the frictional deformation radius.

The three effects which compete to set the width of downwelling are nicely exhibited; one sees

$$(3.6.13) \quad R_d^* \approx \min [R_{\text{fric}}^*, R_{\text{rot}}^*, R_t^*] ;$$

clouds damp each other significantly when $\lambda \lesssim 4R_d^*$ and they start to enter the regions of downwelling induced by their neighbors. In the model just considered, I took v to be uniform, so the frictional deformation radius was smallest except for rotation rates much higher than that of the earth. However, in the real atmosphere, $v_d^* \ll v_c^*$ because turbulence is suppressed in the stably stratified dry air. Taking typical values $N_d^* = 10^{-2} \text{ s}^{-1}$, $v_d^* = 10 - 100 \text{ m}^2/\text{s}$, $h = 2 \text{ km}$, $f^* = 10^{-1} \text{ s}^{-1}$, $\Omega^* \gtrsim 10^{-3} \text{ s}^{-1}$ for boundary layer convection,

$$(3.6.14a) \quad R_{\text{fric}}^* = 25 - 250 \text{ km},$$

$$(3.6.14b) \quad R_{\text{rot}}^* = 60 \text{ km},$$

$$(3.6.14c) \quad R_t^* \gtrsim 6 \text{ km},$$

so rotation and especially rapid growth limit the extent of downwelling as much or more than turbulent mixing.

3.7 The Stability of Separable Eigenmodes

So far I've restricted attention to convection with separable vertical structure $\sin(z)$ and showed that the fastest growing mode consists of a cloud with a single updraft surrounded by an infinite region of downwelling. Integration of (3.2.11) forward in time from many initial conditions suggests (as the analysis of section (4.2) will show for widely spaced updrafts) that at large time this mode is always the asymptotic solution to the separated problem.

However, I haven't considered the possibility of exponentially growing modes with curved cloud edges which could grow faster than this separable mode. I do not believe such solutions to (3.2.1)-(3.2.4) exist, but this is extremely difficult to prove, requiring the solution of a two-dimensional free-boundary problem with an unknown eigenvalue, the growth rate. A first step is to show no such solutions exist adjacent to the separable mode.

I employ an interesting variational technique. I derive a linear equation for the evolution of small perturbations to the separable eigenmode and its variational formulation. This can be used to bound the growth rate of all perturbations whose vertical structure is not $\sin(z)$ below that of the separable mode; at large time they become negligible to it. Therefore, the single updraft separable mode is stable to all small perturbations on it and no faster growing modes with slightly curved boundaries can exist.

I look for solutions of (3.2.1)-(3.2.4) which are a normal mode \tilde{L}_0 plus a small perturbation $\epsilon \tilde{L}_1$,

$$(3.7.1a) \quad \tilde{L}(x, z, t) = \tilde{L}_0(x, z, t) + \epsilon \tilde{L}_1(x, z, t) + O(\epsilon^2)$$

$$(3.7.1b) \quad \tilde{L}_0(x, z, t) \equiv L_0(x) \sin z \cdot e^{\Omega_0 t} .$$

The boundaries of the resulting cloud are at

$$(3.7.2) \quad \alpha_{\pm}(z, t) = \pm(a_0/2) + \epsilon \alpha_{1\pm}(z, t) .$$

Since

$$\begin{aligned} 0 = B_{\rho}(\alpha_{\pm}, z, t) &= \tilde{L}_{0x}(\alpha_{\pm}, z, t) + \epsilon \tilde{L}_{1x}(\alpha_{\pm}, z, t) , \\ &= \epsilon \alpha_1 \tilde{L}_{0xx}(\pm(a_0/2), z, t) + \epsilon \tilde{L}_{1x}(\pm(a_0/2), z, t) + O(\epsilon^2), \\ (3.7.3) \quad \alpha_{1\pm}(z, t) &= - \frac{\tilde{L}_{1x}(\pm(a_0/2), z, t)}{\tilde{L}_{0xx}(\pm(a_0/2), z, t)} \end{aligned}$$

In (3.7.3) one sees how movement of the cloud boundary is related to the perturbation. How does this movement influence the boundary conditions? As in the case in which the cloud had vertical boundaries, L and its first five normal and tangential derivatives are continuous across the cloud edge, so in particular

$$(3.7.4) \quad \tilde{L}, \tilde{L}_x, \tilde{L}_{xx}, \dots, \tilde{L}_{xxxxx} \text{ are continuous across } \alpha_{\pm} .$$

Rather than working with a free boundary, I translate these conditions into effective jumps of L and its derivatives between the solutions

inside and outside (continuously extended if necessary) at $\pm a_0/2$.

Let this jump be denoted

$$(3.7.5) \quad f \Big|_c^d = f_d\left(\frac{a_0}{2}, z, t\right) - f_c\left(\frac{a_0}{2}, z, t\right) .$$

Taylor expand (3.7.4):

$$(3.7.6) \quad \frac{\partial^n(\tilde{L}_0 + \epsilon \tilde{L}_1)}{\partial x^n}\left(\frac{a_0}{2}, z, t\right) \Big|_c^d + \alpha_{1\pm} \frac{\partial^{n+1} \tilde{L}_0}{\partial x^{n+1}}\left(\frac{a_0}{2}, z, t\right) \Big|_c^d = O(\epsilon^2), \quad 0 \leq n \leq 5.$$

Now, from (3.2.14),

$$(3.7.7a) \quad \frac{\partial^6 \tilde{L}_0}{\partial x^6} \Big|_c^d = -(N_c^2 + N_d^2) \frac{\partial^2 \tilde{L}_0}{\partial x^2}\left(\frac{a_0}{2}, z, t\right) = -\Gamma \frac{\partial^2 \tilde{L}_0}{\partial x^2}\left(\frac{a_0}{2}, z, t\right) ,$$

$$(3.7.7b) \quad \frac{\partial^n \tilde{L}_0}{\partial x^n} \Big|_c^d = 0, \quad 0 \leq n \leq 5,$$

so, substituting (3.7.3) into (3.7.6)

$$(3.7.8a) \quad \frac{\partial^5 \tilde{L}_1}{\partial x^5} \Big|_c^d = \Gamma \alpha_{1+} \tilde{L}_{0xx}\left(\frac{a_0}{2}, z, t\right) = -\tilde{\Gamma} \tilde{L}_{1x}\left(\frac{a_0}{2}, z, t\right) ,$$

$$(3.7.8b) \quad \frac{\partial^n \tilde{L}_1}{\partial x^n} \Big|_c^d = 0, \quad 0 \leq n \leq 4.$$

Having established the matching conditions, I round out the problem by noting that, since $\tilde{L}_0 + \epsilon \tilde{L}_1$ and \tilde{L}_0 both obey (3.2.8), and except within $O(\epsilon)$ of $\pm a_0/2$, both have the same N^2 , which for the infinite wavelength separable eigenmode is

$$(3.7.9a) \quad N^2 = N_0^2 \cong \begin{cases} -N_c^2 & |x| < a_o/2, \\ N_d^2 & |x| > a_o/2, \end{cases}$$

I can subtract to find

$$(3.7.9b) \quad (\partial_t - \nabla^2)^2 \nabla^2 \tilde{L}_1 = -N_0^2 \tilde{L}_{1xx}.$$

Unlike (3.2.8), (3.7.8) and (3.7.9) are linear equations for \tilde{L}_1 so I can break \tilde{L}_1 into its separable components.

$$(3.7.10a) \quad \tilde{L}_1 = \sum_{n=1}^{\infty} \hat{L}_{1n}(x,t) \sin nz,$$

$$(3.7.10b) \quad \hat{L}_{1n} = \frac{2}{\pi} \int_0^{\pi} \tilde{L}_1(x,z,t) \sin nz \, dz.$$

Integrating (3.7.9) with $\sin nz$ and using the boundary conditions

$$(3.7.11) \quad \tilde{L}_1 = \tilde{L}_{1zz} = \tilde{L}_{1zzzz} = 0,$$

one obtains

$$(3.7.12) \quad (\partial_t + n^2 - \partial_x^2)^2 (\partial_x^2 - n^2) \hat{L}_{1n} = -N_0^2 \hat{L}_{1xx},$$

together with the matching conditions (3.7.8) with \tilde{L}_1 replaced by \hat{L}_{1n} . There is a discrete spectrum of exponentially growing solutions and a continuous spectrum of viscously damped modes. The fastest growing discrete mode will dominate the large-time behavior, so let

$$(3.7.13) \quad \hat{L}_{1n} = L_{1n}(x)e^{\Omega_n t} + \text{slower growing part} .$$

Clearly, Ω_n satisfies

$$(3.7.14) \quad (\Omega_n + n^2 - \partial_x^2)^2 (\partial_x^2 - n^2) L_{1n} = -N_0^2 L_{1nxx}$$

with matching conditions (3.7.8) on L_{1n} .

Rather than explicitly finding Ω_n (which is not analytically possible) I seek a bound upon it by formulating (3.7.14) variationally. Integrate (3.7.14) with $L_1(x)$, assuming $L_{1n}(x)$ is localized around the cloud so

$$(3.7.15) \quad L_{1n}(x) \rightarrow 0 \quad \text{as } x \rightarrow \pm\infty ,$$

and use (3.7.8). After several integrations by parts

$$(3.7.16a) \quad 0 = - \int_{-\infty}^{\infty} dx L_{1n}(x) [(\Omega_n + n^2 - \partial_x^2)^2 (\partial_x^2 - n^2) L_{1n}(x)] \\ + N_0^2 L_{1n}(x) L_{1nxx} \\ = (\Omega_n + n^2)^2 n^2 \int_{-\infty}^{\infty} L_{1n}^2 dx + (\Omega_n + n^2)(\Omega_n + 3n^2) \int_{-\infty}^{\infty} L_{1nx}^2 dx \\ + (2\Omega_n + 3n^2) \int_{-\infty}^{\infty} L_{1nxx}^2 dx + \int_{-\infty}^{\infty} N_0^2 L_{1nx}^2 dx + N_0^2 L_{1n} L_{1nx} \Big|_{-a_0^-/2}^{-a_0^+/2} \\ + N_0^2 L_{1n} L_{1nx} \Big|_{a_0^-/2}^{a_0^+/2} + L_{1n} L_{1nxxxxx} \Big|_{-a_0^-/2}^{-a_0^+/2} + L_{1n} L_{1nxxxxx} \Big|_{-a_0^-/2}^{-a_0^+/2} .$$

Although L_{1n} and L_{1nx} are continuous across $\pm a_0/2$, N_0^2 has a jump of $\pm \Gamma$, while L_{1nxxxx} has a jump of $\mp \Gamma L_{1nx}$. Therefore, the boundary terms cancel to yield

$$(3.7.16b) \quad 0 = I(L_{1n}) = I_0(L_{1n}) + 2I_1(L_{1n})\Omega_n + I_2(L_{1n})\Omega_n^2,$$

where $I(L_{1n})$ is the integral in (3.7.16a) and

$$(3.7.16c) \quad I_0(L_{1n}) = n^6 \int_{-\infty}^{\infty} L_{1n}^2 dx + 3n^4 \int_{-\infty}^{\infty} L_{1nx}^2 dx + 2n^2 \int_{-\infty}^{\infty} L_{1nxx}^2 dx \\ + \int_{-\infty}^{\infty} L_{1nxxxx}^2 dx - \int_{-\infty}^{\infty} N_0^2 L_{1nx}^2 dx$$

$$(3.7.16d) \quad I_1(L_{1n}) = n^4 \int_{-\infty}^{\infty} L_{1n}^2 dx + 2n^2 \int_{-\infty}^{\infty} L_{1nx}^2 dx + \int_{-\infty}^{\infty} L_{1nxx}^2 dx > 0$$

$$(3.7.16e) \quad I_2(L_{1n}) = n^2 \int_{-\infty}^{\infty} L_{1n}^2 dx + \int_{-\infty}^{\infty} L_{1nx}^2 dx > 0$$

The variation of $I(L_{1n})$ over functions which satisfy the matching conditions (3.7.8) and decay as $x \rightarrow \pm\infty$ is easily calculated to be zero, iff L_{1n} satisfies (3.7.14),

$$(3.7.17) \quad \delta I(L_{1n}) = 0 \quad \text{for a solution of (3.7.14).}$$

Together, (3.7.16) and (3.7.17) allow me to recast (3.7.14) to write the true growthrate as the minimum of a functional $\Omega^*(L_{1n})$. For any admissible trial function, solve (3.7.16a) for Ω_0^* , discarding the negative root.

$$(3.7.18) \quad \Omega_n^* \equiv \frac{-I_1 + (I_1^2 - I_0 I_2)^{1/2}}{I_2} .$$

Now when L_{1n} is a solution of (3.7.14), $\Omega_n = \Omega_n^*(L_{1n})$. Thus at that point (3.7.17) implies

$$(3.7.19) \quad \delta I_0 + 2\delta I_1 \Omega_n^* + \delta I_2 \cdot \Omega_n^{*2} = 0 .$$

However, since Ω_n^* is defined so that for any L_{1n}

$$(3.7.20) \quad I_0 + 2I_1 \Omega_n^*(L_{1n}) + I_2 \Omega_n^{*2}(L_{1n}) = 0 ,$$

when L_{1n} is varied,

$$(3.7.21) \quad \delta I_0 + 2\delta I_1 \Omega_n^* + \delta I_2 \cdot \Omega_n^{*2} + \delta \Omega_n^* [2I_1 + 2I_2 \Omega_n^*] = 0 .$$

Since $2I_1 + 2I_2 \Omega_n^* > 0$ when $\Omega_n = \Omega_n^* > 0$, (3.7.19) can be subtracted from (3.7.21) to get

$$(3.7.22) \quad \delta \Omega_n^* = 0$$

for any solution of (3.7.14); the true growth rate is an extremum (in fact a maximum) of Ω_n^* over all functions $L_{1n}(x)$ which satisfy the boundary and matching conditions.

I would now like to show Ω_n is a decreasing function of n , so that modes of increasing oscillatory vertical structure $\sin(nz)$ grow

increasingly slowly. To do this, pick any admissible trial function, and for the moment, regard n as a continuous variable, calculating how Ω^* varies with n . Glancing back at (3.7.16c) - (3.7.16e),

$$(3.7.23) \quad \frac{\partial I_0}{\partial n}, \frac{\partial I_1}{\partial n}, \frac{\partial I_2}{\partial n} > 0$$

so

$$(3.7.24) \quad \frac{\partial I_0}{\partial n} + 2\Omega^* \frac{\partial I_1}{\partial n} + \Omega^{*2} \frac{\partial I_2}{\partial n} > 0, \quad \Omega^* > 0 .$$

We are finding the larger root of an upward-bending parabola which is rising higher as n increases, so Ω^* decreases with n . To show this formally, differentiate (3.7.20) with respect to n ,

$$(3.7.25) \quad \frac{\partial I_0}{\partial n} + 2\Omega^* \frac{\partial I_1}{\partial n} + \Omega^{*2} \frac{\partial I_2}{\partial n} + 2 \frac{\partial \Omega^*}{\partial n} (I_1 + \Omega^* I_2) = 0 .$$

Since $I_1 + I_2 \Omega^* = (I_1^2 - I_0 I_2)^{1/2} > 0$, (3.7.23b) shows

$$(3.7.26) \quad \frac{\partial \Omega^*}{\partial n} < 0,$$

so for any trial function $L_1(x)$

$$(3.7.27) \quad \Omega_1^*(L_1) > \Omega_2^*(L_1) > \Omega_3^*(L_1) \dots$$

so the maximum value of Ω_1^* must be larger than the maximum of $\Omega_2^*, \Omega_3^*, \dots$. But these maxima, from our variational principle (3.7.22) are just the true growth rates, so

$$(3.7.28) \quad \Omega_0 = \Omega_1 > \Omega_2 > \Omega_3 \dots$$

Thus the fastest growing perturbations are those with vertical structure $\sin(z)$ which leave the cloud boundary vertical and the solution separable, and are governed by (3.2.11). As shown in section 3.5, these modes have $\Omega_1 = \Omega_0$ for a single updraft mode only for perturbations which represent translations in x of the original eigenmode. Non-trivial perturbations all grow less fast than the eigenmode.

3.8 A Variational Principle and the Nonexistence of Oscillatory Modes

Even though even small perturbations from an exactly saturated static state of the atmosphere are governed by a nonlinear equation, variational principles for several kinds of potential eigenmodes can be found. In this section, I show by such means that there are no growing travelling wave solutions, nor any growing oscillatory solutions. Since squall lines and thunderstorms in the atmosphere are often observed not to travel with the mean wind, this strongly indicates rain is very important in their dynamics. It also shows there is no linear "wave-CISK" possible, i.e. no self-exciting gravity wave of wavelength many times the inter-cloud spacing which relies on the fact that convection can generate kinetic energy (and perhaps feed it into the wave) even though the horizontally averaged stratification is stable.

Firstly, I derive a variational principle for steadily growing eigenmodes, not necessarily separable in x and z ,

$$(3.8.1) \quad \tilde{L} = \tilde{L}(x, z)e^{\Omega t} .$$

Multiplying (3.2.8) by $-\tilde{L}$ (with ∂_t replaced by the real growth rate Ω), averaging over all space using the operator $\langle \rangle$ defined by (2.3.20), and integrating by parts using (3.2.9),

$$(3.8.2) \quad I(\tilde{L}) = -\langle \tilde{L} \{ (\Omega - \nabla^2)^2 \nabla^2 \tilde{L} + N^2 \tilde{L}_{xx} \} \rangle = 0 ,$$

$$0 = \Omega^2 \langle (\nabla \tilde{L})^2 \rangle + 2\Omega \langle (\nabla^2 \tilde{L})^2 \rangle + \langle [\nabla(\nabla^2 \tilde{L})]^2 \rangle + \langle N^2 \tilde{L}_x^2 \rangle ,$$

where N^2 is

$$(3.8.3) \quad N^2 = \begin{cases} N_d^2 & \tilde{L}_x < 0, \\ -N_c^2 & \tilde{L}_x > 0. \end{cases}$$

Taking the variation of I with respect to all functions L satisfying the boundary conditions (3.2.9) at $z = 0$ and π which are continuously five times differentiable across $\tilde{L}_x = 0$ recovers the original equation (3.2.8) since, integrating by parts and using the continuity of $\tilde{L}, \dots, \tilde{L}_{xxxxx}$,

$$(3.8.4) \quad \begin{aligned} \delta I = I(L + \delta L) - I(L) &= \Omega^2 \langle 2\nabla(\delta\tilde{L}) \cdot \nabla\tilde{L} \rangle + 2\Omega \langle 2\nabla^2(\delta\tilde{L}) \nabla^2(\tilde{L}) \rangle + \\ &+ \langle 2\nabla(\nabla^2\tilde{L}) \cdot \nabla(\nabla^2\delta\tilde{L}) \rangle + \langle 2N_x^2 \tilde{L} \delta\tilde{L}_x \rangle \\ &= -2\Omega^2 \langle \delta\tilde{L} \nabla^2\tilde{L} \rangle + 4\Omega \langle \delta\tilde{L} \cdot \nabla^4\tilde{L} \rangle - 2 \langle \delta\tilde{L} \nabla^6\tilde{L} \rangle + \\ &+ \lim_{L \rightarrow \infty} \left\{ \iint_{L_x > 0} -2N_c^2 \tilde{L}_x \delta\tilde{L}_x + \iint_{L_x < 0} 2N_d^2 \tilde{L}_x \delta\tilde{L}_x \right\} \frac{1}{2\pi L} + \\ &+ o([\delta L]^2). \end{aligned}$$

The last term must be treated with care since N^2 is not a continuous function of \tilde{L}_x , so cannot directly be integrated by parts. However

$$\begin{aligned}
& \lim_{L \rightarrow \infty} \left\{ \iint_{L_x > 0} -2N_c^2 \tilde{L}_x \delta \tilde{L}_x + \iint_{L_x < 0} 2N_d^2 \tilde{L}_x \delta \tilde{L}_x \right\} \frac{1}{2\pi L} = \\
& = \lim_{L \rightarrow \infty} \left\{ \iint_{L_x > 0} 2N_c^2 \tilde{L}_{xx} \delta \tilde{L} + \iint_{L_x < 0} 2N_d^2 \tilde{L}_{xx} \delta \tilde{L} \right\} \frac{1}{2\pi L} - \sum_{\substack{\text{cloud} \\ \text{edges}}} \int_{L_x=0} [2N_c^2 \tilde{L}_x + 2N_d^2 \tilde{L}_x] \cdot \hat{x}_c \frac{1}{2\pi L} \\
& = - \langle 2N_c^2 \tilde{L}_{xx} \delta \tilde{L} \rangle ,
\end{aligned}$$

since the boundary terms vanish because $\tilde{L}_x = 0$ there (\hat{x}_c is the normal vector in the x direction pointing out of the cloud). It follows that

$$(3.8.5) \quad \delta I = -2 \langle \delta \tilde{L} \cdot \{ (\Omega - \nabla^2)^2 \nabla^2 \tilde{L} + N_c^2 \tilde{L}_{xx} \} \rangle + O((\delta \tilde{L})^2)$$

will vanish for all infinitesimal variations $\delta \tilde{L}$ iff (3.2.8) is satisfied.

If it is assumed

$$(3.8.6) \quad s \equiv N_c^2 / N_d^2$$

is fixed (although if N_c^2 or N_d^2 were fixed, analogous procedures would follow) then from (3.8.2), for the true solution,

$$(3.8.7) \quad N_c^2 = \frac{\Omega^2 \langle (\nabla \tilde{L})^2 \rangle + 2\Omega \langle (\nabla^2 \tilde{L})^2 \rangle + \langle [\nabla(\nabla^2 \tilde{L})]^2 \rangle}{\langle -(N_c^2 / N_d^2) \tilde{L}_x^2 \rangle} = \frac{I_1(\tilde{L})}{I_2(\tilde{L})}$$

However, since for this true solution,

$$(3.8.8a) \quad \delta I(\tilde{L}) = \delta I_1 - N_c^2 \delta I_2 = 0,$$

$$(3.8.8b) \quad \delta N_c^2 = \frac{\delta I_1}{I_2} - \frac{I_1 \delta I_2}{I_2^2} = \frac{1}{I_2} \{ \delta I_1 - N_c^2 \delta I_2 \} = 0 .$$

So N_c^2 is extremized (in fact, minimized) at the true eigenmode:

$$(3.8.9) \quad N_c^2 = \min_{\tilde{L}} \frac{\Omega^2 \langle (\nabla \tilde{L})^2 \rangle + 2\Omega \langle (\nabla^2 \tilde{L})^2 \rangle + \langle [\nabla(\nabla^2 \tilde{L})]^2 \rangle}{\langle -(N^2/N_c^2) \tilde{L}_x^2 \rangle}.$$

This allows a variational determination of the lowest N_c^2 at which growing modes of any growth rate Ω are possible and nicely shows how the solution is a compromise between smoothness, which reduces the numerator, and amplitude mainly in the unstable region $N^2 = -N_c^2$ inside the cloud, which increases the denominator.

A similar idea shows there are no growing, steadily translating wavelike solutions to (3.2.8),

$$(3.8.10) \quad \tilde{L} = e^{\Omega t} L(x-ct, z),$$

where Ω is again real. Such solutions obey

$$(3.8.11) \quad (\Omega - c\partial_x - \nabla^2)^2 \nabla^2 L = -N^2 L_{xx},$$

which when multiplied by L_x and integrated implies

$$(3.8.12) \quad 0 = \langle L_x (\Omega - c\partial_x - \nabla^2)^2 \nabla^2 L + N^2 L_x L_{xx} \rangle$$

$$= \Omega^2 \{ \langle L_x L_{xx} \rangle + \langle L_x L_{zz} \rangle \} - 2\Omega c \{ \langle L_x L_{xxx} \rangle + \langle L_x L_{xzz} \rangle \}$$

$$- 2\Omega \langle L_x (\partial_x^2 + \partial_z^2)^2 L \rangle + c^2 \langle (\partial_x^2 + \partial_z^2) L_{xx} \cdot L_x \rangle + 2c \langle (\partial_x^2 + \partial_z^2)^2 L_x \cdot L_x \rangle$$

$$+ \langle (\partial_x^2 + \partial_z^2) L \cdot L_x \rangle - \frac{1}{2\pi L} \sum_{\substack{\text{cloud} \\ \text{edges}}} \int_{L_x=0} (N_c^2 + N_d^2) L_x^2 dx.$$

All the terms with an odd number of derivatives inside an average can be integrated by parts into averages of perfect differentials which vanish, while the rest can be written

$$(3.8.13) \quad 2\Omega c \langle L_{xx}^2 + L_{xz}^2 \rangle + 2c \langle [(\partial_x^2 + \partial_z^2)L_x]^2 \rangle = 0 .$$

If $\Omega \geq 0$ so that the wave grows, either $c = 0$ or $L_x \equiv 0$ so there are no growing travelling wave solutions.

A similar technique rules out growing periodic oscillations of some period τ :

$$(3.8.14a) \quad \tilde{L}(x,z,t) = e^{\Omega t} L(x,z,t) ,$$

$$(3.8.14b) \quad L(x,z,t+\tau) = L(x,z,t) .$$

This time, L obeys

$$(3.8.15) \quad (\partial_t + \Omega - \nabla^2)^2 \nabla^2 L + N^2 L_{xx} = 0 .$$

Multiply by L_t and integrate over x,z , and a period in time, denoted by an over bar:

$$(3.8.16) \quad \bar{f} = \int_0^\tau \langle f(x,z,t) \rangle dt .$$

Then, integrating by parts in space (again the boundary term due to the discontinuity in N^2 vanishes)

$$\begin{aligned}
(3.8.17) \quad 0 &= \overline{L_t(\partial_t + \Omega - \nabla^2)^2 \nabla^2 L} + \overline{N^2 L_t L_{xx}} \\
&= \overline{L_t \nabla^2 L_{tt}} + \overline{2L_t(\Omega - \nabla^2) \nabla^2 L_t} + \overline{L_t(\Omega - \nabla^2)^2 \nabla^2 L} + \overline{N^2 L_t L_{xx}} \\
&= -\overline{\nabla L_t \cdot \nabla L_{tt}} - \overline{2[\Omega(\nabla L_t)^2 + (\nabla^2 L_t)^2]} - \overline{[(\Omega - \nabla^2) \nabla L] \cdot [(\Omega - \nabla^2) \nabla L_t]} \\
&\quad - \overline{N^2 L_t L_{xt}} .
\end{aligned}$$

The first and third terms are averages over a period of the perfect derivatives of periodic functions, so they vanish. Interchanging the order of integration in the last term,

$$\begin{aligned}
(3.8.18) \quad \overline{N^2 L_x L_{xt}} &= \int_0^\tau \langle N^2 L_x L_{xt} \rangle dt \\
&= \langle \int_0^\tau N^2 L_x L_{xt} dt \rangle .
\end{aligned}$$

The time integral can be divided into segments for which $L_x > 0$ and $L_x < 0$. The function L is periodic so either there is one segment, N^2 is constant, so the integral is the perfect time derivative of $\frac{1}{2} N^2 L_x^2$ averaged over a period, or there are several segments, and $L_x(x, z, t_0) = 0$ for some t_0 . Then

$$\begin{aligned}
(3.8.19) \quad \int_0^\tau N^2 L_x L_{xt} dt &= \int_{t_0}^{\tau+t_0} N^2 L_x L_{xt} dt \\
&= \sum_{\text{segments}} \frac{1}{2} N^2_{\text{segment}} \left\{ L_x^2 \Big|_{\text{segment end}} - L_x^2 \Big|_{\text{segment beginning}} \right\} \\
&= 0 ,
\end{aligned}$$

since $L_x = 0$ at the ends of a segment by definition. In either case, from (3.8.18),

$$(3.8.20) \quad \overline{N^2 L_x L_{xt}} = 0 ,$$

so from (3.8.17),

$$(3.8.21) \quad \overline{2 \Omega (\nabla L_t)^2 + (\nabla^2 L_t)^2} = 0 ,$$

which requires L_t be constant. Since L is periodic, the constant is zero, and

$$(3.8.22) \quad L \equiv 0 ,$$

so there are no growing periodic oscillations. The same argument with τ taken infinite establishes there are no exponentially growing aperiodic oscillations either.

This severely restricts the possible asymptotic states of the "linear" system at $t \rightarrow \infty$. Section 3.7 suggests that all of the eigenmodes have vertical cloud boundaries and are "separable." This section indicates that if clouds grow at all, their boundaries asymptote to fixed positions. Numerical experiments and the upcoming results of chapter four show that separable clouds do not coexist for infinite time. Symptotically, the only plausible state is a single isolated cloud such as described in section 3.2, surrounded by subsiding dry air.

3.9 A Summary of "Linear" Moist Convection

The study of small amplitude perturbations of an exactly saturated static atmosphere has led to several interesting results. The fastest growing solutions are isolated cylindrical clouds whose radius is almost equal to the depth of convection, surrounded by a broad area of subsidence exponentially decaying away from the cloud in a radius which is the minimum of the frictional, Rossby, and transient deformation radii. For a growing cloud, the transient deformation radius is smallest under conditions typical of boundary layer convection, but is still upward of 6 km.

Each cloud is centered on an updraft with evaporatively driven downdrafts near its edges. Clouds with several updrafts can grow, but are unstable to the growth of perturbations which in the end collect all the upward motion into a single updraft.

Arguments based on variational techniques show single-updraft clouds are stable to the growth of perturbations, and that convection cannot take the form of travelling waves or oscillations. This strongly suggests that almost any initial conditions will result in one isolated, single updraft cloud growing in place with vertical cloud boundaries.

However, moist convective updrafts are not infinitely far apart in deep moist convection even when little precipitation is falling. In the next chapter I will explore within this model the reasons why this can be so by extending this study to include a nonlinear equilibration of a field of growing cumuli, possibly in a region of large-scale vertical motion.

CHAPTER 4

The Interaction of Weakly Nonlinear Clouds
in Mean Vertical Motion

4.1 Introduction

The "linear" theory of moist convection explored in chapter 3 left some important questions unanswered. No mechanism for producing a finite intercloud spacing was found, so what is it that sets the horizontal distance between clouds? Often, large scale processes such as baroclinic instability, frontal uplifting, or nonuniform surface heating can induce a mean slow vertical motion. How does this influence the convection? As convection intensifies, the nonlinear advections of heat and water can be expected to stabilize the convection. How does this occur and what are the consequences for a field of clouds? Does this cause clouds to cluster as is often observed?

In this chapter I will derive equations for the amplitudes of weakly nonlinear, sparsely distributed clouds in the presence of a mean vertical motion induced by a slowly varying temperature perturbation of the lower boundary. To do this N_c^2 is reduced until the fastest growing linear mode grows at a very small rate $\mu \ll 1$, and $\mu^{1/2}$ is used as the basis of an asymptotic solution of the equations. In section 4.2 I sketch the method of the expansion, and in section 4.3 carry it out in detail to obtain evolution equations for the strength and position of each cloud. In section 4.4 I discuss the equilibrium solutions of these

equations and their stability. A minimum cloud spacing varying inversely with the linear growth rate and upward motion emerges. In section 4.5 I show that long-wavelength modulations of the cloud field are governed by a diffusion equation whose diffusivity is a function of the local cloud spacing, but is always positive when the minimum stable spacing is exceeded. While the situation discussed is highly idealized, the equations are quite interesting and may be generalizable to more realistic models of moist convection.

4.2 An Overview of the Asymptotic Expansion

When N_c^2 is close to its marginal value N_{co}^2 for any fixed N_d^2 , I can use Stewart-Watson expansion to perturb the marginal "linear" cloud eigenfunction to produce a solution of the non-linear problem. The same framework can handle the weak effects of widely spaced clouds on each other and of a mean vertical motion on each cloud.

I will consider the distinguished limit in which all these effects contribute roughly equally to the evolution of each cloud. Were $N_c^2 = N_{co}^2$, an infinitesimally weak isolated steady cloud of the form

$$(4.2.1a) \quad \tilde{B}_\ell(x, z, t) = AB_{\ell 1}(x) \sin z,$$

$$(4.2.1b) \quad \tilde{\Psi}(x, z, t) = A\psi_1(x) \sin z,$$

where $(B_{\ell 1}(x), \psi_1(x))$ is the neutral isolated cloud eigenfunction, could persist. If

$$(4.2.2) \quad N_c^2 = N_{c0}^2 + \mu, \quad \mu \ll 1,$$

an isolated cloud has a growthrate proportional to μ , while maintaining approximately the same horizontal structure. A field of such clouds embedded in a mean flow can approximately be represented (see figure 4.1)

$$(4.2.3a) \quad \begin{bmatrix} \tilde{B}_\ell(x, z, t) \\ \tilde{\psi}(x, z, t) \end{bmatrix} \approx \mu^{1/2} \sum_j A_j(\tau) \begin{bmatrix} \tilde{B}_{\ell 1}(x - x_j(\tau)) \\ \tilde{\psi}_1(x - x_j(\tau)) \end{bmatrix} \sin z + \begin{bmatrix} \tilde{B}_{\ell m} \\ \tilde{\psi}_m \end{bmatrix},$$

$$(4.2.3b) \quad \tau \equiv \mu t.$$

The j^{th} cloud has slowly varying amplitude $\mu^{1/2} A_j(\tau)$ and center $x_j(\tau)$. The factor $\mu^{1/2}$ is the characteristic amplitude at which nonlinear advections of heat and water, which are then $O(\mu)$, stabilize the mean profiles of temperature and water enough to counteract the $O(\mu)$ supercriticality of N_c^2 .

The cloud spacing

$$(4.2.4) \quad \Delta x_j(\tau) = x_{j+1}(\tau) - x_j(\tau)$$

must be large enough so that the subsidence

$$(4.2.5) \quad w_{j+1}(x_j) \propto \mu^{1/2} A_{j+1} \exp\{-\rho_{d1} \Delta x_j\}$$

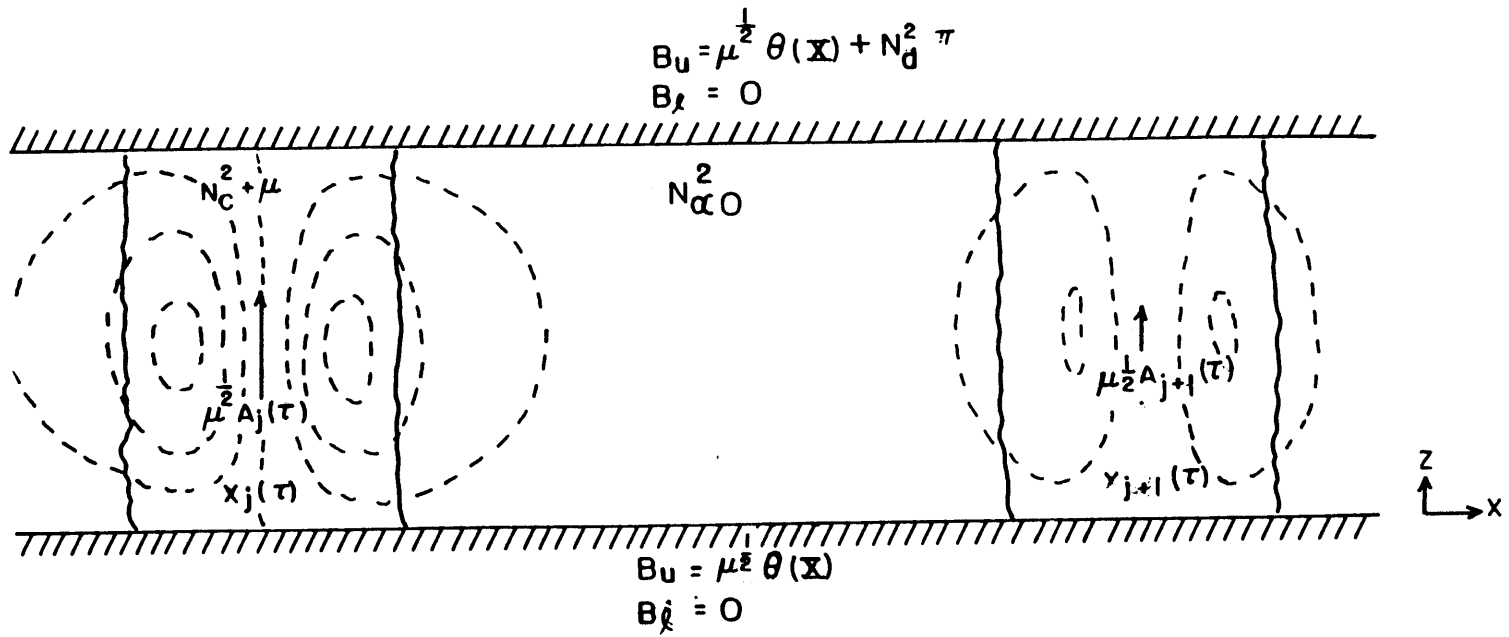


Figure 4.1

Part of a representative field of clouds considered in chapter four.
 Streamlines are dashed and the wavy solid lines are cloud boundaries.

induced by the $j+1$ 'st cloud near the j 'th cloud does not overwhelm the growth $\mu^{3/2}A_{j\tau}$ of the j 'th cloud. Therefore

$$(4.2.6a) \quad \zeta_j = \exp\{-\rho_{d1} \Delta x_j\} \lesssim O(\mu)$$

$$(4.2.6b) \quad \Delta x_j \gtrsim \frac{1}{\rho_{d1}} \{\log(1/\mu) + O(1)\} .$$

Notice that the effect of the $j+2$ 'nd cloud on the j 'th cloud is $O(\mu^2)$; only adjacent clouds affect each other significantly.

The mean vertical motion w_m , which I induce by slow horizontal variations of the temperature on the boundaries, must also not overwhelm $\mu^{3/2}A_{j\tau}$, so

$$(4.2.7) \quad w_m \lesssim O(\mu^{3/2}) .$$

I will now outline a consistent asymptotic theory which predicts the evolution of such a cloud field. The equations which are to be solved are (2.3.25-26):

$$(4.2.8a) \quad (\partial_t - \nabla^2) \nabla^2 \tilde{\psi} + J(\tilde{\psi}, \nabla^2 \tilde{\psi}) = \tilde{B}_x$$

$$(4.2.8b) \quad (\partial_t - \nabla^2) \tilde{B}_\ell + J(\tilde{\psi}, \tilde{B}_\ell) = \Gamma \tilde{\psi}_x$$

$$(4.2.8c) \quad J(\tilde{F}, \tilde{G}) \equiv \tilde{F}_x \tilde{G}_z - \tilde{G}_x \tilde{F}_z .$$

First, I generate a mean flow consistent with (4.2.7) by choosing

$$(4.2.9a) \quad \tilde{B}_{um} = \mu^{1/2} \theta(X) \quad \text{at } z = 0,$$

$$(4.2.9b) \quad \tilde{B}_{lm} = 0$$

$$(4.2.9c) \quad X = \mu^{1/2} x .$$

At the boundaries, small gradual variations of the temperature force upward motion near temperature maxima. Since the boundaries saturate the air with water, there will be more liquid water available to fuel convection in such regions. There are mean fields in the absence of convection:

$$(4.2.10a) \quad \tilde{B}_{lm}(x, z, t) = \mu^{3/2} \tilde{B}_{lm3}(X, z) \dots$$

$$(4.2.10b) \quad \tilde{B}_{um}(x, z, t) = \mu^{1/2} \theta(X) + \mu^{3/2} \tilde{B}_{um3}(X, z) + \dots$$

$$(4.2.10c) \quad \tilde{\psi}_m(x, z, t) = \mu \tilde{\psi}_{m2}(X, z) + O(\mu^2) \dots$$

where

$$(4.2.11a) \quad \tilde{\psi}_{m2}(X, z) = \theta_X(X) S_1(z),$$

$$(4.2.11b) \quad \begin{bmatrix} \tilde{B}_{lm3}(X, z) \\ \tilde{B}_{um3}(X, z) \end{bmatrix} = \theta_{XX}(X) S_2(z) \cdot \begin{bmatrix} -\Gamma_0 \\ N_d^2 \end{bmatrix},$$

$$(4.2.11c) \quad \Gamma_0 = N_d^2 + N_{co}^2,$$

and $S_1(z)$ and $S_2(z)$ are fixed polynomials in z derived in appendix II. To a good approximation,

$$(4.2.11d) \quad S_1(z) \approx S_2(z) \approx \frac{4}{\pi} \sin z .$$

Each variable is broken up into its mean value and a perturbation due to convection, denoted by a prime. The induced mean flow alters the formula (2.3.23) for \tilde{B} to

$$(4.2.12) \quad \tilde{B} = \begin{cases} \tilde{B}_{um} + \tilde{B}_{\ell m} + (N_c^2/\Gamma)\tilde{B}'_{\ell} , & \tilde{B}'_{\ell} + \tilde{B}_{\ell m} > 0 \\ \tilde{B}_{um} - (N_d^2/\Gamma)\tilde{B}'_{\ell} & , \quad \tilde{B}'_{\ell} + \tilde{B}_{\ell m} < 0 \end{cases}$$

In the neighborhood of the j 'th cloud, expand

$$(4.2.13a) \quad \tilde{\psi}' = \mu^{1/2}\tilde{\psi}'_1 + \mu\tilde{\psi}'_2 + \mu^{3/2}\tilde{\psi}'_3 \dots ,$$

$$(4.2.13b) \quad \tilde{B}_{\ell} = \mu^{1/2}\tilde{B}'_{\ell 1} + \mu\tilde{B}'_{\ell 2} + \mu^{3/2}\tilde{B}'_{\ell 3} \dots ,$$

where

$$(4.2.14a) \quad \tilde{\psi}'_1 = A_j(\tau)\psi_1(x - x_j(\tau)) \sin z ,$$

$$(4.2.14b) \quad \tilde{B}'_{\ell 1} = A_j(\tau)B_1(x - x_j(\tau)) \sin z .$$

The presence of the $j+1$ 'st and $j-1$ 'st clouds enforces boundary conditions

$$(4.2.15a) \quad \tilde{\psi}' \rightarrow \begin{cases} \mu^{1/2}A_{j+1}(\tau)\psi_1(x - x_{j+1}(\tau)) \sin z & \text{as } x \rightarrow \text{"}\infty\text{"} \\ & \text{(really } 1 \ll x - x_j \ll \Delta x_j) \\ \mu^{1/2}A_{j-1}(\tau)\psi_1(x - x_{j-1}(\tau)) \sin z & \text{as } x \rightarrow \text{"}\infty\text{"} \\ & (1 \ll x_j - x \ll \Delta x_{j-1}) , \end{cases}$$

and similarly for \tilde{B}'_ℓ .

Since $\psi_1(x_j - x_{j+1}) = O(\mu)$ these boundary conditions imply

$$(4.2.15b) \quad \tilde{\psi}'_1, \tilde{\psi}'_2 \rightarrow 0 \quad \text{as } x \rightarrow \pm\infty,$$

and similarly for $\tilde{B}'_{\ell 1,2}$, but affect $\tilde{\psi}'_3$ and $\tilde{B}'_{\ell 3}$.

Lastly, at every cloud boundary, the six independent matching conditions derivable from (2.3.28) are

$$(4.2.15c) \quad \tilde{B}_\ell, \tilde{B}_{\ell x}, \tilde{\psi}, \tilde{\psi}_x, \tilde{\psi}_{xx}, \tilde{\psi}_{xxx} \text{ are continuous across } \tilde{B}_\ell = 0.$$

The cloud boundaries are no longer at $x_j \pm a_0/2$; instead their positions must be expanded as

$$(4.2.16a) \quad \tilde{B}_\ell(x, z, t) = 0 \quad \text{at } x = \tilde{\alpha}_\pm(z, t),$$

$$(4.2.16b) \quad \tilde{\alpha}_\pm = \tilde{\alpha}_{0\pm} + \mu^{1/2} \tilde{\alpha}_{1\pm} + \mu \tilde{\alpha}_{2\pm} \dots,$$

$$(4.2.16c) \quad \tilde{\alpha}_{0\pm} = x_j(\tau) \pm a_0/2$$

The equations (4.2.10a-b) must now be solved accurate to successively higher powers of $\mu^{1/2}$ until solvability conditions determining the evolution of $A_j(\tau)$ and $x_j(\tau)$ emerge. I will outline the calculation here, leaving the calculation of specific terms for the next section.

$$(4.2.17a) \quad \nabla^4 \tilde{\psi}'_1 - (N_o^2/\Gamma_o) \tilde{B}'_{\ell 1x} = 0, \quad \underline{O(\mu^{1/2})}$$

$$(4.2.17b) \quad \nabla^2 \tilde{B}'_{\ell 1} + \Gamma_o \tilde{\psi}'_{1x} = 0,$$

$$(4.2.17c) \quad N_o^2 = \begin{cases} -N_{co}^2 & \tilde{B}'_{\ell 1x} > 0 \\ N_d^2 & \tilde{B}'_{\ell 1x} < 0 \end{cases}.$$

These equations, by the construction of N_{co} , indeed do have solutions of the form (4.2.14a,b), where from section 3.2 the neutral eigenmode can be written

$$(4.2.18a) \quad \psi_1(x) = \begin{cases} \sum_i \gamma_{ci} b_{ci} g(x, \rho_{ci}) & |x| \leq a_o/2, \\ \sum_i \gamma_{di} b_{di} g(x, \rho_{di}) & |x| \geq a_o/2, \end{cases}$$

$$(4.2.18b) \quad B_1(x) = \begin{cases} \sum_i b_{ci} f(x, \rho_{ci}) & |x| \leq a_o/2, \\ \sum_i b_{di} f(x, \rho_{di}) & |x| \geq a_o/2. \end{cases}$$

where the γ_{ci}, γ_{di} are defined as in (3.5.10b),

$$(4.2.18c) \quad \gamma_{c,di} = (1 - \rho_{c,di}^2)/\Gamma_o.$$

$$(4.2.19a) \quad \nabla^4 \tilde{\psi}'_2 - (N_o^2/\Gamma_o) \tilde{B}'_{\ell 2x} + \partial_z^4 \tilde{\psi}'_{m2} + \theta_x = J(\tilde{\psi}'_1, \nabla^2 \tilde{\psi}'_1), \quad \underline{O(\mu)}$$

$$(4.2.19b) \quad \nabla^2 \tilde{B}'_{\ell 2} + \Gamma_o \tilde{\psi}'_{2x} = J(\tilde{\psi}'_1, \tilde{B}'_{\ell 1}),$$

The mean fields, which persist in the absence of convection, obey

$$(4.2.20) \quad \partial_z^4 \tilde{\psi}_{m2} + \theta_X = 0 .$$

The remainder of the equation is solved in section 4.3 to obtain

$$(4.2.21) \quad \begin{bmatrix} \tilde{\psi}'_2 \\ \tilde{B}'_{\ell 2} \end{bmatrix} = A_j^2 \sin 2z \begin{bmatrix} \psi_2(\mathbf{x}) \\ B_2(\mathbf{x}) \end{bmatrix}$$

and the cloud boundary perturbations

$$(4.2.22) \quad \hat{\alpha}_{1\pm} = \pm A_j \alpha_1 \cos z .$$

$$\underline{O(\mu^{3/2})}$$

$$(4.2.23a) \quad \nabla^4 \tilde{\psi}'_3 - (N_o^2/\Gamma_o) \tilde{B}'_{\ell 3x} = J(\tilde{\psi}'_1, \nabla^2 \tilde{\psi}'_2) + J(\tilde{\psi}'_2, \nabla^2 \tilde{\psi}'_1) + \partial_\tau \nabla^2 \tilde{\psi}'_1 \\ + \left\{ \frac{N^2 - N_o^2}{\mu \Gamma_o} - \frac{N_o^2}{\mu \Gamma_o^2} (\Gamma - \Gamma_o) \right\} \tilde{B}'_{\ell 1x} \\ + J(\tilde{\psi}'_1, \tilde{\psi}'_{2mzz}) + J(\tilde{\psi}'_{2m}, \nabla^2 \tilde{\psi}'_1) ,$$

$$(4.2.23b) \quad \nabla^2 \tilde{B}'_{\ell 3} + \Gamma_o \tilde{\psi}'_{3x} = J(\tilde{\psi}'_1, \tilde{B}'_{\ell 2}) + J(\tilde{\psi}'_2, \tilde{B}'_{\ell 1}) + \partial_\tau \tilde{B}'_{\ell 1} \\ - \mu^{-1} (\Gamma - \Gamma_o) \tilde{\psi}'_{1x} + \partial_z^2 \tilde{B}'_{\ell m3} + \Gamma_o \tilde{\psi}'_{m2x} .$$

$\tilde{B}'_{\ell 3m}$ is determined from

$$(4.2.24) \quad \partial_z^2 \tilde{B}'_{\ell m3} = -\Gamma_o \tilde{\psi}'_{m2x} .$$

The mean fields enter to this order not only through their contribution to vorticity advection, but also implicitly by perturbing the cloud boundary, which is at

$$(4.2.25) \quad \tilde{B}_\ell = \tilde{B}'_\ell + \tilde{B}_{\ell m} = 0 .$$

At this order solvability conditions arise when the parts of $\tilde{\Psi}'_3$ and $\tilde{B}'_{\ell 3}$ proportional to $\sin(z)$ are matched across the cloud boundary, and these will be the goal of section 4.3. Their derivation is tremendously complicated, and the reader is urged to skip to section 4.4, where the resulting evolution equations for the cloud field are stated.

Given their underlying assumptions, these equations contain all of the physical effects modifying the growth rates at least $O(\mu)$. The shearing of the mean flow on each cloud at a rate $du_m/dz = O(\mu)$ reduces the growth rate by $O(\mu^2)$, a negligible effect, as do the nonlinear interactions of neighboring clouds. The three physical effects which are important are

- (1) The stabilization of a cloud by its own nonlinear buoyancy fluxes;
- (2) The moistening of the basic atmosphere by upward motion;
- (3) The two-fold competition of clouds with each other due to their linear interaction, first by competing for inflow air and second, suppressing each other by drying the environment through forced subsidence.

4.3 Derivation of the Amplitude Equations

In this section I will carry through the method outlined in section 4.2 to obtain equations for the slowly varying amplitude and position of each cloud and to examine the nonlinear modification of the structure of each cloud.

$O(\mu)$

To find the leading nonlinear corrections to the cloud structure, I must solve (4.2.19a,b). The solution can consistently be assumed to have the form (4.2.20). I first compute the Jacobians

$$(4.3.1a) \quad J(\tilde{\Psi}'_1, \nabla^2 \tilde{\Psi}'_1) = A_j^2 \sin 2z J_1(x - x_j(\tau)) ,$$

$$(4.3.1b) \quad J(\tilde{\Psi}'_1, \tilde{B}'_{\lambda 1}) = A_j^2 \sin 2z J_2(x - x_j(\tau)) .$$

From (4.2.14a,b), in the cloudy air,

$$(4.3.2) \quad J_{1c}(x) = \frac{1}{2} \sum_i \sum_j \gamma_{ci} \gamma_{cj} (\rho_{cj}^2 - 1) [f_c(x, \rho_{ci}) g_c(x, \rho_{cj}) - f_c(x, \rho_{cj}) g_c(x, \rho_{ci})] b_{ci} b_{cj} .$$

Noting that $\rho_{cj}^2 - 1$ can be rewritten as $-\gamma_{cj} \Gamma_o$ and using multiplication formulas from appendix II to write the products as sums of characteristic functions,

$$(4.3.3a) \quad J_{1c}(x) = \sum_i \sum_j \{ a_{11c}^{(i,j)} g_c(x, \rho_{ci} + \rho_{cj}) + a_{12c}^{(i,j)} g_c(x, \rho_{ci} - \rho_{cj}) \} ,$$

where

$$(4.3.3b) \quad a_{11c}^{(i,j)} = -(\Gamma_o/2)\gamma_{ci}\gamma_{cj}^2 \left\{ \frac{\rho_{ci} + \rho_{cj}}{2\rho_{cj}} - \frac{\rho_{ci} + \rho_{cj}}{2\rho_{ci}} \right\} b_{ci}b_{cj}$$

$$= -(\Gamma_o/4)\gamma_{ci}\gamma_{cj}^2 \frac{(\rho_{ci} + \rho_{cj})(\rho_{ci} - \rho_{cj})}{\rho_{ci}\rho_{cj}} b_{ci}b_{cj} ,$$

$$(4.3.3c) \quad a_{12c}^{(i,j)} = -(\Gamma_o/2)\gamma_{ci}\gamma_{cj}^2 \left\{ \frac{\rho_{ci} - \rho_{cj}}{2\rho_{cj}} - \frac{\rho_{ci} - \rho_{cj}}{2\rho_{ci}} \right\} b_{ci}b_{cj}$$

$$= -a_{11c}^{(i,j)} .$$

In the dry air, (4.3.3a) holds with subscript "c" replaced by "d" and

$$(4.3.4a) \quad a_{11d}^{(i,j)} = -(\Gamma_o/2)\gamma_{di}\gamma_{dj}^2 \frac{(\rho_{di} + \rho_{dj})(\rho_{di} - \rho_{dj})}{\rho_{di}\rho_{dj}} b_{di}b_{dj} ,$$

$$(4.3.4b) \quad a_{12d}^{(i,j)} = 0 .$$

Similarly,

$$(4.3.5a) \quad J_{2c}(x) = \frac{1}{2} \sum_i \sum_j \gamma_{ci} [f_c(x, \rho_{ci})f_c(x, \rho_{cj}) -$$

$$- \gamma_{cj}^2 g_c(x, \rho_{cj})g_c(x, \rho_{ci})] b_{ci}b_{cj} ,$$

$$= \sum_i \sum_j a_{21c}^{(i,j)} f_c(x, \rho_{ci} + \rho_{cj}) + a_{22c}^{(i,j)} f_c(x, \rho_{ci} - \rho_{cj}) ,$$

where

$$(4.3.5b) \quad a_{21c}^{(i,j)} = \frac{1}{4} \gamma_{ci} \frac{\rho_{ci} - \rho_{cj}}{\rho_{ci}}$$

$$(4.3.5c) \quad a_{22c}^{(i,j)} = \frac{1}{4} \gamma_{ci} \frac{\rho_{ci} + \rho_{cj}}{\rho_{ci}},$$

and in the dry air

$$(4.3.6a) \quad a_{21d}^{(i,j)} = \frac{1}{2} \gamma_{di} \frac{\rho_{di} + \rho_{dj}}{\rho_{di}},$$

$$(3.3.6b) \quad a_{22d}^{(i,j)} = 0$$

Consulting appendix IV, I can find particular inhomogeneous solutions in the cloudy and the dry air by substituting the a_1 's and a_2 's for the R_1 and R_2 of the appendix.

$$(4.3.7a) \quad \begin{aligned} \tilde{\psi}_{2c}(x) &= \sum_i \sum_j Q_1 \{ m_{11c}^{(i,j)} g_c(x, \rho_{ci} + \rho_{cj}) + m_{12c}^{(i,j)} g_c(x, \rho_{ci} - \rho_{cj}) \} \\ &= \sum_i \sum_j \{ \psi_{21c}^{(i,j)} g_c(x, \rho_{ci} + \rho_{cj}) + \psi_{22c}^{(i,j)} g_c(x, \rho_{ci} - \rho_{cj}) \}, \end{aligned}$$

$$(4.3.7b) \quad \begin{aligned} \tilde{\psi}_{2d}(x) &= \sum_i \sum_j Q_1 \{ m_{21d}^{(i,j)} g_d(x, \rho_{di} + \rho_{dj}) \} \\ &= \sum_i \sum_j \psi_{21d}^{(i,j)} g_d(x, \rho_{di} + \rho_{dj}). \end{aligned}$$

Since $\rho_i \pm \rho_j$ is never a characteristic root of $p_2(\rho)$, I have used (IV.3e) to eliminate the operator Q_1 in favor of new coefficients

$$(4.3.7c) \quad \psi_{21c}^{(i,j)} = m_{11c}^{(i,j)} / p_{c2}(\rho)$$

(likewise for the other coefficients).

The most general solution is of the form

$$(4.3.8a) \quad \psi_{2c}(x) = \psi_{2hc}(x) + \tilde{\psi}_{2c}(x) ,$$

$$(4.3.8b) \quad \psi_{2hc}(x) = \sum_i \gamma_{ci}^{(2)} b_{ci}^{(2)} g_c(x, \rho_{ci}^{(2)}) ,$$

and similarly in the dry air. To find the unknown coefficients $b_{ci}^{(2)}$ and $b_{di}^{(2)}$ I derive matching conditions at $x = \frac{1}{2}a_0$. The right cloud boundary $x = \tilde{\alpha}_+(z, \tau)$ is where

$$(4.3.9) \quad 0 = \tilde{B}_\rho(x, z, \tau) = \mu^{1/2} A_j B_1(x) \sin z + \mu A_j^2 B_2(x) \sin 2z + O(\mu^{3/2}) .$$

Recalling $\beta \equiv B_{1x}(\frac{1}{2}a_0)$ and Taylor-expanding about $x = a_0/2$,

$$(4.3.10a) \quad \tilde{\alpha}_+(z, \tau) = (a_0/2) + \mu^{1/2} \tilde{\alpha}_1(z, \tau) + O(\mu) ,$$

$$(4.3.10b) \quad \beta A_j \tilde{\alpha}_1 \sin z = -A_j^2 B_2(a_0/2) \sin 2z .$$

From (2.3.28), the appropriate nonlinear matching conditions are the same as for the "linear" problem, namely continuity of \tilde{B}_ρ and its first x -derivative and of $\tilde{\psi}$ and its first three x -derivatives. Using the jump notation (3.7.5), for any function continuous across the cloud boundary

$$(4.3.11) \quad \tilde{F}(x, z, \tau) = \mu^{1/2} \tilde{F}_1(x, z, \tau) + \mu \tilde{F}_2(x, z, \tau) \dots ,$$

the effective jump condition at $x = a_0/2$ is found by Taylor expansion to be

$$(4.3.12) \quad F_2 \Big|_c^d = -\alpha_1 \frac{\partial F_1}{\partial x} \Big|_c^d .$$

Now by construction

$$(4.3.13) \quad \nabla^4 \tilde{\psi}_1 \Big|_c^d = \tilde{\psi}_{1xxxx} \Big|_c^d = -\tilde{B}_x \Big|_c^d = - \left(-\frac{N_{do}^2}{\Gamma_o} - \frac{N_{co}^2}{\Gamma_o} \right) \tilde{B}_{\ell x}(a_0/2, z, \tau) \\ = \tilde{B}_{\ell x}(a_0/2, z, \tau),$$

so

$$(4.3.14) \quad \psi_2 \Big|_c^d = \psi_{2x} \Big|_c^d = \psi_{2xx} \Big|_c^d = \psi_{2xxx} \Big|_c^d - B_{\ell 2}(a_0/2) \\ = B_{\ell 2} \Big|_c^d = B_{\ell 2x} \Big|_c^d = 0 .$$

By splitting ψ_2 and $B_{\ell 2}$ into their homogeneous and inhomogeneous parts, matching conditions for the homogeneous solution are obtained which can be written in the manner of (IV.16) with

$$(4.3.15a) \quad \Delta_{ns}[\psi_{2h}] = \Delta_n^+[\psi_{2h}] = -\frac{d^{n-1}}{dx^{n-1}} \{ \check{\psi}_{2d}(x) - \check{\psi}_{2c}(x) \} \Big|_{x=\frac{1}{2}a_0} + \delta_{n4} B_{\ell 2} \left(\frac{a_0}{2} \right),$$

$$(4.3.15b) \quad \Delta_{na}[\psi_{2h}] = 0 .$$

and similarly for B_{2h} . The unknown coefficients $b_{ci}^{(2)}$ and $b_{di}^{(2)}$ can now be found from (IV.20) of the appendix.

$$\underline{O(\mu^{3/2})}$$

The leading nonlinear correction term could be found without imposing any conditions on the solution. To find such solvability conditions, I go one order further in the expansion and solve (4.2.23a,b) for the $\sin(z)$ components $\hat{\psi}_3(x, \tau)$ and $\hat{B}_{\ell 3}(x, \tau)$ of $\tilde{\psi}'_3$ and $\tilde{B}'_{\ell 3}$. Components of the right hand sides of (4.2.23a) proportional to higher harmonics do not lead to further conditions on the solution. Let

$$(4.3.16) \quad \hat{f}(x, t) = \frac{2}{\pi} \int_0^\pi \tilde{f}(x, z, \tau) \sin z \, dz$$

denote the $\sin(z)$ component of any function f . Then

$$(4.3.17a) \quad \nabla_1^4 \hat{\psi}_3 - \frac{Nc}{\Gamma_0} \hat{B}_{\ell 3x} = \hat{R}_{11} + \hat{R}_{12} + \hat{R}_{13} + \hat{R}_{14},$$

$$(4.3.17b) \quad \nabla_1^2 \hat{\psi}_3 + \Gamma_0 \hat{\psi}_{3x} = \hat{R}_{21} + \hat{R}_{22} + \hat{R}_{23},$$

where

$$(4.3.18a) \quad \hat{R}_{11} = \hat{J}(\tilde{\psi}'_1, \nabla^2 \tilde{\psi}'_2) + \hat{J}(\tilde{\psi}'_2, \nabla^2 \tilde{\psi}'_1),$$

$$(4.3.18b) \quad \hat{R}_{21} = \hat{J}(\tilde{\psi}'_1, \tilde{B}'_{\ell 2}) + \hat{J}(\tilde{\psi}'_2, \tilde{B}'_{\ell 1}),$$

are nonlinear self-interaction terms,

$$(4.3.19a) \quad \hat{R}_{12} = \partial_\tau \nabla^2 \hat{\psi}_1,$$

$$(4.3.19b) \quad \hat{R}_{22} = \partial_{\tau} \hat{B}_{\ell 1},$$

depend on the slow variation of the clouds,

$$(4.3.20a) \quad \hat{R}_{13} = \left\{ \frac{N^2 - N_0^2}{\mu \Gamma_0} - \frac{N_0^2}{\mu \Gamma_0^2} (\Gamma - \Gamma_0) \right\} \hat{B}_{\ell 1x} = - \frac{N_d^2}{\Gamma_0^2} \hat{B}_{\ell 1x},$$

$$(4.3.20b) \quad \hat{R}_{23} = - \mu^{-1} (\Gamma - \Gamma_0) \hat{\psi}_{1x} = - \hat{\psi}_{1x},$$

depend on the supercriticality, and

$$(4.3.21) \quad \hat{R}_{14} = \hat{J}(\tilde{\psi}'_1, \tilde{\psi}_{m2zz}) + \hat{J}(\tilde{\psi}_{m2}, \nabla^2 \tilde{\psi}'_1)$$

depends on the mean field (but will turn out to be zero).

There are two complications. Firstly, the boundary conditions at this order must finally take into account the presence of other clouds.

From (4.2.14a),

$$(4.3.22) \quad \hat{\psi}_3 \sim \begin{cases} \mu^{-1} A_{j+1}(\tau) \psi_1(x - x_{j+1}(\tau)) & x \gg x_j(\tau) \\ \mu^{-1} A_{j-1}(\tau) \psi_1(x - x_{j-1}(\tau)) & x \ll x_j(\tau) \end{cases}$$

and similarly for $\hat{B}_{\ell 3}$. The intercloud spacing has been chosen in (4.2.6a) to make $\mu^{-1} \psi_1(x - x_{j+1}(\tau))$ an $O(1)$ quantity near the j^{th} cloud. Secondly, the cloud boundaries at

$$(4.3.23) \quad 0 = \tilde{B}_{\ell} = \mu^{\frac{1}{2}} A_j B_1(x_c) \sin z + \mu A_j^2 B_2(x_c) \sin 2z \\ + \mu^{3/2} [\tilde{B}_{\ell 3}'(x_c, z, \tau) + \tilde{B}_{\ell 3m}] \dots$$

are affected by the mean circulation.

In Appendix V I calculate the inhomogeneous terms and find particular inhomogeneous solutions in the neighborhood of the j^{th} cloud:

$$(4.3.24) \quad \check{\psi}_3(x, \tau) = \check{\psi}_3^{(n)}(x - x_j)A_j^3 + \check{\psi}_3^{(t)}(x - x_j)A_{j\tau} + \check{\psi}_3^{(x)}(x - x_j)A_{jx}A_{j\tau} \\ + \check{\psi}_3^{(g)}(x - x_j)A_j + \check{\psi}_3^{(e)}(x - x_j)\{\zeta_j A_{j+1} + \zeta_{j-1} A_{j-1}\} \\ + \check{\psi}_3^{(0)}(x - x_j)\{\zeta_j A_{j+1} - \zeta_{j-1} A_{j-1}\}$$

in the cloudy and dry air which satisfy the boundary conditions at $x = \pm\infty$. Next I add to them homogeneous solutions $\psi_{3h}(x, \tau)$ to satisfy the matching conditions at the two cloud boundaries. The singular matrix equations which result are solvable only given two constraints which lead to evolution equations for the amplitude and position of each cloud.

The Matching Conditions

$B_{\ell 3}$, its first x -derivative, ψ_3 , and its first three x -derivatives are continuous across the cloud boundaries $\tilde{\alpha}_{\pm}(z, \tau)$. $\tilde{\alpha}_{+}(z, \tau)$ can be expanded

$$(4.3.25) \quad \tilde{\alpha}_{+} = x_j + \frac{1}{2}a_0 + \mu^{\frac{1}{2}}\tilde{\alpha}_1 + \mu\tilde{\alpha}_2 \dots$$

(in this and what follows, all functions are evaluated at $x = \frac{1}{2}a_0$ unless explicitly stated and arguments 'z' and 'τ' are omitted.) By definition,

$$\begin{aligned}
(4.3.26a) \quad 0 &= \tilde{B}_\ell(\tilde{\alpha}_+) \\
&= \mu^{1/2} \{ \tilde{B}'_{\ell 1} + \mu^{1/2} (\tilde{\alpha}_1 + \mu^{1/2} \tilde{\alpha}_2) \tilde{B}'_{\ell 1x} + \frac{1}{2} \mu \tilde{\alpha}_1^2 \tilde{B}'_{\ell 1xx} \} \\
&\quad + \mu \{ \tilde{B}'_{\ell 2} + \mu^{1/2} \tilde{\alpha}_1 \tilde{B}'_{\ell 2x} \} + \mu^{3/2} \{ \tilde{B}'_{\ell 3} + \tilde{B}'_{\ell m3} \} + O(\mu^2) .
\end{aligned}$$

Equating the $O(\mu^{3/2})$ terms to zero,

$$(4.3.26b) \quad \tilde{B}'_{\ell 3} + \tilde{\alpha}_2 \tilde{B}'_{\ell 1x} = -\tilde{\alpha}_1 \tilde{B}'_{\ell 2x} - (\tilde{\alpha}_1^2/2) \tilde{B}'_{\ell 1xx} - \tilde{B}'_{\ell m3} .$$

Let \tilde{F} be any function continuous across the cloud boundary with a functional form \tilde{F}_c inside the cloud and \tilde{F}_d outside it. Like \tilde{B}_ℓ , $\tilde{F}_c - \tilde{F}_d$ is zero at the cloud boundary. The same procedure shows that

$$(4.3.27) \quad \tilde{F}_3 \Big|_c^d + \tilde{\alpha}_2 \tilde{F}_{1x} \Big|_c^d = -\tilde{\alpha}_1 \tilde{F}_{2x} \Big|_c^d - \frac{1}{2} \tilde{\alpha}_1^2 \tilde{F}_{1xx} \Big|_c^d .$$

$\tilde{\psi}_1$ and its first three derivatives, $\tilde{\psi}_2$ and its first two derivatives, $\tilde{B}_{\ell 1}$ and its first four derivatives, and $\tilde{B}_{\ell 2}$ and its first three derivatives are continuous across $x = \frac{1}{2}a_0$. Consequently, (4.3.27) implies

$$(4.3.28a) \quad \tilde{\psi}_3 \Big|_c^d = \tilde{\psi}_{3x} \Big|_c^d = \tilde{B}'_{\ell 3} \Big|_c^d = \tilde{B}'_{\ell 3x} \Big|_c^d = 0 ,$$

$$(4.3.28b) \quad \tilde{\psi}_{3xx} \Big|_c^d = -\tilde{\alpha}_1 \tilde{\psi}_{2xxx} \Big|_c^d - \frac{1}{2} \tilde{\alpha}_1^2 \tilde{\psi}_{1xxxx} \Big|_c^d ,$$

$$(4.3.28c) \quad \tilde{\psi}_{3xxx} \Big|_c^d + \tilde{\alpha}_2 \tilde{\psi}_{1xxxx} \Big|_c^d = -\tilde{\alpha}_1 \tilde{\psi}_{2xxxx} \Big|_c^d - \frac{1}{2} \tilde{\alpha}_1^2 \tilde{\psi}_{1xxxxx} \Big|_c^d .$$

The matching condition (4.3.28b) can be simplified using (4.3.13,14):

$$(4.3.29a) \quad \tilde{\psi}_{1xxxx} \Big|_c^d = \tilde{B}_{\ell 1x} ,$$

$$(4.3.29b) \quad \tilde{\psi}_{2xxx} \Big|_c^d = \tilde{B}_{\ell 2} .$$

Only the components of the matching conditions proportional to $\sin(z)$ contribute to the solvability conditions. Let \hat{F} denote the $\sin(z)$ component of \tilde{F} and recall (4.3.10b),

$$(4.3.30a) \quad \tilde{\alpha}_1 = -2A_j \beta^{-1} B_{\ell 2} \cos z ,$$

$$(4.3.30b) \quad \beta = B_{1x} .$$

Then

$$(4.3.31) \quad \psi_{3xx} \Big|_c^d = -2A_j^3 \beta^{-1} B_2^2 \overbrace{\cos z \sin 2z} + \frac{1}{2} \cdot 4A_j^3 \beta^{-1} B_2^2 \overbrace{\cos^2 z \sin z} \\ = -\frac{1}{2} A_j^3 \beta^{-1} B_2^2 .$$

With (4.3.29a) and (4.3.26b) I can eliminate $\tilde{\alpha}_2$ from (4.3.28c),

$$(4.3.32) \quad \tilde{\psi}_{3xxx} \Big|_c^d - \tilde{B}'_{\ell 3} = -\tilde{\alpha}_1 \{ \tilde{\psi}_{2xxxx} \Big|_c^d - \tilde{B}'_{\ell 2x} \} \\ + \frac{1}{2} \tilde{\alpha}_1^2 \{ \tilde{\psi}_{1xxxxx} \Big|_c^d - \tilde{B}'_{\ell 1xx} \} + \tilde{B}_{\ell m3} .$$

From appendix II,

$$(4.3.33a) \quad \tilde{B}_{\ell m 3} = \Gamma_0 w_m ,$$

where w_m is the approximate maximum vertical velocity

$$(4.3.33b) \quad w_m = -\frac{4}{\pi} \theta_{XX} ,$$

The rest of (4.3.32) has $\sin(z)$ component

$$(4.3.34) \quad \hat{\psi}_{3xxx} \Big|_c^d - \hat{B}_{\ell 3} = 2A_j^3 \beta^{-1} \{ \psi_{2xxxx} \Big|_c^d - B_{\ell 2x} \} \cos z \sin 2z \\ - 2A_j^3 \beta^{-2} \{ \psi_{1xxxx} \Big|_c^d - B_{\ell 1xx} \} \cos^2 z \sin z - \hat{B}_{\ell m 3} \\ = A_j^3 \{ \beta^{-1} [\psi_{2xxxx} \Big|_c^d - B_{\ell 2x}] - \frac{1}{2} \beta^{-2} [\psi_{1xxxx} \Big|_c^d - B_{\ell 1xx}] \} \\ + \Gamma_0 w_m .$$

The Solvability Conditions

Knowing the matching conditions, I attempt to satisfy them at both cloud boundaries by adding "symmetric" and "antisymmetric" homogeneous solutions to $\tilde{\psi}_3(x, \tau)$ and $\tilde{B}_{\ell 3}(x, \tau)$. The "symmetric" homogeneous solution takes care of jumps in the parts of the inhomogeneous solution which are symmetric about the cloud center. The "antisymmetric" homogeneous solution takes care of the unbalanced effects of the two neighboring clouds. Write

$$(4.3.35a) \quad \hat{\psi}_3(x, \tau) = \hat{\psi}_3^{(s)}(x, \tau) + \hat{\psi}_3^{(a)}(x, \tau) ,$$

$$(4.3.35b) \quad \hat{\psi}_3^{(s)}(x, \tau) = \hat{\psi}_{3h}^{(s)}(x, \tau) + \check{\psi}_3^{(s)}(x, \tau) ,$$

$$(4.3.35c) \quad \hat{\psi}_3^{(a)}(x, \tau) = \hat{\psi}_{3h}^{(a)}(x, \tau) + \check{\psi}_3^{(a)}(x, \tau) ,$$

where from (4.3.24)

$$(4.3.36a) \quad \check{\psi}_3^{(s)}(x, \tau) = \check{\psi}_3^{(n)}(x - x_j) A_j^3 + \check{\psi}_3^{(t)}(x - x_j) A_j + \psi_3^{(g)}(x - x_j) A_j \\ + \check{\psi}_3^{(e)}(x - x_j) \{ \zeta_j A_{j+1} + \zeta_{j-1} A_{j-1} \} ,$$

$$(4.3.36b) \quad \check{\psi}_3^{(a)} = \check{\psi}_3^{(o)}(x - x_j) \{ \zeta_j A_{j+1} - \zeta_{j-1} A_{j-1} \} + \psi_3^{(x)}(x - x_j) A_j x_j \tau ,$$

while the symmetric and antisymmetric homogeneous solutions which decay as $x \rightarrow \pm \infty$ are given in appendix IV, equations (IV.14-15):

$$(4.3.37a) \quad \hat{\psi}_{3hd}^{(s)} = \sum_i \gamma_{di} b_{dsi} g_d(x, \rho_{di}) ,$$

$$(4.3.37b) \quad \hat{\psi}_{3hc}^{(s)} = \sum_i \gamma_{ci} b_{csi} g_c(x, \rho_{ci}) ,$$

$$(4.3.37c) \quad \hat{\psi}_{3hd}^{(a)} = \begin{pmatrix} + \\ - \end{pmatrix} \sum_i \gamma_{di} b_{dai} g_d(x, \rho_{di}) \quad \left\{ \begin{array}{l} x > \frac{1}{2} a_0 \\ x < -\frac{1}{2} a_0 \end{array} \right\} ,$$

$$(4.3.37d) \quad \hat{\psi}_{3hc}^{(a)} = \sum_i \gamma_{ci} b_{cai} f_c(x, \rho_{ci}) ,$$

and similarly for \hat{B}_{3h} .

The jumps in the matching conditions are symmetric, so $\hat{\psi}_3^{(s)}(x, \tau)$ obeys the same conditions as $\hat{\psi}_3(x, \tau)$, while there are no jumps in the antisymmetric solution. Therefore, the homogeneous solutions obey

$$(4.3.38a) \quad \frac{d^{n-1} \psi_{3h}^{(s)}}{dx^{n-1}} \Big|_c^d - \delta_{n4} B_{3h}^{(s)}(a_0) = \Delta_n[\psi_{3h}^{(s)}],$$

$$(4.3.38b) \quad \frac{d^{n-1} B_{3h}^{(s)}}{dx^{n-1}} \Big|_c^d = \Delta_n[B_{3h}^{(s)}],$$

and similarly for the asymmetric solution; from (4.3.28a, 31, 34)

$$(4.3.39a) \quad \Delta_n[\psi_{3h}^{(r)}] = - \frac{d^{n-1} \tilde{\psi}_3^{(r)}}{dx^{n-1}} \Big|_c^d + \delta_{n4} \tilde{B}_3^{(r)} +$$

$$+ \begin{cases} 0 & n = 1, 2, r = s; n = 1, 2, 3, 4, r = a \\ -\frac{1}{2} \beta^{-1} B_{2A_j}^{23}, & n = 3, r = 2 \\ A_j^3 \{ \beta^{-1} [\psi_{2xxxx} \Big|_c^d + B_{2x}] - \frac{1}{2} \beta^{-2} [\psi_{1xxxx} \Big|_c^d - B_{1xx}] \} \\ + \Gamma_{om}^w, & n = 4, r = s, \end{cases}$$

$$(4.3.39b) \quad \Delta_n[B_{3h}^{(r)}] = - \frac{d^{n-1} \tilde{B}_{l3}^{(r)}}{dx^{n-1}} \Big|_c^d \quad n = 1, 2, r = s, a.$$

Consulting (IV.19), two matrix equations for the coefficients $b_{d,csi}$ of the symmetric homogeneous solution and the coefficients $b_{d,cai}$ of the antisymmetric homogeneous solution are obtained. Using the notation of the appendix:

$$(4.3.40a) \quad M_{-s}^{(1)} b_{-s} = R_{-s} = R_{-s}^{(n)} A_j^3 + R_{-s}^{(\tau)} A_{j\tau} + R_{-s}^{(g)} A_j \\ + R_{-s}^{(e)} \{ \zeta_j A_{j+1} + \zeta_{j-1} A_{j-1} \},$$

$$(4.3.40b) \quad M_a^{(1)} b_{-a} = R_{-a} = R_{-a}^{(x)} A_{jx} A_{j\tau} + R_{-a}^{(o)} \{ \zeta_j A_{j+1} - \zeta_{j-1} A_{j-1} \} .$$

The matrices are both singular, with left null vectors \underline{u}_{-s} and \underline{u}_{-a} respectively. For a solution to exist the solvability conditions

$$(4.3.41a) \quad \underline{u}_{-s} \cdot R_{-s} = 0 ,$$

$$(4.3.41b) \quad \underline{u}_{-a} \cdot R_{-a} = 0 .$$

must hold. They can be solved for the slow evolution of A_j and x_j :

$$(4.3.42a) \quad A_{j\tau} = \sigma A_j - \eta_j A_{j+1} - \eta_{j-1} A_{j-1} - k A_j^3 + \omega w_m ,$$

$$A_{jx} A_{j\tau} = -d_j A_{j+1} + d_{j-1} A_{j-1} ,$$

where

$$(4.3.42c) \quad \eta_j, d_j = \eta, d \cdot \zeta_j = \eta, d \cdot \mu^{-1} \exp \{ -\rho_{d1} (x_{j+1} - x_j) \} .$$

Numerical values of the coefficients except for k for various N_{do}^2 are tabulated in Appendix VI. As a check of σ and η , I can use these equations to predict the "linear" growth rate Ω of a periodic array of clouds

spaced a distance λ apart. From (4.3.42a),

$$(4.3.43) \quad \Omega = (N_c^2 - N_{co}^2)\sigma - 2\eta \exp\{-\rho_{d1}\lambda\}.$$

In figure (4.2a) this prediction is compared with the true growth rates of the "linear" eigenmodes found in section 3.2; it is quite accurate for clouds more than a frictional deformation radius apart whose linear growth rate is only a few percent of N_c .

The coefficients d and ω can be checked by solving the linear initial value problem (3.2.1-4) assuming a vertical structure $\sin(z)$ and replacing the effective stratification N^2 of (3.2.4) by that felt in the presence of mean vertical motion

$$(4.3.44) \quad N^2 = \begin{cases} N_d^2 & \tilde{B}_\ell < -\Gamma_o w_m \sin z \\ -N_c^2 & \tilde{B}_\ell > -\Gamma_o w_m \sin z \end{cases}.$$

By first taking $w_m = 0$ and then considering two clouds of equal amplitude a distance x apart, (4.3.42b) predicts

$$(4.3.45a) \quad \frac{dx}{dt} = 2d \exp\{-\rho_{d1}x\},$$

$$(4.3.45b) \quad \frac{d}{dt} [\exp(\rho_{d1}x)] = 2d\rho_{d1}.$$

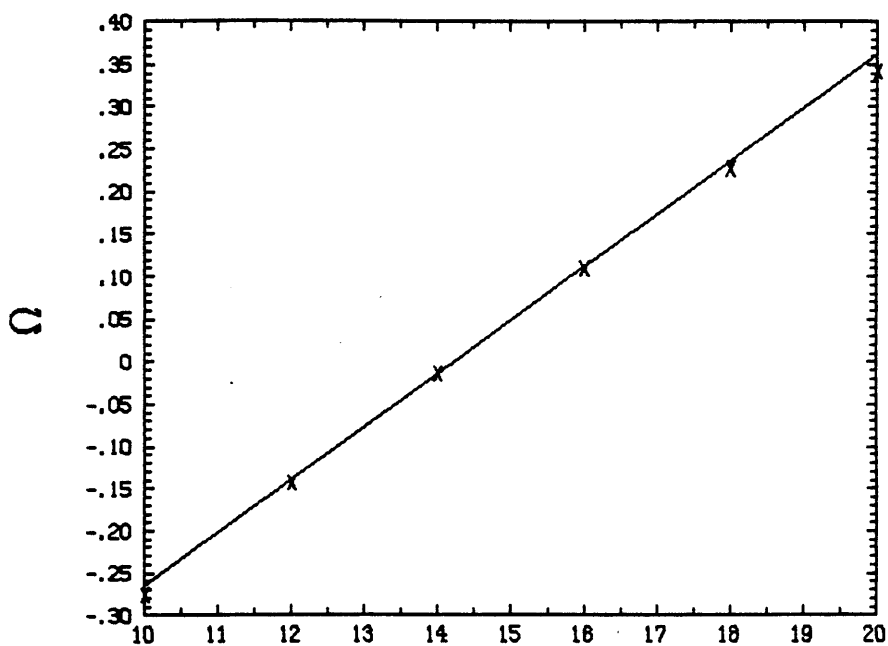
If $w_m \neq 0$ but only one isolated cloud is present, (4.3.42a) predicts that if $N_c^2 = N_{co}^2$,

$$(4.3.46) \quad \frac{dA}{dt} = \omega w_m$$

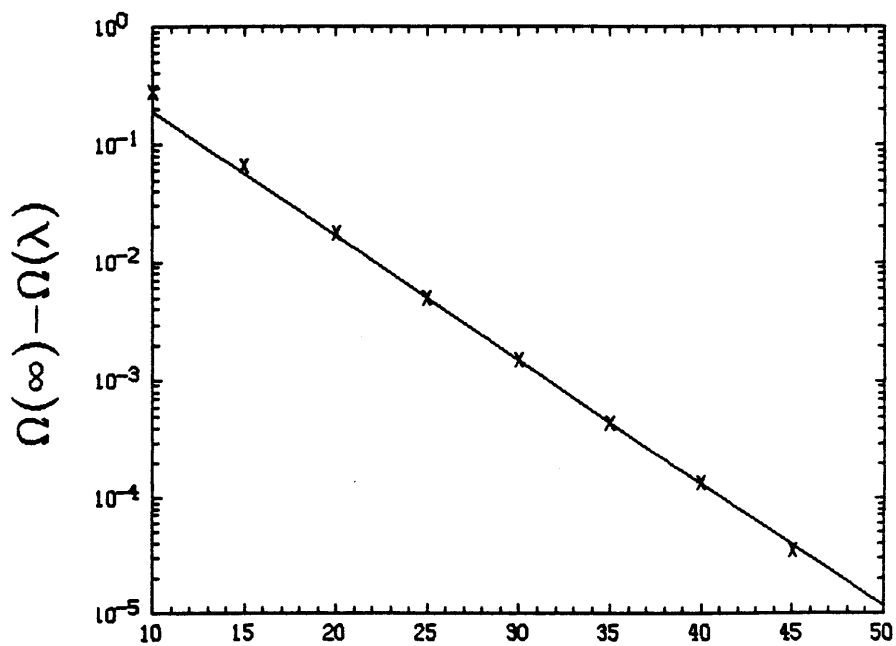
for small w_m . These predictions are checked in figure (4.2b).

I did not feel able to reliably carry out the labyrinthine computation of the Landau constant k without a check, which requires a full nonlinear simulation of the equations; I have not done this.

The numerical values of the constants are important in testing theory against reality, but I emphasize that they do not effect the qualitative behavior of the solution. Only η/d cannot be scaled out of the equations.



(I) Ω vs N_c^2 for $\lambda = \infty$, $N_d^2 = 14.23$ N_c^2



(II) Ω vs λ when $N_c^2 = N_d^2 = 14.23$, λ
 $\Omega(\infty) = 0$.

Figure 4.2a

A comparison of the "linear" eigenfunctions (crosses) with the predicted growth rates based on the asymptotic cloud interaction theory (solid).

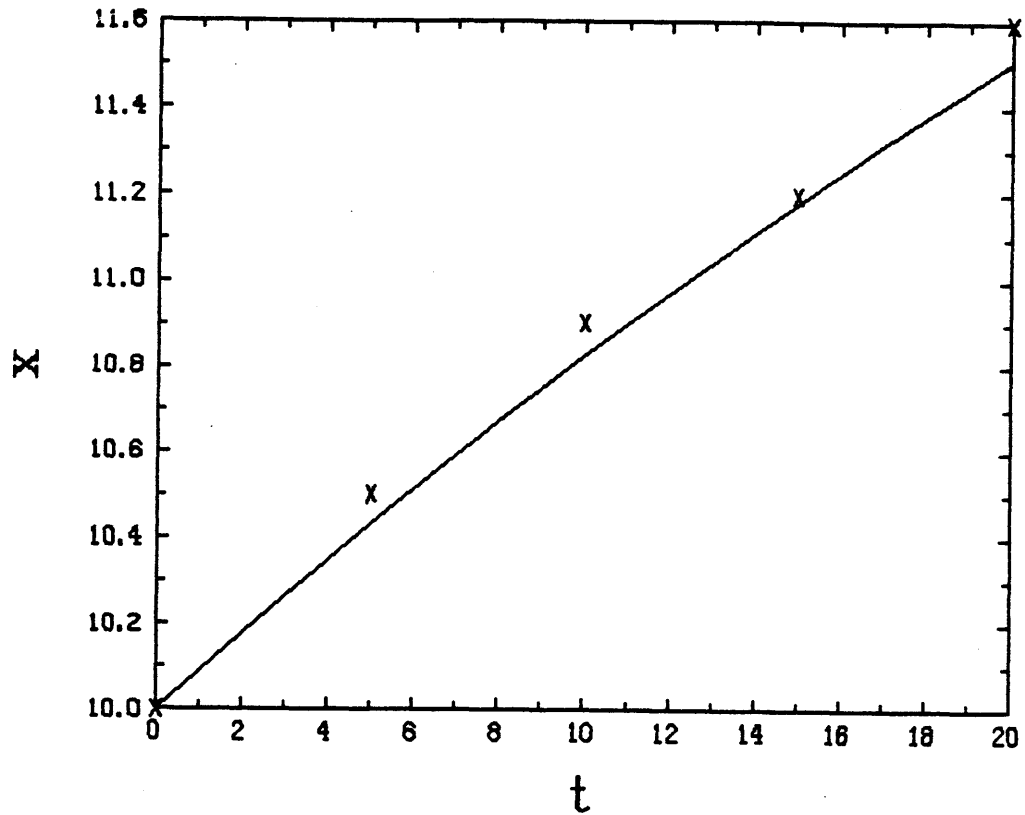


Figure 4.2b

Further comparisons between linear critical value problem calculations (crosses) and asymptotic theory (line).

- (a) The spacing x between two clouds isolated from all others increases with time t .

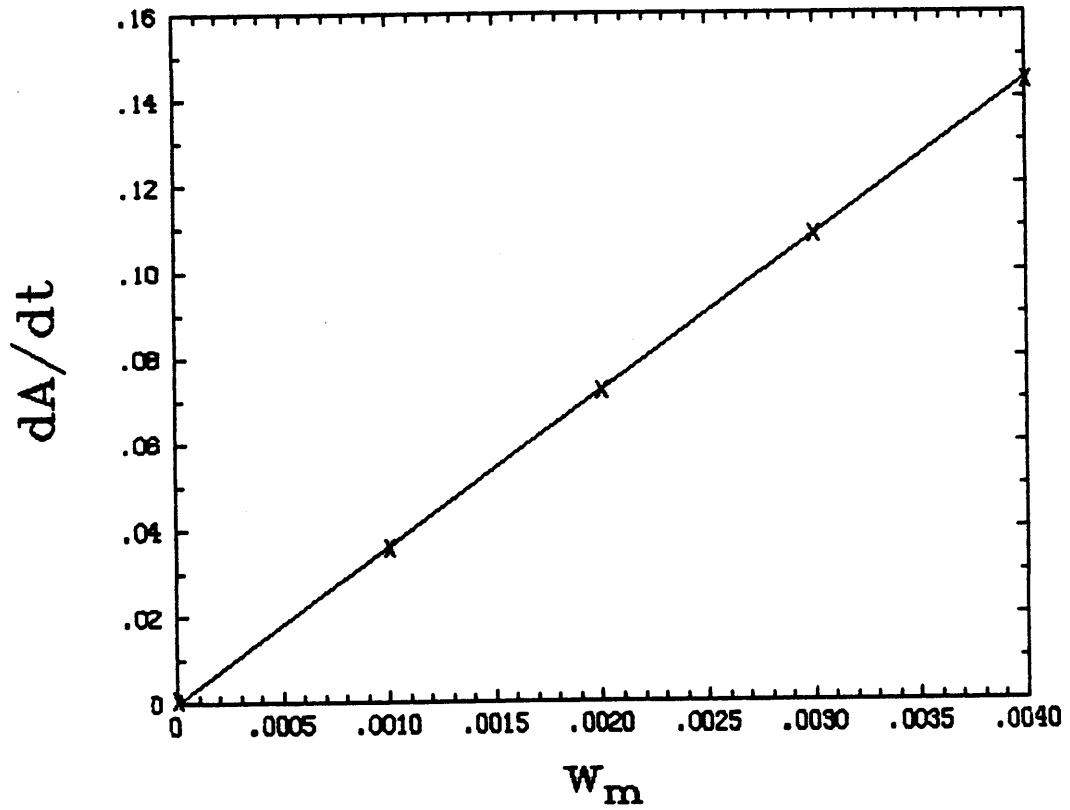


Figure 4.2b -- continued

- (b) The amplitude of a cloud A grows linearly with time t proportional to W_m .

4.4 The Amplitude Equations and Cloud Spacing

In the previous section I derived equations for the amplitudes and positions of a field of widely spaced clouds. The essential fact that allows each cloud to be determined by its amplitude and position was that its horizontal structure is always approximately that of a "linear" isolated eigenmode; motions inside and outside the cloud are completely coupled. The idealized model considered was very special; if the boundaries are not saturated, or the nonlinear behavior of $q^*(p,T)$, the saturation mixing ratio, is considered, or if a more realistic upper boundary (such as a region of strongly stratified air) were used, the equations would change.

However, the qualitative character of their solutions would be little altered, as I will show. As long as N_c^2 is near the critical value N_{co}^2 for the onset of convection, there is a stable steady solution in which clouds are equally spaced at least a critical distance λ_c apart. If clouds are closer than this distance, they strongly suppress each other. A subharmonic instability which amplifies every second cloud leads to a field of clouds with twice the spacing which can achieve much larger amplitude and thus increase the buoyancy flux. A second type of equilibrium in which clouds of two amplitudes intermingle in any combination is probably always unstable.

Having established that clouds are (at least locally) equally strong and equally spaced, I will turn to "large-scale" variations of the cloud field in which cloud amplitude and spacing change slowly compared to the intercloud distance. I will obtain a diffusion equation for the cloud

spacing in which the diffusivity is positive precisely if the cloud spacing exceeds λ_c ; all such variations decay by a slow adjustment in the position of the clouds.

The Equations

The equations (4.3.42) of the previous section can be written

$$(4.4.1a) \quad dA_j/d\tau = -\eta_j A_{j+1} - \eta_{j-1} A_{j-1} + p(A_j), \quad A_j > 0,$$

$$(4.4.1b) \quad A_j(dx_j/d\tau) = -d_j A_{j+1} + d_{j-1} A_{j-1},$$

where

$$(4.4.1c) \quad \tau = \mu t,$$

$$(4.4.1d) \quad \eta_j, d_j = \eta, d \cdot \mu^{-1} \cdot \exp\{-\rho_{1d} \Delta x_j\},$$

$$(4.4.1e) \quad \mu = N_c^2 - N_{co}^2.$$

The restriction that $A_j > 0$ is necessary to ensure each cloud really is saturated. Notice that this allows the number of clouds in the field to change. A cloud which is suppressed until $A_j = 0$ is thereafter deleted from the equations. Conversely, new clouds can grow at any new position x at which mean upward motion more than compensates for the subsidence induced by the two nearest clouds.

For my model,

$$(4.4.2) \quad p(A_j) = \sigma A_j - k A_j^3 + \omega w_m$$

where σ , k , ω , η , and d are constants depending only on N_{co}^2 and N_{do}^2 , and $\mu^{3/2} w_m$ is the mean vertical velocity at midheight. Different boundary conditions or non-Boussinesq thermodynamics lead to the same equations with different forms of $p(A_j)$, different η and d , and perhaps a different subsidence radius ρ_{d1}^{-1} . If convection is not too penetrative, it will stabilize the environment by its upward buoyancy flux so

$$(4.4.3a) \quad d^2 p(\alpha) / d\alpha^2 > 0, \quad \alpha > 0.$$

This does not mean that moist convection is supercritical, however.

If $w_m < 0$ any cloud requires a finite amplitude kick to grow.

I will also assume the linear growth rate σ of an isolated cloud is positive. Physically, this is reasonable because it is viscosity which allows convection to be damped in a conditionally unstable environment, yet an eddy viscosity is generated only as the cloud grows. Thus $p(\alpha)$ has a maximum,

$$(4.4.3b) \quad dp/d\alpha = 0, \quad \alpha = \alpha_{\max}.$$

If $p(\alpha)$ has these properties then the equilibria and their stability behave identically to the case (4.4.2). In this sense the equations

(4.4.1) and the solutions I will discuss are generic. I now seek their equilibria.

The Equilibria of an Adjacent Pair of Clouds

Steady solutions of (4.4.2 a,b) obey (since $d_j \propto \eta_j$)

$$(4.4.4a) \quad 0 = p(A_j) - \eta_j A_{j+1} - \eta_{j-1} A_{j-1} ,$$

$$(4.4.4b) \quad 0 = -\eta_j A_{j+1} + \eta_{j-1} A_{j-1} .$$

Consider a specific pair of adjacent clouds i and $i+1$. Equation (4.4.4b) can be used to eliminate A_{i+2} and A_{i-1} from the equation (4.4.4a) for each cloud to yield a pair of simultaneous equations for A_i and A_{i+1} ,

$$(4.4.5a) \quad A_i = p(A_{i+1})/2\eta_i ,$$

$$(4.4.5b) \quad A_{i+1} = p(A_i)/2\eta_i .$$

If these equations hold for every cloud pair, then direct substitution into (4.4.4) shows the cloud field is steady.

The number of solutions depends on $p(0)$ and η_i . In my model $p(0)$ is proportional to the mean vertical velocity w_m and the solutions are shown in figure 4.3. However, more generally $p(0)$ measures the moisture in the basic state and would be reduced if, for instance, the air at the plates were less than completely saturated.

If $p(0) > 0$ there is always one equilibrium in which both clouds have equal strength:

$$(4.4.6a) \quad A_i = A_{i+1} = \alpha_1(\eta_i) ,$$

$$(4.4.6b) \quad \alpha_1 = p(\alpha_1)/2\eta_i ,$$

Since $p(\alpha)/2\eta - \alpha$ is a decreasing function of α near α_1 , $d\alpha_1/d\eta < 0$; when the damping of a cloud on its neighbor increases, its neighbor does not grow as strong.

If $dp/d\alpha$ were not a monotone decreasing function of α , as might occur were the convection penetrative, there could be a pair of much smaller equilibria of this type for some range of η_i , corresponding to a subcritical instability. A finite amplitude "kick" would then be necessary to realize the strongly convecting equilibrium; otherwise only the barely convecting weaker equilibrium of the pair would be attained.

If the clouds are close together (case I) the equal strength equilibrium is the only possible solution to (4.4.5). But if the clouds are far enough apart (case II) so that

$$(4.4.7a) \quad \eta_i < \eta_c = \eta(\lambda_c) ,$$

where

$$(4.4.7b) \quad (1/2\eta_c)(dp/d\alpha)(\alpha_1(\eta_c)) = -1 > (1/2\eta_i)(dp/d\alpha)(\alpha_1(\eta_i)) ;$$

there is a pair of solutions in which adjacent clouds are unequal,

$$(4.4.8a) \quad (A_i, A_{i+1}) = (\alpha_2(\eta_i), \alpha_3(\eta_i)) \quad \text{or} \quad (\alpha_3(\eta_i), \alpha_2(\eta_i)),$$

$$(4.4.8b) \quad \alpha_2 (= p(\alpha_3)/2\eta_i) < \alpha_3 (= p(\alpha_2)/2\eta_i),$$

which bifurcate from the equal strength solution at $\eta_i = \eta_c$.

When $p(0) < 0$, there are no equilibria at all when clouds are very closely spaced (case III). This occurs if $\eta_i > \eta_{\text{damp}}$, $q(\alpha; \eta_i) = (2\eta_i)^{-1}p(\alpha) - \alpha < 0$ for all α . At η_{damp} , $q(\alpha)$ reaches its maximum of 0 at $\alpha = \alpha_{\text{damp}}$:

$$(4.4.9) \quad q(\alpha_{\text{damp}}; \eta_{\text{damp}}) = (dq/d\alpha)(\alpha_{\text{damp}}; \eta_{\text{damp}}) = 0.$$

For my form (4.4.2) of $p(\alpha)$, η_{damp} is given by

$$(4.4.10) \quad \sigma - 2\eta_{\text{damp}} = \left[\frac{3}{2}(3k)^{1/2}(-\omega_w)_m \right]^{2/3} = \sigma_{\text{damp}};$$

η_{damp} decreases proportional to the two-thirds power of the subsidence.

In sufficiently strong subsidence (case IV) $\sigma < \sigma_{\text{damp}}$ and the convection is entirely suppressed.

If $\sigma > \sigma_{\text{damp}}$ and $\eta_j < \eta_{\text{damp}}$ there are two equilibria in which both clouds have equal strength (case V). If $\eta_i < \eta_{\text{crit}}$ there also are two unequal equilibria as in case II (case VI).

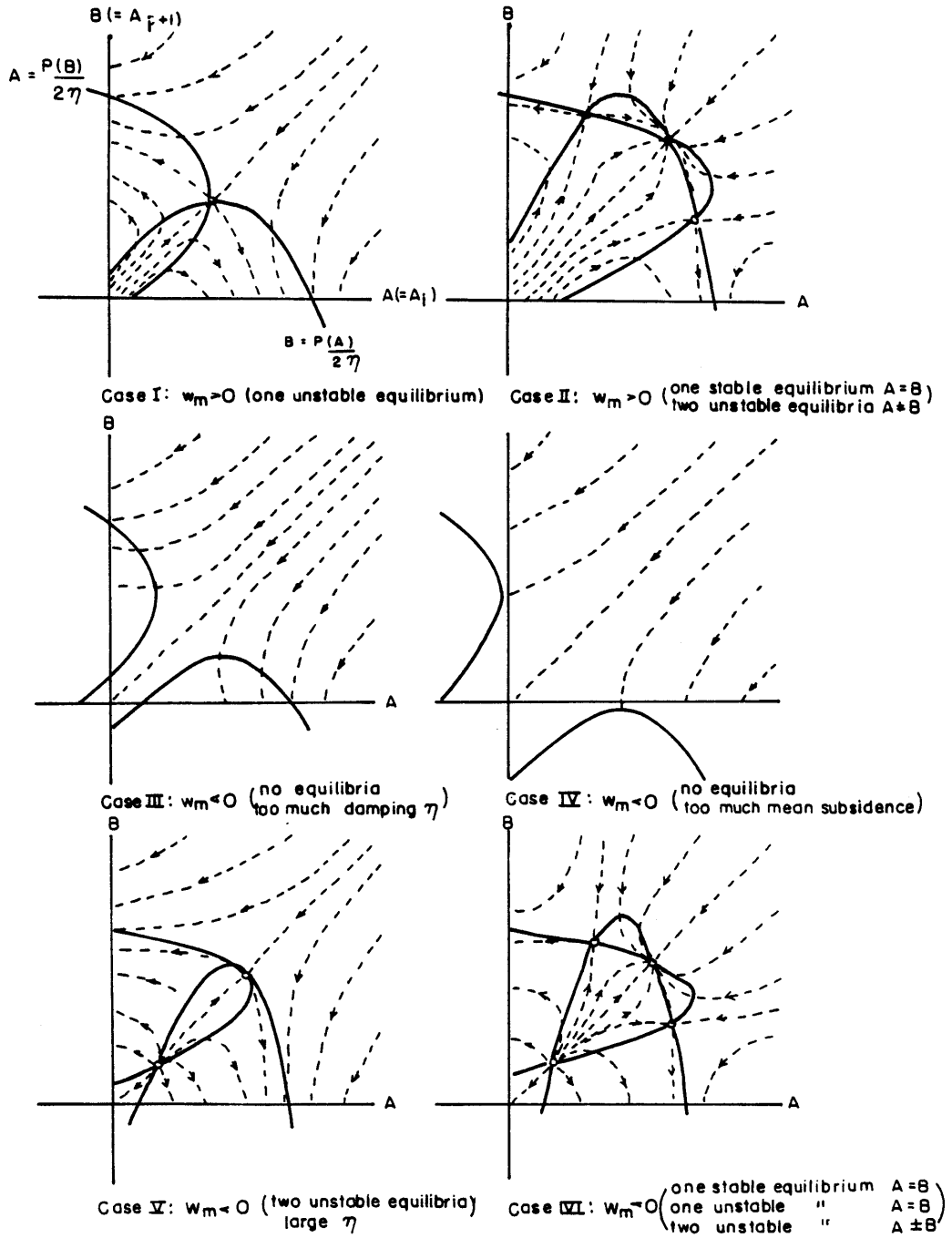


Figure 4.3

The equilibria of adjacent clouds and their stability. The solid lines are the curves $B = p(A)/2\eta$ and $A = p(B)/2\eta$. Their intersections give the equilibria and are shown as solid circles if they are stable and as unfilled circles if they are unstable. The dotted lines are the trajectories of (4.4.5).

Equilibria of a Field of Clouds

So far I have just constructed solutions in which a particular pair of clouds can be in equilibrium. That such relations hold between every adjacent pair of clouds is a necessary condition for an equilibrium of an infinite field of clouds.

If all the clouds are of equal strength, (4.4.5a) shows that they must be equally spaced. If $w_m > 0$ their spacing uniquely determines their amplitude; if $w_m < 0$ there will either be no solutions or two possible cloud amplitudes if the spacing is large enough.

If all the clouds are not of equal strength, I can show they all have one of two different amplitudes. There must be a pair (A_i, A_{i+1}) of adjacent clouds with different strengths; assume without loss of generality that $A_i = \alpha_3(\eta_i)$ is stronger than $A_{i+1} = \alpha_2(\eta_i)$ and consider A_{i-1} . It is either equal to A_{i-1} or unequal to it. In the latter case, I will show it must also be spaced a distance $\Delta x_{i-1} = \Delta x_i$ away from A_i and have amplitude $\alpha_2(\eta_i)$. To prove this, I will show first that

$$(4.4.11) \quad \frac{d\alpha_2}{d\eta} > 0 > \frac{d\alpha_3}{d\eta} .$$

Differentiate (4.4.8b) with respect to η ,

$$(4.4.12a) \quad \frac{\partial \alpha_2}{\partial \eta} = -s_3 \frac{\partial \alpha_3}{\partial \eta} - \frac{1}{2\eta^2} p(\alpha_3) ,$$

$$(4.4.12b) \quad \frac{\partial \alpha_3}{\partial \eta} = s_2 \frac{\partial \alpha_2}{\partial \eta} - \frac{1}{2\eta^2} p(\alpha_2) ,$$

$$(4.4.12c) \quad s_3 \equiv -\frac{1}{2\eta} \frac{dp}{d\alpha}(\alpha_3) > -\frac{1}{2\eta} \frac{dp}{d\alpha}(\alpha_1(\eta_i)) > 1.$$

$$(4.4.12d) \quad s_2 \equiv \frac{1}{2\eta} \frac{dp}{d\alpha}(\alpha_2) > 0.$$

These equations can be simultaneously solved,

$$(4.4.13a) \quad \begin{aligned} \frac{\partial \alpha_2}{\partial \eta} &= -\frac{1}{2\eta^2(1+s_2s_3)} \{p(\alpha_3) - s_3p(\alpha_2)\} \\ &= -\frac{1}{\eta(1+s_2s_3)} \{\alpha_2 - s_3\alpha_3\} > 0, \end{aligned}$$

$$(4.4.13b) \quad \frac{\partial \alpha_3}{\partial \eta} = -\frac{1}{\eta(1+s_2s_3)} \{s_2\alpha_2 + \alpha_3\} < 0,$$

where I used (4.4.8b) and (4.4.12c,d).

Since $\eta_i < \eta_{\text{crit}}$ and from the definition of η_{crit} ,

$$(4.4.14) \quad \alpha_2(\eta_{\text{crit}}) = \alpha_3(\eta_{\text{crit}}) = \alpha_1(\eta_{\text{crit}}),$$

this shows that for any choices of η_{i-1} and η_i ,

$$(4.4.15) \quad \alpha_2(\eta_{i-1}) < \alpha_1(\eta_{\text{crit}}) < \alpha_3(\eta_i).$$

Consequently, A_i cannot be the smaller of the pair (A_{i-1}, A_i) . If it is larger,

$$(4.4.16) \quad \alpha_3(\eta_i) = \alpha_3(\eta_{i-1}),$$

so from (4.4.11) A_{i-1} is equally far from A_i as is A_{i+1} ,

$$(4.4.17a) \quad \eta_i = \eta_{i-1},$$

and so is equally big,

$$(4.4.17b) \quad A_{i-1} = \alpha_2(\eta_{i-1}) = A_{i+1} = \alpha_2(\eta_i).$$

It is also possible that $A_{i-1} = A_i = \alpha_3(\eta_i)$. This uniquely specifies η_{i-1} to be

$$(4.4.18) \quad \eta_{i-1} = \frac{p(\alpha_3)}{2\alpha_3} = \frac{\alpha_2(\eta_i)}{\alpha_3(\eta_i)} \eta_i.$$

By extending this reasoning in both directions along the line of clouds, I can show that every pair of unequal adjacent clouds must have amplitudes $\alpha_2(\eta_i)$ and $\alpha_3(\eta_i)$. The only equilibria of (4.4.1) are fields of clouds, each of which has amplitude $\alpha_2(\eta)$ or $\alpha_3(\eta)$ for some η . The distance between the clouds is such that

$$(4.4.19) \quad \eta_i = \begin{cases} \eta & A_i = \alpha_2, \quad A_{i+1} = \alpha_3 \quad \text{or vice versa} \\ \frac{\alpha_2}{\alpha_3} \eta & A_i = A_{i+1} = \alpha_3 \\ \frac{\alpha_3}{\alpha_2} \eta & A_i = A_{i+1} = \alpha_2 \end{cases}$$

It is easily verified by direct substitution that all such solutions are indeed equilibria, as they satisfy (4.4.1a,b).

Physically, what are these equilibria? One can easily understand the equilibria in which all clouds are equal. If the intercloud spacing is large, clouds damp their neighbors little and achieve almost the amplitude of an isolated cloud. The stability of such a cloud field depends on the stability of the equilibrated isolated cloud; physically, the nonlinearity is what keeps the linearly unstable convection down to a finite amplitude, so the isolated cloud which is the result of this process is always stable. If $w_m < 0$ there are two equilibria $p(\alpha) = 0$ for an isolated cloud, but the smaller one represents the amplitude above which a cloud is established enough to grow against the mean subsidence and below which it is squelched by mean subsidence. This solution is clearly an unstable equilibrium. Thus, there will always be one stable equilibrium in which clouds are widely, but equally spaced.

If the intercloud spacing is small, clouds damp each other much more, and do not come close to the amplitude of an isolated, steady cloud. Then an array of equally spaced clouds is unstable, because if a cloud is bigger than its neighbors, it induces greater subsidence around itself, damping them more. As they decay, it is no longer held down by the subsidence they induced and grows further. Consequently, a cloud can force its neighbors to disappear entirely if they are too close; this sets a minimum intercloud spacing.

Next I turn to the equilibria in which clouds of two amplitudes coexist. These are always unstable. To see why, I consider the extreme case in which clouds alternate in strength between amplitudes $\alpha_2(\eta)$ and $\alpha_3(\eta)$, so are all equidistant. The larger clouds are little affected by the smaller ones, and have grown almost to the amplitude of

an isolated cloud. The smaller clouds, however, are balanced on a razor edge. Were they any smaller, they would be wiped out entirely by the subsidence around the larger clouds. Were they larger, they could damp the larger clouds more and decrease the subsidence they induce, allowing further growth of the smaller clouds.

On physical grounds, I have concluded the only stable steady cloud fields have uniformly strong clouds spaced a sufficiently large uniform distance apart. Now I turn to the mathematical justification of this statement.

The Stability of Equilibrium Solutions

Unfortunately, a complete stability analysis of this infinite set of coupled equations appears intractable to me. I will content myself with the stability analysis of two important special cases to a particular kind of perturbation. The first case is that of alternating larger and smaller clouds, the second case is that of uniformly strong equidistant clouds, and I do a stability analysis with respect to perturbations which are equal for every second cloud. It will show the alternating equilibrium is unstable, and give a minimum critical cloud spacing for the uniform equilibrium to be unstable. It is reasonable to suppose that if the uniform equilibrium is unstable by means of the mechanism discussed above, the most unstable perturbation should alternately damp and enhance cloud amplitudes and so should have the form I now consider.

Let me assume, then, that

$$(4.4.20a) \quad \dots A_{-2} = A_0 = A_2 \dots = A,$$

$$(4.4.20b) \quad \dots A_{-1} = A_1 = A_3 \dots = B,$$

$$(4.4.20c) \quad \dots \eta_{-2} = \eta_0 = \eta_2 \dots = \eta_0,$$

$$(4.4.20d) \quad \dots \eta_{-1} = \eta_1 = \eta_3 \dots = \eta_1.$$

The equations (4.4.91a,b) reduce to (since $d_i = c \cdot \eta_i$ for some c)

$$(4.4.21a) \quad \frac{dA}{dt} = p(A) - (\eta_0 + \eta_1)B,$$

$$(4.4.21b) \quad \frac{dB}{dt} = p(B) - (\eta_0 + \eta_1)A,$$

$$(4.4.21c) \quad A \frac{dx_0}{dt} = \{-\eta_0 + \eta_1\}B \cdot c,$$

$$(4.4.21d) \quad B \frac{dx_1}{dt} = \{\eta_0 - \eta_1\}A \cdot c.$$

The last pair of equations imply (since x_2 and x_0 change synchronously)

$$(4.4.21e) \quad \frac{d(x_1 - x_0)}{dt} = - \frac{d(x_2 - x_1)}{dt} = c\{\eta_0 - \eta_1\} \left\{ \frac{A}{B} + \frac{B}{A} \right\}.$$

Since $\eta_1 \propto \exp(-\rho_{d1}(x_{i+1} - x_i))$,

$$(4.4.21f) \quad \frac{1}{\eta_0} \frac{d\eta_0}{dt} = - \frac{1}{\eta_1} \frac{d\eta_1}{dt} = -c\rho_{d1}(\eta_0 - \eta_1) \left(\frac{A}{B} + \frac{B}{A} \right),$$

so $\eta_0 - \eta_1$ must decay exponentially,

$$(4.4.22) \quad \frac{d}{dt}\{\eta_0 - \eta_1\} = -\{c\rho_{d1}(\eta_0 + \eta_1)\left(\frac{A}{B} + \frac{B}{A}\right)\}(\eta_0 - \eta_1).$$

It is therefore consistent, and asymptotically necessary for large times, to take

$$(4.4.23) \quad \eta_0 = \eta_1 = \eta ;$$

all clouds become equidistant since their neighbors have the same strength on both sides. Then

$$(4.4.24a) \quad \frac{dA}{dt} = p(A) - 2\eta B,$$

$$(4.4.24b) \quad \frac{dB}{dt} = p(B) - 2\eta A .$$

These equations encompass and allow an examination of the stability of all pairwise equilibria (4.4.8), giving the phase portraits (dotted lines) of each case in figure 4.3. When clouds are close together, there are no stable equilibria; either A or B is forced down to zero and half the clouds disappear. When clouds are further apart, both the uniform and alternating equilibria are possible, but only the uniform equilibrium $A = B$ is stable (cases II and VI). The uniform equilibrium becomes stable when η decreases below η_c and the alternating equilibria bifurcate from it. To calculate η_c , I simultaneously solve (4.4.6b) and (4.4.7b) using the $p(\alpha)$ of my model from (4.4.2),

leading to an implicit equation for η_c in terms of σ , k , and w_m :

$$(4.4.22a) \quad 2 \left[\frac{\sigma - 4\eta_c}{3} \right] \left[\frac{\sigma + 2\eta_c}{3k} \right]^{1/2} + \omega w_m = 0 ,$$

whose solution

$$(4.4.22b) \quad \frac{\eta_c}{\sigma} = N \left[\frac{k^{1/2} \omega w_m}{\sigma^{3/2}} \right]$$

is graphed in figure 4.4. For

$$(4.4.23) \quad w_m < w_{\text{damp}} = - \frac{2}{k^{1/2} \omega} \left(\frac{\sigma}{3} \right)^{3/2} ,$$

convection cannot occur. η_c increases, and the minimum stable cloud spacing decreases, as w_m grows, until for large positive w_m ,

$$(4.4.24) \quad \eta_c \sim \frac{1}{3} \left(\frac{4}{k} \right)^{1/2} (\omega w_m)^{2/3} , \quad w_m \gg 0 .$$

Lastly, as the supercriticality μ decreases, the cloud spacing

$$(4.4.25) \quad \lambda_c = \log \left\{ \frac{\eta}{\mu \eta_c} \right\} / \rho_{d1}$$

corresponding to η_c increases -- in the "linear" limit $\mu \rightarrow 0$ no finite cloud spacing is stable, confirming a conjecture of chapter three.

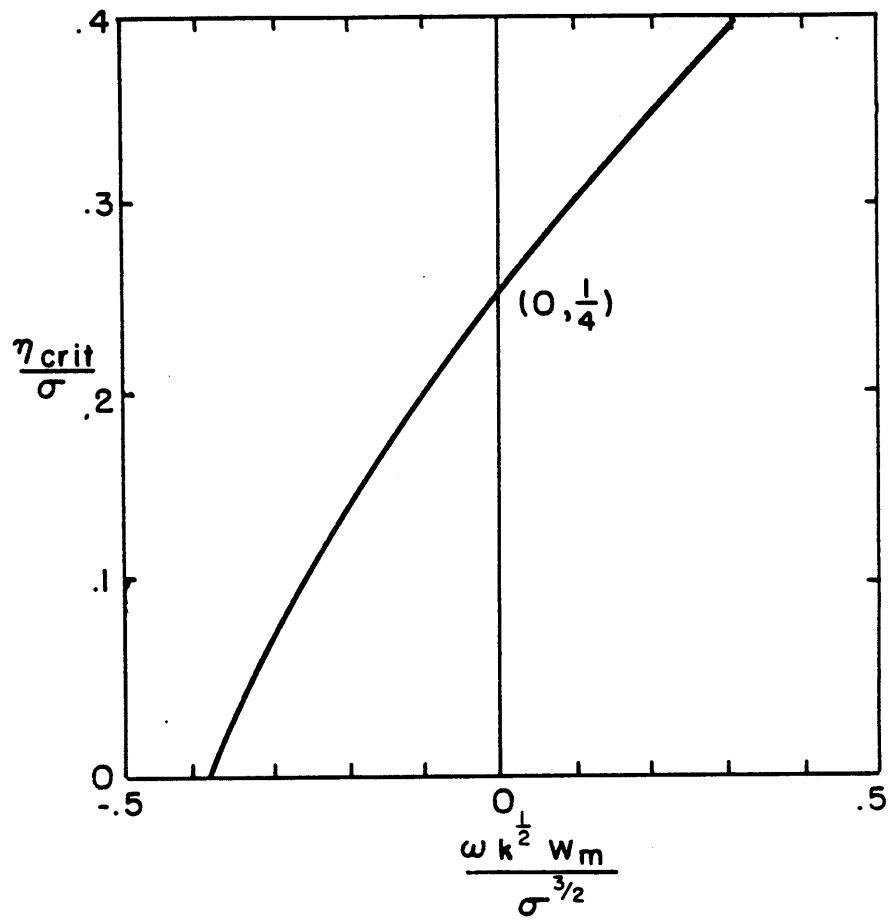


Figure 4.4

The relationship between the minimum critical cloud spacing $\Delta x \propto -\rho_{dl}^{-1} \log \eta_{crit}$ and the mean vertical motion ω_m and growth rate σ of an isolated cloud.

4.5 Collective Disturbances of a Cloud Field

The stability theory just presented was restricted to the shortest wavelength disturbances possible on a cloud field. It is also interesting that disturbances of long wavelength compared to the cloud spacing obey a diffusion equation whose diffusivity is positive, so long wavelength disturbances are smoothed away, precisely when $\lambda > \lambda_c$.

In a long wavelength disturbance, the spacing $\lambda = \Delta x_j$ and amplitude $A = A_j$ are slowly varying functions of x, τ . From equations (4.4.1a), $A(x, \tau)$ equilibrates to

$$(4.5.1) \quad 2\eta(\lambda)A(x, \tau) = p(A(x, \tau))$$

in time $\tau = O(1)$, but λ itself changes on a much slower timescale as a result of the small imbalance of the effects of its neighbors. On this scale, (4.5.1) implicitly determines A as a function of λ ,

$$(4.5.2) \quad A = a(\lambda) .$$

Now, from (4.4.1b), omitting the argument " τ " of A and λ ,

$$(4.5.3a) \quad \begin{aligned} A(x_j)x_{j\tau} &= -d(\lambda(x_j))A(x_j + \lambda(x_j)) + d(\lambda(x_j - \lambda(x_j)))A(x_j - \lambda(x_j)) \\ &= -d(\lambda(x_j))[A(x_j) + \lambda(x_j)A_x(x_j)] \\ &\quad + [d(\lambda(x_j)) - \lambda(x_j)d_x(\lambda(x_j))][A(x_j) - \lambda(x_j)A_x(\lambda(x_j))] \\ &\quad + O(\lambda^2) \end{aligned}$$

$$= F(\lambda(\mathbf{x}_j)) \cdot \lambda_{\mathbf{x}}(\mathbf{x}_j)$$

where

$$(4.5.3b) \quad d(\lambda) = \mu^{-1} d \exp\{-\rho_{1d} \lambda\} ,$$

$$(4.5.3c) \quad F(\lambda) = -\lambda\{2da_{\lambda} + ad_{\lambda}\} .$$

Similarly

$$(4.5.3d) \quad A(\mathbf{x}_j + \lambda(\mathbf{x}_j))_{\mathbf{x}_{j+1,\tau}} = F(\lambda(\mathbf{x}_j + \lambda(\mathbf{x}_j))) \cdot \lambda_{\mathbf{x}}(\mathbf{x}_j + \lambda(\mathbf{x}_j)) ,$$

so

$$(4.5.4a) \quad \lambda_{\tau}(\mathbf{x}_j) = \mathbf{x}_{j+1,\tau} - \mathbf{x}_{j,\tau} = \lambda(\mathbf{x}_j) \left\{ \frac{F(\lambda)}{a(\lambda)} \lambda_{\mathbf{x}}(\mathbf{x}_j) \right\}_{\mathbf{x}} ,$$

which is a nonlinear diffusion equation for $\tilde{\lambda} = \log \lambda$,

$$(4.5.4b) \quad \tilde{\lambda}_{\tau} = (k(\tilde{\lambda}) \tilde{\lambda}_{\mathbf{x}})_{\mathbf{x}} ,$$

$$(4.5.4c) \quad k(\tilde{\lambda}) = \frac{\lambda F(\lambda)}{a(\lambda)} .$$

The diffusion coefficient is positive as long as $F(\lambda) > 0$. From the definition (4.5.3c) I may rewrite F using the notation $\alpha(\eta)$ for the equilibrium value $a(\lambda)$ when $\eta = \eta(\lambda)$,

$$(4.5.5) \quad \begin{aligned} F(\lambda) &= \lambda d(\lambda) \{a[-d_{\lambda}/d] - 2a_{\lambda}\} \\ &= \lambda \eta(\lambda) \rho_{d1} \{\alpha + 2\eta \alpha_{\eta}\} , \end{aligned}$$

since $d(\lambda), \eta(\lambda) \propto \exp\{-\rho_{d1}\lambda\}$.

$F(\lambda) > 0$, I assert, is precisely equivalent to stability criterion

$$(4.5.6) \quad \frac{1}{2\eta} \frac{dp(\alpha)}{d\alpha} < -1 \quad \text{at} \quad \alpha = \alpha(\eta)$$

for alternating disturbances. Differentiating condition (4.5.1) with respect to η ,

$$(4.5.7) \quad \frac{dp}{d\alpha} \alpha_{\eta} = 2\eta\alpha_{\eta} + 2\alpha \quad ,$$

so (4.5.6) implies

$$(4.5.8a) \quad \frac{dp}{d\alpha} + 2\eta < 0 \quad ,$$

or since $\alpha_{\eta} < 0$

$$(4.5.8b) \quad \alpha_{\eta} \left(\frac{dp}{d\alpha} + 2\eta \right) = 2(2\eta\alpha_{\eta} + \alpha) > 0 \quad ,$$

as claimed.

This is a somewhat remarkable result, since the type of instability which would result when $k(\tilde{\lambda}) < 0$ is an instability of cloud spacing, while the alternating instability changes only the cloud amplitudes. When $k(\tilde{\lambda}) > 0$, i.e. when $\lambda > \lambda_c$ across the whole cloud field, there are no collective instabilities of the system and no propagation of convective disturbances, i.e. no wave-CISK. This is physically reasonable, since buoyancy is generated in phase with vertical motion within each

cloud, and there is no means of decoupling motions in the stably stratified air outside the clouds to allow a gravity wave to grow.

4.6 Summary

In conclusion, it appears the only stable steady solutions of the amplitude equations are uniformly spaced clouds of uniform amplitude $a(\lambda)$ a distance λ apart. If the clouds are packed more closely, subharmonic instability causes every second cloud to grow and annihilate its neighbors. Slow variations of convection simply diffuse away; no wave-CISK can occur.

One may ask whether there is also an upper bound on cloud spacing. Infinitesimal clouds can grow wherever $p(0)$ (or w_m in my model) exceeds the damping due to the two closest clouds, which is smallest halfway between them,

$$(4.6.1) \quad -2\eta(\lambda/2)a(\lambda) + p(0) > 0 \quad (\text{infinitesimal}).$$

However, finite amplitude clouds can be inserted into the cloud field when it is more closely spaced. Clearly, if $\lambda < 2\lambda_c$ such clouds will be damped out by the subharmonic instability mechanism. But if clouds of amplitude $a(\lambda)$ are introduced when $\lambda > 2\lambda_c$, a new stable equilibrium with twice the cloud density is possible. It is quite reasonable to consider such finite amplitude disturbances, for in the real atmosphere dry convection of a heated boundary layer below cloudbase can maintain quite strong circulations when it is not interfered with by a nearby cloud. In the band

$$(4.6.2) \quad \lambda_c < \lambda < 2\lambda_c \quad (\text{finite amplitude})$$

the cloud field is stable both to disturbances of the existing clouds and to the introduction of new clouds. As shown in Appendix VII, the volume average buoyancy flux $\langle wB \rangle$ is maximized for a cloud spacing in this band slightly larger than λ_c . It is nonlinearity, therefore, which permits many clouds to coexist by limiting the strength of each cloud and consequently the damping effect of the subsidence-induced drying near its neighbors.

CHAPTER 5

Conclusion5.1 A Synopsis

I have formulated a thermodynamically accurate but analytically tractable model of conditional instability, obtaining solutions in the "linear" limit of infinitesimal motions and equations for the development of a widely spaced, weakly nonlinear field of clouds. These

which all clouds are of equal amplitude and spacing unless they are too densely packed, in which case every second cloud is suppressed.

In chapter two I showed that if the Boussinesq approximation is made and the saturation mixing ratio can be regarded as a linear function of temperature and pressure over the convecting region, the buoyancy of an air parcel can be simply written

$$(5.1.1) \quad B = \begin{cases} B_u & B_\ell < 0 \\ B_u + B_\ell & B_\ell > 0 \end{cases} .$$

The unsaturated buoyancy B_u is a scaled virtual liquid water potential temperature, and is invariant in adiabatic motions. The liquid buoyancy B_ℓ is proportional to the amount of liquid water in the air (or the deficit of water vapor from that required to saturate the air when it is negative), and increases linearly with height as water condenses

in the adiabatic ascent of a parcel. Both B_u and B_ℓ combine linearly when air parcels are mixed.

If the temperature and water content of the air are specified at an upper and lower plate, then perturbations of the two buoyancies from a hydrostatic, purely diffusive basic state are proportional to one another and the perturbation buoyancy is simply proportional to B_ℓ ; since the constant of proportionality depends on the sign of B_ℓ , the dependence is nonlinear.

Lastly, a constant isotropic eddy viscosity is assumed.

In chapter three I considered the stability of infinitesimal motions. Remarkably, the equations are identical to those posed by Kuo (1961) but the dependent variable is no longer the vertical velocity but the liquid buoyancy. Thus the stability problem is identical, but the solutions are different. Strong evaporatively driven downdrafts near the cloud edge surround an updraft core. Away from the clouds subsidence of dry air slowly decays on a lengthscale which is the minimum of three "deformation radii"--the frictional deformation radius $R_{fr} = Nh(h^2 / \Omega)$ where Ω is the growthrate. In the atmosphere, typically $R_{tr} = 5 - 20\text{km}$ is the smallest; the influence of a growing cloud is limited primarily by the finite maximum horizontal group velocity

section 3.5, the eddy viscosity was taken to be large even in the stably stratified air and the frictional deformation radius artificially became the smallest.

The downwelling around each cloud dries out the air and suppresses

the growth of clouds, so a periodic array of clouds grows fastest when the spacing substantially exceeds the subsidence radius. A circularly symmetric cloud is more unstable than a slab-symmetric cloud. These findings are well known from numerical models and accord with the results of Lilly (1960) and Yamasaki (1972). If the eddy viscosity is decreased to a much smaller constant value outside the cloud, the growth rate increases and less subsidence occurs outside the cloud, but is spread over a much wider region due to the much increased frictional deformation radius. The abrupt change in the diffusion of horizontal momentum causes a pressure jump across the cloud boundary.

One might ask if other solutions of the "linear" equations grow as fast or render the clouds with vertical edges unstable (the nonlinear expression for the buoyancy makes the question of stability meaningful). I proved there are no growing periodically oscillating solutions or growing travelling waves, and that the separable solutions just considered are stable to any nontrivial perturbation of their cloud boundaries. But there are other separable solutions corresponding to clouds with multiple updrafts separated by barely saturated downdrafts; these are a crude response to cloudtop entrainment instability. These solutions are unstable to perturbations which in the end transform them into the faster growing single updraft clouds. Any initial condition evolves toward an ever smaller number of ever stronger stationary single updraft clouds.

The cloud spacing is nonlinearly determined. In chapter four I explored the dynamics of a field of clouds when an individual isolated cloud is slightly linearly unstable and a very weak mean vertical motion

is included by slight horizontal variations of the temperature on the boundaries. Any clouds which persist must not be too close to one another, so each cloud has a structure close to that of the isolated "linear" cloud with a slowly varying amplitude and position found from solvability conditions determined from a very involved amplitude expansion. The procedure is much complicated by having to match two solutions across a moving cloud boundary whose deformation depends on the solutions themselves. Clouds interact linearly to both damp their neighbors and to force them to move away by cutting off their inflow and outflow, but the nonlinear advections due to a cloud affect only itself. A small mean upward motion causes every cloud to grow linearly in time. A cloud is annihilated when its amplitude drops to zero. It can be created in a region in which mean upward motion is strong enough to allow an infinitesimal cloud to grow despite the suppressing effects of its neighbors; the number of clouds is not fixed.

These equations have two types of equilibria--either all clouds are of equal strength or clouds of two distinct amplitudes coexist in an arbitrary ordering. Although a general stability analysis is intractable, a revealing special case can be solved. If every second cloud has equal amplitude the infinite set of equations reduces to two. When the cloud spacing is too small, alternate clouds grow by suppressing their neighbors. But nonlinearity limits the amplitude which clouds can attain. When the spacing exceeds a critical distance proportional to the subsidence radius and inversely related to the supercriticality, clouds cannot wield a great enough influence on each other to stop the growth of their neighbors, and a uniformly strong field of clouds is

stable. In this situation, there is another equilibrium, characteristic of the second class, in which every second cloud is just strong enough to survive against the subsidence induced by its stronger neighbors. All non-uniform equilibria have clouds which balance on this razor edge; I believe they are all unstable.

In general the equations nicely reproduce the features of the nonlinear numerical simulations of Asai and Nakasuji (1982). The minimum cloud spacing increases as the mean vertical velocity decreases, until in sufficiently strong large-scale subsidence no convection is possible. Unless there is mean upward motion there is no maximum possible cloud spacing unless new clouds of finite size are introduced, in which case they can grow if they exceed a threshold amplitude (the razor edge mentioned in the previous paragraph) which decreases exponentially with cloud spacing. The band between one and two times the minimum spacing is stable even to these perturbations. The buoyancy flux is maximized at a spacing in the band just above the minimum.

Lastly, I considered modulations of the cloud amplitude and spacing on a lengthscale much larger than the spacing itself. In this case, a nonlinear diffusion equation for the spacing can be obtained from the evolution equations. The diffusivity is positive, and variations tend to smooth out with time, unless the clouds are closer than the minimum stable spacing. No wavelike modulations can propagate.

5.2 Limitations

The set of coupled amplitude equations I have derived provide an interesting new view of a cloud field. They predict cloud dynamics consistent with the much more nonlinear model of Asai and Nagasuji (1982), while giving greater insight into the processes involved, in particular the nonlinearly determined minimum distance between clouds and the subharmonic instability of a more closely spaced cloud field. Their versatility compensates for their restrictive scope. But, most important, they provide a framework for further questions, to which I now turn.

As a model of nonprecipitating, nonsheared convection, my equations have two serious related deficiencies. Firstly, they do not lead to time dependent convection, and secondly, the assumption of a uniform eddy viscosity is rather poor.

An important drawback of replacing turbulent mixing by an eddy viscosity is to reduce the time-dependence of the flow. In a steady circulation the moisture and temperature fields are coupled, but Randall and Huffman (1982) speculated that a decaying cloud may leave behind primarily a relatively moist region which provides a favorable environment for further clouds to grow, leading to cloud clustering. Their argument must be applied carefully. In the model I have discussed, the unsaturated buoyancy B_u and the total moisture r are linearly proportional in the basic state and remain so regardless of the motion or mixing of air parcels. Perturbations of B_u cannot radiate away without precisely the same thing happening to perturbations in r .

But for deep, moist convection in the atmosphere this is often far from the case. Near the surface, r drops strongly with height, but in the cold air of the upper troposphere, r is nearly zero and cannot further decrease. Over the whole depth, B_u increases at a nearly constant rate with height. Mixing equal quantities of air from the top and bottom of the troposphere produces air much moister than undisturbed air with the same B_u . This may allow convection to leave behind the moisture anomalies required for Randall and Huffman's clustering mechanism to work.

There may be another effect of time-dependence, which can numerically be studied by gradually lowering the viscosity from the value at which steady isolated clouds are marginally stable until a bifurcation to oscillatory behavior occurs. As the viscosity is further lowered the amplitude of the cloud updraft will oscillate increasingly violently until, one may speculate, the cloud splits. It is possible that at this stage isolated convection is no longer possible; bunches of oscillating cells begin to spread outward from the formerly steady updraft, the width of the cell packet determined by a modulational instability. This would provide an intriguing interpretation of the simulation of Delden and Oerlemans (1982). In any case, the bifurcation of the steady isolated updraft into unsteady convection seems a promising area of investigation. A vertical truncation of the equations to $\sin(z)$ and $\sin(2z)$ modes might recreate some of the same dynamics in a simpler model.

The assumption of a large and constant eddy viscosity causes subsidence to occur within a frictional deformation radius of the cloud. As

I discussed earlier, there is in reality very little turbulent mixing except in the vicinity of clouds in a more turbulent subcloud boundary layer generated by thermals and shear instability near the lower boundary. The effect of this is difficult to estimate, but since it covers a small fraction of the domain near the lower boundary, the influence of the subcloud layer on the convective circulation is probably small. It is the finite group velocity of gravity waves which really limits the subsidence radius of a growing cloud. But what happens when the cloud stops growing? The gravity wave response is quite complicated, and becomes even more so when the upper boundary is removed. It is only rotation that can finally corral the thermal perturbations, so the long term effects of a region of intense convection will be felt over a Rossby radius.

5.3 Some Extensions

The base of a convective cloud is always some distance from the ground, and in boundary layer convection in which clouds are not very deep, the aspect ratio is observed to be similar to that of dry convection. How does the aspect ratio vary with the fraction of the depth over which air can be saturated? Some numerical results of Asai and Nagasuji (1982) in which they maintained the boundaries of their domain at various relative humidities indicate that as long as conditional instability is possible the aspect ratio of steady nonlinear convective clouds remains approximately the same. They considered a domain which

was stably stratified to dry convection through its entire depth. Typically, however, convection is induced by surface heating and a dry convective boundary layer forms and deepens to the point where condensation can occur and soon thereafter the clouds rapidly deepen in the conditionally unstable layer above. One might model this in the spirit of Lilly as a domain in which the stability is a function of the sign of the upward motion above a condensation level and search for a most unstable aspect ratio.

Two physical effects that must also be understood are precipitation and shear. Shear is observed to be a powerful organizing force in the atmosphere. The prominence of cloud rows in the study of Malkus and Riehl (1964), however, begs the following question. Is a purely roll-like nonprecipitating moist circulation aligned along the shear unstable to the growth of three-dimensional perturbations which grow into cloud towers, no matter how strong the shear? Such basic states are separable, so this stability problem is analytically tractable.

Rain is perhaps the most interesting dynamical element missing from my model. If the stability of a purely saturated basic state in which all liquid water falls at a constant terminal velocity is examined, convective cells tilt and begin to propagate under certain conditions (Emanuel, personal communication) because this allows the updrafts to shed their load of liquid water and further weigh down the colder return flow. This theory could be extended to a conditionally unstable basic state, albeit only numerically, because clouds with sloping boundaries do not correspond to separable solutions of the equations of my model. Now the downdraft can be further cooled by evaporation if it

is unsaturated. Is there a preference for two-dimensional flow if rain falls fast enough? When can cloud complexes form?

The joint effects of shear and rain can be very powerful, because the updraft can tilt into the shear and release kinetic energy. To summarize the interesting dynamical issues that have been brought up in this area would require many pages.

5.2 Some Mesoscale Convective Phenomena

I will lastly comment on wave-CISK and mesoscale cellular convection, neither of which is yet on a firm theoretical footing.

A very interesting application of simplified equations describing a cloud field is to the concept of wave-CISK, the excitation of a long-wavelength gravity wave whose energy is derived from conditional instability. Usually the mean latent heating due to the convection is parameterized by relating it to the mean vertical motion due to the gravity wave. For instance, Lindzen (1974) assumed that all the upward mass flux through the top of the boundary layer occurs in cumulus towers, so the latent heating is proportional to some vertical structure function multiplied by the low level convergence due to the wave. A very serious problem with simple theories of wave-CISK in an unsheared environment is that there is no reasonable short-wave cutoff unless lag effects which violate the scale separation are also present; waves are predicted to grow at a rate proportional to their horizontal wavenumber.

tackle the problem by trying to find an analogous instability of a field of clouds, all of which are resolved. In the model I have discussed, no "linear" instability of this type exists. This primarily reflects several special restrictions of the model. The rigid upper boundary does not allow the lines of constant phase of a gravity wave to tilt away from the vertical. The large eddy viscosity artificially damps such a wave. The latent heating of a saturated parcel is proportional to its vertical velocity with the same proportionality constant at all heights, rather than being weighted toward the warmer air at the bottom of the domain. However, the model suggests that the parametrization must be carefully thought through, since the dominant effect of a mean upward motion in the model is to moisten the environmental air at the mid-levels of the cloud. This effect depends not on the downward convective fluxes of air. This effect depends not on the boundary layer convergence, but the convergence throughout the whole lower half of the convecting region, and brings the mean vertical velocity and the latent heat release into phase where both are strongest, which is not conducive to the growth of a wave. One of the most exciting applications of my approach is to understand when and if wave-CISK can really occur.

Mesoscale cellular convection, described in the introduction, is a pervasive feature of convection over the oceans. Satellite pictures show the broad cells forming within outbreaks of cold arctic air over the much warmer Gulf Stream waters of the Atlantic or the Kuroshio current off Japan. A shallow boundary layer of convecting air, usually 1-2 km thick, forms and becomes capped by cloud as it moistens. The

large scale descent which typically occurs above such an outbreak and the radiative cooling near the cloudtop encourages the growth of a strong inversion.

Because of the superficial resemblance of open MCC to Bénard cells, it has usually been attributed primarily to convection, despite its broad aspect ratio. A recent paper of Fiedler (1984) summarized the shortcomings of these theories (none of which explicitly takes into account the effects of moisture) in accounting for the aspect ratio. I have shown that latent heating can broaden the aspect ratio substantially. Could this resolve the dilemma? Probably not. Open MCC has characteristics of moist convection--a 15-30:1 aspect ratio and a fractional cloud cover which is fairly low (typically 40%, but often less), and is associated with a convecting boundary layer, but the cloudiness is at the edge of the polygonal cells. In dry convection with a hexagonal planform, the vertical motion in the center of a cell is twice as intense as the maximum along the edges (Chandrasekhar, 1961); the preference of moist convection for stronger updrafts than downdrafts favors upward motion at the center of each hexagon. When the cell width is much larger than the subsidence radius, this is particularly clear. A hexagonal array of nearly isolated cylindrical clouds produces ascent in the center of each cell. A honeycomb of long roll clouds, which have a smaller growth rate, lead to rising motion at the edges. The circulation in cells of open MCC is thus the reverse of that preferred by nonprecipitating moist convection. The cloud is restricted to the upper few hundred meters of the layer, so it is unlikely to drastically increase the most unstable aspect ratio.

Further, the cell width seems to be almost independent of the boundary layer depth (Agee and Dowell, 1973), while the subsidence radius (which determines the distance between convecting clouds) is proportional to it. Lastly, Agee and Lomax (1978) constructed a thermodynamic profile of an open MCC cell from two soundings, one through a cloudy region and one through the clear air in another cell six hours later. To the extent this technique can be trusted, they observed that the virtual potential temperature in the convective layer was well mixed without noticeable mesoscale variations, suggesting that convection was working on a much shorter lengthscale. Large horizontal buoyancy gradients were observed in the inversion above the cell only.

Closed MCC, in which cloudy areas are surrounded by connected regions of clear air has a planform similar to that predicted simply by convection. However, all the other arguments against the convective origin of open MCC apply. In addition, Agee and Rothermel (1982) analyzed data from two flights through two adjacent closed cells, and obtained power spectra of the fluctuations of temperature, moisture and wind. The virtual potential temperature fluctuations were dominated by horizontal scales of a few kilometers, as were the velocity components. A fairly strong mesoscale fluctuation in the mixing ratio was observed well separated from the variations in shorter length scales, suggesting differential entrainment of the very dry air above the mixed layer. In fact, Fiedler (1984) has shown that such entrainment could lead to an instability with the horizontal scale of MCC, at least in a totally cloud-capped mixed layer. Above the entrainment interface there is a strong stable temperature stratification. Clouds which penetrate higher

into this stratification encounter potentially warmer air. Since the entrainment interface consequently is more stable, they entrain less air, and thus dry out less fast than the dips in between. Yet since the air they entrain is warmer, they entrain more buoyancy. Differential entrainment slowly amplifies the perturbation. A rather strong inversion is needed to produce the instability, and it is unclear what the effects of the partial breakup of the cloud cover would be. The hexagonal planform and the difference between open and closed cells remains a mystery, and a picture in Agee and Rothermel taken from Gemini 10 of beautiful hexagons of almost entirely clear air with lines of small cumuli around their edges suggest that a primarily cloud-capped layer may not be necessary. But the large aspect ratio, its relative insensitivity to the boundary layer depth, and the formative conditions of MCC are nicely explained by this theory. It appears that MCC cannot simply be thought of as moist convection, but involves the more subtle interplay of convection, radiation, and entrainment which characterize the oceanic boundary layer.

Perhaps it is now clear why one must always return to a simplistic theoretical model. Such a model allows a clear understanding of the effects of a single physical mechanism such as condensation. Equally important in a complicated system are the features it does not predict. By precisely mapping the frontiers of our knowledge, we, like Columbus, learn where to search next, and perhaps may also stumble upon the New World.

APPENDIX I

Some Thermodynamics(A) The Buoyancy of Moist Air

My aim is to express the buoyancy

$$(I.1) \quad B = -(g/\rho_0)(\rho - \rho_a(z))$$

in terms of quantities invariant in adiabatic motions of an air parcel.

In this section I write B in terms of a quantity θ_v , the virtual potential temperature, which is invariant until condensation occurs, correcting for liquid water loading.

The density of a moist air parcel can be partitioned

$$(I.2) \quad \rho = \rho_d(1 + q_v + q_l) .$$

The pressure is the sum of the partial pressures of dry air and water vapor

$$(I.3) \quad \begin{aligned} p &= p_d + p_v \\ &= (\rho_d R_d + \rho_v R_v)T . \end{aligned}$$

In order to simplify the gas law for a mixture of water vapor and air, the "virtual" temperature T_v is introduced,

$$(I.4a) \quad p = (\rho_d + \rho_v)R_d T_v ,$$

$$(I.4b) \quad T_v = T \left\{ \frac{1 + (R_v/R_d)q_v}{1 + q_v} \right\} = T\{1 + \epsilon q_v\}, \quad q_v \ll 1,$$

$$(I.4c) \quad \epsilon = (R_v/R_d) = 1 = (w_d/w_v) - 1 = .608 ,$$

where $w_d \approx 29$ and $w_v \approx 18$ are the molecular weights of dry air and water vapor. T_v is the temperature dry air must have at the pressure p of the mixture to have the same density as the mixture. As water vapor is less dense than air at a given temperature and pressure, $T_v > T$, but the difference is rarely more than 2°K in the atmosphere.

The virtual temperature is not an invariant, however. For an unsaturated air parcel, the potential temperature

$$(I.5) \quad \theta = T(p_{\text{ref}}/p_d)^{R_d/c_p} \quad (p_{\text{ref}} = 1000 \text{ mb})$$

and q_v are invariants, so the virtual potential temperature

$$(I.6) \quad \theta_v = \theta\{1 + \epsilon q_v\}$$

is also invariant.

I can express the part of the buoyancy not due to liquid water loading in terms of θ_v . In a shallow layer around the reference level

z_0 , $\rho_d q_\ell \approx \rho_0 q_\ell$ so from (I.1) and (I.2) B can be written

$$(I.7a) \quad B = B_u - g q_\ell ,$$

$$(I.7b) \quad B_u = -(g/\rho_0)(\rho_d + \rho_v - \rho_a(z)) .$$

From (I.4b), (I.5) and (I.6),

$$(I.8) \quad \frac{\rho_d + \rho_v - \rho_a(z)}{\rho_0} = \frac{p - p_a(z)}{p_0} - \frac{T_v - T_a(z)}{T_0} = \left(1 + \frac{R_d}{c_p}\right) \frac{p - p_a(z)}{p_0} - \frac{\theta_v - \theta_0}{\theta_0} .$$

The reference state is absolutely dry, so $T_{va}(z) = T_a(z)$, and adiabatic, so $\theta_{va}(z) = \theta_a(z) = \theta_0$.

For the Boussinesq approximation to hold, motions must be slow compared to the speed of sound in air. The relative pressure perturbations from a hydrostatic state due to such motions are much smaller than their density perturbations, so

$$(I.9) \quad \frac{p - p_a(z)}{p_0} \ll \frac{\rho - \rho_a(z)}{\rho_0}, \frac{T_v - T_a(z)}{T_0}, \frac{\theta_v - \theta_0}{\theta_0},$$

and from (I.7) and (I.8)

$$(I.10) \quad B = g \left[\left(\frac{\theta_v - \theta_0}{\theta_0} \right) - q_\ell \right] .$$

Outside a cloud this expresses B in terms of an invariant, but inside θ_v and q_ℓ are not invariant and must be expressed in terms of invariants.

(B) An Invariant θ_{vl} for Moist Air

I will now develop a linearly mixing invariant which reduces to θ_v outside a cloud. Neglect the very weak dependence of the heat capacities C_{pd} of dry air and C_l of liquid water on temperature. The entropy S of a parcel (per unit mass of dry air therein) can be partitioned

$$(I.11) \quad S = S_d + S_v q_v + S_l q_l .$$

The entropy S_d of dry air is

$$(I.12) \quad S_d = C_{pd} \ln T - R_d \ln p_d ,$$

where p_d is the partial pressure of dry air in the mixture. The entropy S_l of the liquid water is

$$(I.13) \quad S_l = C_l \ln T .$$

From the Clausius-Clapeyron equation, if L_v is the latent heat of vaporization,

$$(I.14) \quad S_v - S_l = L_v/T .$$

substituting into (I.11),

$$(I.15a) \quad S = C_{pm} \ln T - R_d \ln p_d + (q_v L_v / T) ,$$

$$(I.15b) \quad C_{pm} = C_{pm} + r C_\ell .$$

Except for neglect of the slight temperature variation of C_{pd} and C_ℓ , this is exact and allows the construct of an exact invariant temperature $\theta_q = \exp\{S/C_{pm}\}$.

However, I will instead use an approximate, but more convenient invariant. Since C_{pm} depends on the water content of a fluid parcel, it is desirable to eliminate it in favor of a fixed constant. Since r is small ($r < .02$ typically), $C_{pm} \approx C_{pd}$ to a fair approximation. However, the systematic error this produces can be partially balanced by replacing $\ln T$ by $\ln T_v$,

$$(I.16) \quad S \approx C_{pd} \ln T_v - R_d \ln p_d + (q_v L_v / T) ,$$

$$\approx C_{pd} \ln \theta_v + (q_v L_v / T) .$$

Since $q_v \ll 1$, in a shallow layer around z_o it is a good approximation to take $q_v L_v / T \approx q_v L_{vo} / T_o$. I eliminate q_v in favor of q_ℓ and define the liquid water virtual potential temperature

$$(I.17) \quad \theta_{v\ell} = \exp\{(S/C_{pd}) - (L_{co}/C_{pd} T_o) \cdot r\}$$

$$= \theta_v \exp\{-(L_{vo}/C_{pd} T_o) \cdot q_\ell\} ,$$

$$(I.18a) \quad \theta_{v\ell} \approx \theta_v - \gamma \cdot q_\ell ,$$

$$(I.18b) \quad \gamma = \theta_{vo} L_{vo} / C_{pf} T_o .$$

Within the shallow layer approximation, $\theta_{v\ell}$ is a function of the invariants S and r , so is itself invariant. Outside a cloud $\theta_{v\ell}$ equals the virtual potential temperature θ_v , but inside it is reduced because of the energy required to evaporate the liquid water. $\theta_{v\ell}$ is also nearly linearly mixing. To understand this take any two parcels of air at some pressure p_1 . Instead of mixing them at that pressure, reversibly lower them to a pressure p_2 at which neither parcel is saturated. Since the enthalpy $H = C_{pm} T$ ($\approx C_{pd} T_v$ by our earlier approximation) is linearly mixing, T_v , and thus $\theta_{v\ell} = \theta_v$, is approximately linearly mixing in the unsaturated air. Now move the mixed parcel back to its original pressure adiabatically, leaving $\theta_{v\ell}$ invariant. The result is the same as if the parcels had been mixed at pressure p_2 , so $\theta_{v\ell}$ is linearly mixing even if either one or both parcels are saturated.

APPENDIX II

The Mean Fields in the Absence of Convection

If mean vertical motions are forced by slow small variations of the temperature at the boundaries

$$(II.1a) \quad \tilde{B}_{um}(X, z) = \mu^{1/2} \theta(X) ,$$

$$(II.1b) \quad \tilde{B}_{lm}(X, z) = 0 , \quad (\text{saturated boundaries})$$

$$(II.1c) \quad X = \mu^{1/2} x .$$

then the equations of motion (4.2.10) reduce to

$$(II.2a) \quad (\partial_z^2 + \mu \partial_X^2) \tilde{\psi}_m + \mu \tilde{B}_{mX} = J(\tilde{\psi}_m, \nabla^2 \tilde{\psi}_m) ,$$

$$(II.2b) \quad (\partial_z^2 + \mu \partial_X^2) \tilde{B}_{lm} + \mu \Gamma \tilde{\psi}_{mX} = J(\tilde{\psi}_m, \tilde{B}_{lm}) ,$$

$$(II.2c) \quad (\partial_z^2 + \mu \partial_X^2) \tilde{B}_{um} - N_d^2 \tilde{\psi}_{mX} = J(\tilde{\psi}_m, \tilde{B}_{um}) .$$

These have the solution

$$(II.3a) \quad \tilde{B}_{um}(X, z) = \mu^{1/2} \theta(X) + \mu^{3/2} B_{um3}(X, z) + O(\mu^2) ,$$

$$(II.3b) \quad \tilde{B}_{\ell m}(X, z) = \mu^{3/2} B_{\ell m 3}(X, z) + O(\mu^2) ,$$

$$(II.3c) \quad \tilde{\psi}_m(X, z) = \mu \tilde{\psi}_{m2}(X, z) + O(\mu^2) ,$$

where, since $\Gamma = N_c^2 + N_d^2 = \mu + \Gamma_0$,

$$(II.4a) \quad \partial_z^4 \tilde{\psi}_{m2} + \theta_X = 0 ,$$

$$(II.4b) \quad \partial_z^2 \tilde{B}_{\ell m 3} + \Gamma_0 \psi_{m2X} = 0 ,$$

$$(II.4c) \quad \partial_z^2 \tilde{B}_{\ell m 3} - N_d^2 \psi_{m2X} = 0 .$$

Using the boundary conditions

$$(II.5) \quad \tilde{\psi}_m(X, z) = \tilde{\psi}_{mzz}(X, z) = \tilde{B}_{\ell, u}(X, z) = 0 \quad \text{at } z = 0, \pi ,$$

I find from (II.4a) that

$$(II.6a) \quad \tilde{\psi}_{m2} = -\theta_X \cdot S_1(z) ,$$

$$(II.6b) \quad S_1(z) = \frac{1}{24}(\zeta^2 - p^2)(\zeta^2 - 5p^2) ,$$

$$(II.6c) \quad \zeta \equiv z - (\pi/2) ,$$

$$(II.6d) \quad p = \pi/2 .$$

From (II.4b,c)

$$(II.7a) \quad \begin{bmatrix} \tilde{B}_{\ell m 3} \\ \tilde{B}_{u m 3} \end{bmatrix} = \begin{bmatrix} -\Gamma_0 \\ N_d^2 \end{bmatrix} \theta_{XX} S_2(z) ,$$

where

$$(II.7b) \quad S_2(z) = -\frac{1}{720} [\zeta^6 - 15\zeta^4 p^2 + 75\zeta^2 p^4 - 61p^6] .$$

I will require the Fourier expansions of $S_1(z)$ and $S_2(z)$,

$$(II.8a) \quad S_1(z) = \sum_{n=1}^{\infty} \hat{S}_{1n} \sin nz ,$$

$$(II.8b) \quad S_2(z) = \sum_{n=1}^{\infty} \hat{S}_{2n} \sin nz .$$

Rather than computing the Fourier coefficients directly from the expressions (II.6b) and (II.7b), I note that by construction,

$$(II.9a) \quad d^4 S_1 / dz^4 = 1 , \quad S_1 = d^2 S_1 / dz^2 = 0 \quad \text{at } z = 0, \pi ,$$

$$(II.9b) \quad d^6 S_2 / dz^6 = -1 , \quad S_2 = d^2 S_2 / dz^2 = d^4 S_2 / dz^4 = 0 \quad \text{at } z = 0, \pi .$$

Integrating by parts,

$$\begin{aligned} S_{1n} &= \frac{2}{\pi} \int_0^{\pi} S_1(z) \sin nz \, dz \\ &= \frac{2}{\pi n^4} \int_0^{\pi} S_{1zzzz} \sin nz \, dz , \end{aligned}$$

$$(II.10a) \quad \hat{S}_{1n} = \begin{cases} 0 & n \text{ even} \\ 4/\pi n^5 & n \text{ odd} \end{cases} .$$

Similarly

$$(II.10b) \quad \hat{S}_{2n} = \begin{cases} 0 & n \text{ even} \\ 4/\pi n^7 & n \text{ odd} \end{cases} .$$

Thus, to a very good approximation (1% for $S_1(z)$ and .1% for $S_2(z)$),

$$(II.11) \quad S_1(z) \approx S_2(z) \approx \frac{4}{\pi} \sin z$$

The mean velocity, from (II.6a),

$$(II.12a) \quad \tilde{v}_m = \mu \theta_X (dS_1/dz) \approx \mu \theta_X \cdot \frac{4}{\pi} \cos z ,$$

$$(II.12b) \quad \tilde{w}_m = -\mu^{3/2} \theta_{XX} S_1 \approx -\mu^{3/2} \theta_{XX} \cdot \frac{4}{\pi} \sin z ,$$

is an inflow at low levels and an outflow at high levels from a region of boundary heating, where there is a weak upward motion which produces a liquid water maximum,

$$(II.12c) \quad \tilde{B}_{\ell m} = -\Gamma_o \mu^{3/2} \theta_{XX} S_2 \approx -\Gamma_o \mu^{3/2} \theta_{XX} \cdot \frac{4}{\pi} \sin z \approx \Gamma_o \tilde{w}_m .$$

This source of liquid water is the most important effect of the mean flow on the convection. The relationship is exact for the $\sin(z)$ component of (II.12c), which I denote by carats:

$$(II.12d) \quad \hat{B}_{\ell m 3}(X, \tau) = \Gamma_o \hat{w}_{m 3}(X, \tau) .$$

APPENDIX III

Product Formulas

I derive in this appendix identities which allow products of characteristic functions to be simplified. In the cloudy air, if p and q are nonzero,

$$(III.1a) \quad f_c(x,p) = \cosh px ,$$

$$(III.1b) \quad g_c(x,p) = \sinh px/p ,$$

so

$$(III.2a) \quad f_c(x,p)f_c(x,q) = \cosh px \cosh qx \\ = \frac{1}{2}\{f_c(x,p+q) + f_c(x,p-q)\} ,$$

$$(III.2b) \quad f_c(x,p)f_c(x,q) = \frac{1}{q} \cosh px \sinh qx \\ = \frac{p+q}{2q} g_c(x,p+q) - \frac{p-q}{2q} g_c(x,p-q) ,$$

$$(III.2c) \quad g_c(x,p)g_c(x,q) = \frac{1}{pq} \sinh px \sinh qx \\ = \frac{1}{2pq} \{f_c(x,p+q) - f_c(x,p-q)\} .$$

If either p or q is zero, one simply takes the limits of the formulas above:

$$(III.3a) \quad f_c(x,0) = 1 ,$$

$$(III.3b) \quad g_c(x,0) = x ,$$

$$(III.4a) \quad f_c(x,p)f_c(x,0) = f_c(x,p) ,$$

$$(III.4b) \quad f_c(x,p)g_c(x,0) = \frac{\partial}{\partial p}\{pg_c(x,p)\} ,$$

$$(III.4c) \quad g_c(x,p)f_c(x,p) = g_c(x,p) ,$$

$$(III.4d) \quad g_c(x,p)g_c(x,0) = p^{-1} \frac{\partial f_c(x,p)}{\partial p} .$$

In the dry air

$$(III.5) \quad f_d(x,p) = -pg_d(x,p) = \exp\{-p(|x| - a_0/2)\} ,$$

so

$$(III.6a) \quad f_d(x,p)f_d(x,q) = f_d(x,p+q) ,$$

$$(III.6b) \quad f_d(x,p)g_d(x,q) = \frac{p+q}{q} g_d(x,p+q) ,$$

$$(III.6c) \quad g_d(x,p)g_d(x,q) = \frac{1}{pq} f_d(x,p+q) .$$

The case that p or q is zero never appears in the calculation and will not be considered.

APPENDIX IV

Inverting the "Linear" Operator

I will repeatedly be forced to find particular solutions of inhomogeneous equations

$$(IV.1a) \quad \nabla_m^4 \psi - (N_o^2 / \Gamma_o) B_{\ell x} = R_1(x) ,$$

$$(IV.1b) \quad \nabla_m^2 B_{\ell} + \Gamma_o \psi = R_2(x) ,$$

where

$$(IV.1c) \quad \nabla_m^2 = (d^2/dx^2) - m^2 ,$$

and N_o^2 can be either $-N_{co}^2$ or N_d^2 , depending on whether $|x| > a_o/2$, the cloud boundary for the neutral isolated linear mode. In general, the inhomogeneities will be sums of terms

$$(IV.2a) \quad R_1(x) = R_1 g(x, \rho) ,$$

$$(IV.2b) \quad R_2(x) = R_2 f(x, \rho) .$$

For this choice of R_1 and R_2 , there is an inhomogeneous solution

$$(IV.3a) \quad \psi = Q_1[m_1 g(x, \rho)] ,$$

$$(IV.3b) \quad B_\lambda = Q_1[m_2 f(x, \rho)] ,$$

where

$$(IV.3c) \quad m_1 = R_1(\rho^2 - m^2) + R_2 \cdot N_o^2 \rho^2 / \Gamma_o ,$$

$$(IV.3d) \quad m_2 = -R_1 \Gamma_o + R_2(\rho^2 - m^2) ,$$

and the operator Q_1 is defined

$$(IV.3e) \quad Q_1 F(\rho) = \begin{cases} \frac{F(\rho)}{p_m(\rho)} & \text{if } p_m(\rho) \neq 0 , \\ \frac{dF/d\rho}{dp_m/d\rho} & \text{if } p_m(\rho) = 0 , \end{cases}$$

$$(IV.3f) \quad p_m(\rho) = (\rho^2 - m^2)^3 + N_o^2 \rho^2 .$$

This can easily be verified by direct substitution for $p_m(\rho) \neq 0$,
after recalling

$$(IV.4a) \quad \frac{\partial^2 f}{\partial x^2}(x, \rho) = \rho^2 f(x, \rho) ,$$

$$(IV.4b) \quad \frac{\partial^2 f}{\partial x^2}(x, \rho) = \rho^2 g(x, \rho) ,$$

$$(IV.4c) \quad f(x, \rho) = \frac{\partial g}{\partial x}(x, \rho) .$$

Suppose $p_n(\rho_0) = 0$. Then

$$(IV.5a) \quad h = m_1(\rho_0) \frac{g(x, \rho_0)}{p_m(\rho)},$$

$$(IV.5b) \quad B_h = m_2(\rho_0) \frac{f(x, \rho_0)}{p_m(\rho)},$$

solves the homogeneous equation (IV.1) for any ρ in the neighborhood of ρ_0 and may be subtracted from the inhomogeneous solution already found. Taking the limit $\rho \rightarrow \rho_0$, I find an inhomogeneous solution by l'Hopital's rule:

$$(IV.6a) \quad \psi = \lim_{\rho \rightarrow \rho_0} \frac{m_1 g(x, \rho) - m_1(\rho_0) g(x, \rho_0)}{p_m(\rho)} = Q_1 m_1 g(x, \rho_0)$$

$$(IV.6b) \quad B_\rho = \lim_{\rho \rightarrow \rho_0} \frac{m_2 f(x, \rho) - m_2(\rho_0) f(x, \rho_0)}{p_m(\rho)} = Q_1 m_2 f(x, \rho_0),$$

which is exactly as claimed in (IV.3e).

In fact, I will also need to evaluate derivatives of ψ and B with respect to x , so I will have to calculate

$$(IV.7) \quad Q_{n+1}(x, \rho) \equiv (\partial^n / \partial x^n) Q_1 F(x, \rho).$$

when $F(x, \rho) = f(x, \rho)$ or $g(x, \rho)$. This can be done quite neatly by noting that since Q_1 depends on ρ alone, it commutes with $\partial / \partial x$. This allows one to conclude

$$(IV.8a) \quad \frac{\partial^n \psi(x, \rho)}{\partial x^n} = Q_{n+1} m_1 g(x, \rho)$$

$$(IV.8b) \quad \frac{\partial^n B_\ell(x, \rho)}{\partial x^n} = Q_{n+1} m_2 f(x, \rho)$$

where

$$(IV.9a) \quad Q_{n+1} g(x, \rho) = \begin{cases} \frac{1}{p_m(\rho)} \begin{cases} \rho^n g(x, \rho) & n \text{ even} \\ \rho^{n+1} f(x, \rho) & n \text{ odd} \end{cases} & p_m(\rho) \neq 0 \\ \frac{1}{dp_m/d\rho} \begin{cases} [n\rho^{n-1} + \rho \frac{n\partial}{\partial\rho}] g(x, \rho) & n \text{ even} \\ [(n-1)\rho^{n-2} + \rho^{n-1} \frac{\partial}{\partial\rho}] f(x, \rho) & n \text{ odd} \end{cases} & p_m(\rho) = 0 \end{cases}$$

$$(IV.9b) \quad Q_{n+1} f(x, \rho) = \begin{cases} \frac{1}{p_m(\rho)} \begin{cases} \rho^n f(x, \rho) & n \text{ even} \\ \rho^{n+1} g(x, \rho) & n \text{ odd} \end{cases} & p_m(\rho) \neq 0 \\ \frac{1}{dp_m/d\rho} \begin{cases} [n\rho^{n-1} + \rho \frac{n\partial}{\partial\rho}] f(x, \rho) & n \text{ even} \\ [(n+1)\rho^n + \rho^{n+1} \frac{\partial}{\partial\rho}] g(x, \rho) & n \text{ odd} \end{cases} & p_m(\rho) = 0 \end{cases}$$

To explicitly compute these derivatives I recollect from (3.2.20) and (3.2.23) that in the cloudy air

$$(IV.10a) \quad f_c(x, \rho) = \cosh \rho x, \quad \frac{\partial f_c}{\partial \rho} = x \sinh \rho x$$

$$(IV.10b) \quad g_c(x, \rho) = \frac{\sinh \rho x}{\rho}, \quad \frac{\partial g_c}{\partial \rho} = \frac{x \cosh \rho x}{\rho} - \frac{\sinh \rho x}{\rho^2}$$

or if $\rho = 0$,

$$(IV.10c) \quad f_c(x,0) = 1 ,$$

$$(IV.10d) \quad g_c(x,0) = x ,$$

while in the "dry", i.e. unsaturated, air

$$(IV.11a) \quad f_d(x,\rho) = \exp\{-\rho(x - \frac{a_0}{2})\}, \quad \frac{\partial f_d}{\partial \rho} = -(x - \frac{a_0}{2}) \exp\{-\rho(x - \frac{a_0}{2})\} ,$$

$$(IV.11b) \quad g_d(x,\rho) = -\frac{1}{\rho} \exp\{-\rho(x - \frac{a_0}{2})\}, \quad \frac{\partial g_d}{\partial \rho} = \left\{ \frac{x - \frac{a_0}{2}}{\rho} + \frac{1}{\rho^2} \right\} \exp\{-\rho(x - \frac{a_0}{2})\} .$$

It is also convenient to define the simpler operator

$$(IV.12) \quad D_{n+1}F(x) \equiv (d^n/dx^n)F(x) .$$

The effect of applying D_{n+1} to $g(x,\rho)$ and $f(x,\rho)$ is

$$(IV.13a) \quad D_{n+1}g(x,\rho) = \begin{cases} \rho^n g(x,\rho) & n \text{ even} \\ \rho^{n-1} f(x,\rho) & n \text{ odd} \end{cases} ,$$

$$(IV.13b) \quad D_{n+1}f(x,\rho) = \begin{cases} \rho^n f(x,\rho) & n \text{ even} \\ \rho^{n+1} g(x,\rho) & n \text{ odd} \end{cases} .$$

Lastly, it is necessary to add homogeneous solutions to the inhomogeneous solutions (IV.3a,b) to satisfy appropriate matching conditions at $x = \pm a_0/2$. The most general homogeneous solution of (IV.1a,b) which decays as $x \rightarrow \pm\infty$ and for which $B_\rho(x)$ is symmetric about $x = 0$ is

$$(IV.14a) \quad \psi_s^{(m)}(x) = \begin{cases} \psi_{sd}^{(m)}(x) = \sum_i \gamma_{di}^{(m)} b_{dsi}^{(m)} g_d(x, \rho_{di}^{(m)}) & |x| > a_0/2 \\ \psi_{sc}^{(m)}(x) = \sum_i \gamma_{ci}^{(m)} b_{csi}^{(m)} g_c(x, \rho_{ci}^{(m)}) & |x| < a_0/2 \end{cases},$$

$$(IV.14b) \quad B_{\ell s}^{(m)}(x) = \begin{cases} B_{sd}^{(m)}(x) = \sum_i b_{dsi}^{(m)} f_d(x, \rho_{di}^{(m)}) & |x| > a_0/2 \\ B_{sc}^{(m)}(x) = \sum_i b_{csi}^{(m)} f_c(x, \rho_{ci}^{(m)}) & |x| < a_0/2 \end{cases},$$

where

$$(IV.14c) \quad \gamma_{c,di}^{(m)} = (1/\Gamma_0)(m^2 - \rho_{di}^{(m)2}).$$

The most general homogeneous solution for which $B_\ell(x)$ is antisymmetric about $x = 0$ is

$$(IV.15a) \quad \psi_a^{(m)}(x) = \begin{cases} \psi_{ad}^{(m)}(x) = \begin{pmatrix} + \\ - \end{pmatrix} \sum_i \gamma_{di}^{(m)} b_{dai}^{(m)} g_d(x, \rho_{di}^{(m)}) & \begin{cases} x > \frac{1}{2}a_0 \\ x < -\frac{1}{2}a_0 \end{cases} \\ \psi_{sc}^{(m)}(x) = \sum_i \gamma_{ci}^{(m)} b_{cai}^{(m)} f_c(x, \rho_{ci}^{(m)}) & |x| < \frac{1}{2}a_0 \end{cases},$$

$$(IV.15b) \quad B_{\ell s}^{(m)}(x) = \begin{cases} B_{ad}^{(m)}(x) = \begin{pmatrix} + \\ - \end{pmatrix} \sum_i b_{dci}^{(m)} f_d(x, \rho_{di}^{(m)}) & \begin{cases} x > \frac{1}{2}a_0 \\ x < -\frac{1}{2}a_0 \end{cases} \\ B_{ac}^{(m)}(x) = \sum_i \rho_{ci}^{(m)2} b_{cai}^{(m)} g_c(x, \rho_{ci}^{(m)}) & |x| < \frac{1}{2}a_0 \end{cases}.$$

The six matching conditions (that $\tilde{B}_\ell(x, z, t)$ and its first x -derivative and $\tilde{\psi}(x, z, t)$ and its first three x -derivatives match at the cloud boundary) translate into jump conditions at $x = \pm \frac{1}{2}a_0$ on the homogeneous solution:

$$(IV.16a) \quad \lim_{\epsilon \rightarrow 0} \frac{d^{n-1} \psi^{(m)}}{dx^{n-1}} \bigg|_{\pm(\frac{a_0}{2} \pm \epsilon)} + \delta_{n4} B_\ell^{(m)}(\frac{1}{2}a_0) = \Delta_n^\pm[\psi], \quad n = 1, 2, 3, 4,$$

$$(IV.16b) \quad \lim_{\epsilon \rightarrow 0} \frac{d^{n-1} B_\ell^{(m)}}{dx^{n-1}} \Bigg|_{\pm(\frac{a_0}{2} \pm \epsilon)} = \Delta_n^\pm [B_\ell], \quad n = 1, 2,$$

where I assume that Δ_n^\pm are known. Decompose $\psi^{(m)}$ and $B_\ell^{(m)}$ into parts associated with the symmetric solution and the antisymmetric solution:

$$(IV.17a) \quad \psi^{(m)}(x) = \psi_s^{(m)}(x) + \psi_a^{(m)}(x),$$

$$(IV.17b) \quad B_\ell^{(m)}(x) = B_s^{(m)}(x) + B_a^{(m)}(x).$$

$\psi_a^{(m)}(x)$ and $B_s^{(m)}(x)$ are even, while $\psi_s^{(m)}(x)$ and $B_a^{(m)}(x)$ are odd.

Thus

$$(IV.18a) \quad \frac{d^{n-1} \psi_s}{dx^{n-1}} \Bigg|_{\frac{a_0}{2} \pm \epsilon} = \frac{1}{2} \frac{d^{n-1}}{dx^{n-1}} \left\{ \psi^{(m)}(x) - \psi^{(m)}(-x) \right\} \Bigg|_{\frac{a_0}{2} \pm \epsilon},$$

$$(IV.18b) \quad \Delta_{ns}[\psi] = \frac{1}{2} \{ \Delta_n^+[\psi] + (-1)^n \Delta_n^-[\psi] \}.$$

Similarly

$$(IV.18c) \quad \Delta_{na}[\psi] = \frac{1}{2} \{ \Delta_n^+[\psi] - (-1)^n \Delta_n^-[\psi] \},$$

$$(IV.18d) \quad \Delta_{ns}[B_\ell] = \frac{1}{2} \{ \Delta_n^+[B_\ell] - (-1)^n \Delta_n^-[B_\ell] \},$$

$$(IV.18e) \quad \Delta_{na}[B_\ell] = \frac{1}{2} \{ \Delta_n^+[B_\ell] + (-1)^n \Delta_n^-[B_\ell] \}.$$

The conditions (IV.16a,b) generate two matrix equations, one for the coefficients in the symmetric homogeneous solution and one for the coefficients in the antisymmetric homogeneous solution,

$$(IV.19a) \quad M_s^{(m)} \underline{b}_s^{(m)} = \underline{R}_s ,$$

$$(IV.19b) \quad M_a^{(m)} \underline{b}_a^{(m)} = \underline{R}_a ,$$

where

$$(IV.20a) \quad \underline{b}_s^{(m)} = [b_{ds1}^{(m)} \ b_{ds2}^{(m)} \ b_{ds3}^{(m)} \ -b_{cs1}^{(m)} \ -b_{cs2}^{(m)} \ -b_{cs3}^{(m)}]^T ,$$

$$(IV.20b) \quad \underline{R}_s^{(m)} = [\Delta_{1s} [B_\varrho] \Delta_{2s} [B_\varrho] \Delta_{1s} [\psi] \Delta_{2s} [\psi] \Delta_{3s} [\psi] \Delta_{4s} [\psi]]^T ,$$

and similarly for $\underline{b}_a^{(m)}$ and \underline{R}_a with "s" replaced by "a". The matching matrices are

$$(IV.21a) \quad M_s^{(m)} = \begin{bmatrix} D_1 f_{d1} & D_1 f_{d2} & D_1 f_{d3} & D_1 f_{c1} & D_1 f_{c2} & D_1 f_{c3} \\ D_2 f_{d1} & D_2 f_{d2} & D_2 f_{d3} & D_2 f_{c1} & D_2 f_{c2} & D_2 f_{c3} \\ \gamma_{d1}^{D_1} g_{d1} & \gamma_{d2}^{D_1} g_{d2} & \gamma_{d3}^{D_1} g_{d3} & \gamma_{c1}^{D_1} g_{c1} & \gamma_{c2}^{D_1} g_{c2} & \gamma_{c3}^{D_1} g_{c3} \\ \gamma_{d1}^{D_2} g_{d1} & \gamma_{d2}^{D_2} g_{d2} & \gamma_{d3}^{D_2} g_{d3} & \gamma_{c1}^{D_2} g_{c1} & \gamma_{c2}^{D_2} g_{c2} & \gamma_{c3}^{D_2} g_{c3} \\ \gamma_{d1}^{D_3} g_{d1} & \gamma_{d2}^{D_3} g_{d2} & \gamma_{d3}^{D_3} g_{d3} & \gamma_{c1}^{D_3} g_{c1} & \gamma_{c2}^{D_3} g_{c2} & \gamma_{c3}^{D_3} g_{c3} \\ (\gamma_{d1}^{D_4} g_{d1} & (\gamma_{d2}^{D_4} g_{d2} & (\gamma_{d3}^{D_4} g_{d3} & \gamma_{c1}^{D_4} g_{c1} & \gamma_{c2}^{D_4} g_{c2} & \gamma_{c3}^{D_4} g_{c3} \\ - D_1 f_{d1}) & - D_1 f_{d2}) & - D_1 f_{d3}) \end{bmatrix} ,$$

(IV.21b)

$$M_a^{(m)} = \begin{bmatrix} D_1^f d_1 & D_1^f d_2 & D_1^f d_3 & \rho_{c1}^2 D_1^g c_1 & \rho_{c2}^2 D_1^g c_2 & \rho_{c3}^2 D_1^g c_3 \\ D_2^f d_1 & D_2^f d_2 & D_3^f d_3 & \rho_{c1}^2 D_2^g c_1 & \rho_{c2}^2 D_2^g c_2 & \rho_{c3}^2 D_2^g c_3 \\ \gamma_{d1} D_1^g d_1 & \gamma_{d2} D_1^g d_2 & \gamma_{d3} D_1^g d_3 & \gamma_{c1} D_1^f c_1 & \gamma_{c2} D_1^f c_2 & \gamma_{c3} D_1^f c_3 \\ \gamma_{d2} D_2^g d_1 & \gamma_{d2} D_2^g d_2 & \gamma_{d3} D_2^g d_3 & \gamma_{c1} D_2^f c_1 & \gamma_{c2} D_2^f c_2 & \gamma_{c3} D_2^f c_3 \\ \gamma_{d1} D_3^g d_1 & \gamma_{d2} D_3^g d_2 & \gamma_{d3} D_3^g d_3 & \gamma_{c1} D_3^f c_1 & \gamma_{c2} D_3^f c_2 & \gamma_{c3} D_3^f c_3 \\ (\gamma_{d1} D_4^g d_1 & (\gamma_{d2} D_4^g d_2 & (\gamma_{d3} D_4^g d_3 & \gamma_{d1} D_4^f c_1 & \gamma_{c2} D_4^f c_2 & \gamma_{c3} D_4^f c_3 \\ - D_1^f d_1) & - D_1^f d_2) & - D_1^f d_3) \end{bmatrix},$$

where

$$(IV.21c) \quad \binom{f}{g}_{c,di} = \binom{f}{g}_{c,d} \left(\frac{a_0}{2}, \rho_{c,di} \right),$$

as in section 3.5.

The matrices $M_s^{(m)}$ and $M_u^{(m)}$ govern steady symmetric and anti-symmetric perturbations of the isolated neutral cloud eigenfunction. In sections 3.4 and 3.7 I showed that unforced perturbations with vertical structure $\sin(mz)$, $m > 1$, cannot grow as fast as the eigenfunction itself, and thus cannot be steady. Therefore

$$(IV.22) \quad M_s^{(m)}, M_u^{(m)} \text{ are nonsingular, } m > 1.$$

However there is a steady symmetric perturbation proportional to $\sin(z)$,

$$(IV.23a) \quad \underline{b}_{-so}^{(1)} = [b_{d1} \ b_{d2} \ b_{d3} \ -b_{c1} \ -b_{c2} \ -b_{c3}]^T,$$

which represents a slight change in amplitude of the eigenmode, so

$$(IV.23b) \quad M_s^{(1)} \underline{b}_{so}^{(1)} = 0.$$

A slight translation of the eigenmode produces a steady antisymmetric perturbation

$$(IV.24a) \quad \underline{b}_{-ao}^{(1)T} = [-\rho_{d1} b_{d1} \ -\rho_{d2} b_{d2} \ -\rho_{d3} b_{d3} \ -b_{c1} \ -b_{c2} \ -b_{c3}],$$

corresponding to the representation of dL/dx in the basis of characteristic functions, for which

$$(IV.24b) \quad M_a^{(1)} \underline{b}_{so}^{(1)} = 0.$$

The right hand sides \underline{R}_s and \underline{R}_a must be orthogonal to the null vectors of the adjoint matrices, which are computed in appendix VI:

$$(IV.25a) \quad \underline{u}_s \cdot \underline{R}_s = 0, \quad M_s^{(1)T} \underline{u}_s = 0.$$

$$(IV.25b) \quad \underline{u}_a \cdot \underline{R}_a = 0, \quad M_a^{(1)T} \underline{u}_a = 0.$$

APPENDIX V

The $O(\mu^{3/2})$ Inhomogeneous Solutions

I calculate the four sets of inhomogeneous terms (4.3.18-21) due to nonlinearity, time dependence, supercriticality, and the mean fields, and for each set I find a particular solution to the equations (4.3.17) in the cloudy and the dry air. To the sum of these solutions I add a homogeneous solution in the dry air which accounts for the growing exponential behavior at large x due to neighboring clouds.

Nonlinear Self Interaction Terms

From (4.3.18),

$$\begin{aligned}
 \text{(V.1a)} \quad \hat{R}_{11} &= \hat{J}(A_j \psi_1(x) \sin z, A_j^2 \nabla_2^2 \psi_2(x) \sin 2z) \\
 &\quad + \hat{J}(A_j^2 \psi_2(x) \sin 2z, A_j \nabla_1^2 \psi_1(x) \sin z) \\
 &= A_j^3 [J_{31}(x-x_j) + J_{32}(x-x_j)] ,
 \end{aligned}$$

$$\begin{aligned}
 \text{(V.1b)} \quad J_{31}(x-x_j) &= \psi_{1x} \nabla_2^2 \psi_2 \overbrace{\sin z \quad 2 \cos 2z} - \psi_1 \nabla_2^2 \psi_{2x} \overbrace{\cos z \quad \sin 2z} \\
 &= -\psi_{1x} \nabla_2^2 \psi_2 \quad \frac{1}{2} \psi_1 \nabla_2^2 \psi_{2x} ,
 \end{aligned}$$

$$\begin{aligned}
 \text{(V.1c)} \quad J_{32}(x-x_j) &= \psi_{2x} \nabla_1^2 \psi_1 \overbrace{\sin 2z \quad \cos z} - \psi_2 \nabla_1^2 \psi_{1x} \overbrace{2 \cos 2z \quad \sin z} \\
 &= \frac{1}{2} \psi_{2x} \nabla_1^2 \psi_1 + \psi_2 \nabla_1^2 \psi_{1x} ,
 \end{aligned}$$

while

$$\begin{aligned}
 \hat{R} &= \hat{J}(A_1 \psi_1(x) \sin z, A_j^2 B_2(x) \sin 2x) \\
 &\quad + \hat{J}(A_j^2 \psi_2(x) \sin 2z, A_j B_1(x) \sin z) \\
 &= A_j^3 [J_{33}(x) + J_{34}(x)] ,
 \end{aligned}
 \tag{V.2a}$$

$$J_{33}(x-x_j) = -\psi_{1x} B_2 - \frac{1}{2} \psi_1 B_{2x} ,
 \tag{V.2b}$$

$$J_{34}(x-x_j) = \frac{1}{2} \psi_{2x} B_1 + \psi_2 B_{1x} .
 \tag{V.2c}$$

Using the explicit formulas (4.2.18) and (4.3.7-8) to expand the ψ 's and B 's,

$$\begin{aligned}
 J_{31}(x) &= -\left[\sum_k \gamma_{ck} b_{ck} f_c(x, \rho_{ck}) \right] \left[\sum_i \gamma_{ci}^{(2)} b_{ci}^{(2)} (-\Gamma_o \gamma_{ci}^{(2)}) g(x, \rho_{ci}^{(2)}) \right. \\
 &\quad + \sum_{i,j} \psi_{21c}^{(i,j)} (\rho_{ci} + \rho_{cj})^2 g_c(x, \rho_{ci} + \rho_{cj}) \\
 &\quad \left. + \psi_{22c}^{(i,j)} (\rho_{ci} - \rho_{cj})^2 g_c(x, \rho_{ci} - \rho_{cj}) \right] \\
 &\quad - \frac{1}{2} \left[\sum_k \gamma_{ck} b_{ck} g_c(x, \rho_{ck}) \right] \left[\sum_i \gamma_{ci}^{(2)} b_{ci}^{(2)} (-\Gamma_o \gamma_{ci}^{(2)}) f_c(x, \rho_{ci}^{(2)}) \right. \\
 &\quad + \sum_{i,j} \psi_{21c}^{(i,j)} (\rho_{ci} + \rho_{cj})^2 f_c(x, \rho_{ci} + \rho_{cj}) \\
 &\quad \left. + \psi_{22c}^{(i,j)} (\rho_{ci} - \rho_{cj})^2 f_c(x, \rho_{ci} - \rho_{cj}) \right] \\
 &= \sum_{i,k} \Gamma_o \gamma_{ck} \gamma_{ci}^{(2)2} b_{ck} b_{ci}^{(2)} [f_c(x, \rho_{ck}) g_c(x, \rho_{ci}^{(2)}) \\
 &\quad + \frac{1}{2} g_c(x, \rho_{ck}) f_c(x, \rho_{ci}^{(2)})]
 \end{aligned}
 \tag{V.3}$$

$$\begin{aligned}
& + \sum_{i,j,k} \gamma_{ck} (\rho_{ci} + \rho_{cj})^2 \psi_{21c}^{(i,j)} b_{ck} [-f_c(x, \rho_{ck}) g_c(x, \rho_{ci} + \rho_{cj}) \\
& \quad - \frac{1}{2} g_c(x, \rho_{ck}) f_c(x, \rho_{ci} + \rho_{cj})] \\
& + \sum_{i,j,k} \gamma_{ck} (\rho_{ci} - \rho_{cj})^2 \psi_{22c}^{(i,j)} b_{ck} [-f_c(x, \rho_{ck}) g_c(x, \rho_{ci} - \rho_{cj}) \\
& \quad - \frac{1}{2} g_c(x, \rho_{ck}) f_c(x, \rho_{ci} - \rho_{cj})] .
\end{aligned}$$

Simplifying the products using appendix III, in the cloudy air

$$\begin{aligned}
(V.4a) \quad J_{31c}(x) &= \sum_{i,k} \{c_{ik+}^{(1)} g_c(x, \rho_{ck} + \rho_{ci}^{(2)}) + c_{ik-}^{(1)} g_c(x, \rho_{ck} - \rho_{ci}^{(2)})\} \\
& + \sum_{i,j,k} \{d_{ijk+}^{(1)} g_c(x, \rho_{ck} + \rho_{ci} + \rho_{cj}) + d_{ijk-}^{(1)} g_c(x, \rho_{ck} - \rho_{ci} - \rho_{cj})\} \\
& + \sum_{i,j,k} \{e_{ijk+}^{(1)} g_c(x, \rho_{ck} + \rho_{ci} - \rho_{cj}) + e_{ijk-}^{(1)} g_c(x, \rho_{ck} - \rho_{ci} + \rho_{cj})\},
\end{aligned}$$

where

$$(V.4b) \quad c_{ik\pm}^{(1)} = \frac{1}{2} (\rho_{ck} \pm \rho_{ci}^{(2)}) \left\{ \frac{\pm 1}{\rho_{ci}^{(2)}} + \frac{1}{2\rho_{ck}} \right\} \gamma_{ck} \gamma_{ci}^{(2)^2} \Gamma_o b_{ck} b_{ci}^{(2)}$$

$$(V.4c) \quad d_{ijk\pm}^{(1)} = \frac{1}{2} (\rho_{ck} \pm [\rho_{ci} + \rho_{cj}]) \left\{ \frac{\mp 1}{\rho_{ci} + \rho_{cj}} - \frac{1}{2\rho_{ck}} \right\} \gamma_{ck} (\rho_{ci} + \rho_{cj})^2 \psi_{21c}^{(i,j)} b_{ck}$$

$$\begin{aligned}
(V.4d) \quad e_{ijk\pm}^{(1)} &= \frac{1}{2} (\rho_{ck} \pm [\rho_{ci} - \rho_{cj}]) \left\{ \frac{\mp 1}{\rho_{ci} - \rho_{cj}} - \frac{1}{2\rho_{ck}} \right\} \gamma_{ck} (\rho_{ci} - \rho_{cj})^2 \psi_{22c}^{(i,j)} b_{ck} \\
& \quad (= 0 \quad \text{if } i=j)
\end{aligned}$$

In the dry air, analogous manipulations show

$$(V.5a) \quad J_{31d}(x) = \sum_{i,j} c_{ikd}^{(1)} g_d(x, \rho_{dk} + \rho_{di}^{(2)}) + \sum_{i,j,k} d_{ijkd}^{(1)} g_d(x, \rho_{dk} + \rho_{di} + \rho_{dj})$$

$$(V.5b) \quad c_{ikd}^{(1)} = (\rho_{dk} + \rho_{di}^{(2)}) \left\{ \frac{1}{\rho_{di}^{(2)}} + \frac{1}{2\rho_{dk}} \right\} \Gamma_o \gamma_{dk} \gamma_{di}^{(2)^2} b_{dk} b_{di}^{(2)}$$

$$(V.5c) \quad d_{ijkd}^{(1)} = (\rho_{dk} + \rho_{di} + \rho_{dj}) \left\{ -\frac{1}{\rho_{di} + \rho_{dj}} - \frac{1}{2\rho_{dk}} \right\} \gamma_{dk} (\rho_{di} + \rho_{dj})^2 \psi_{21d}^{(i,j)} b_{dk}$$

Next,

$$(V.6a) \quad J_{32c}(x) = \frac{1}{2} \left[\sum_k \gamma_{ck} b_{ck} (-\Gamma_o \gamma_{ck}) g_c(x, \rho_{ck}) \right] \left[\sum_i \gamma_{ci}^{(2)} b_{ci}^{(2)} f_c(x, \rho_{ci}^{(2)}) \right. \\ \left. + \sum_{i,j} \{ \psi_{21c}^{(i,j)} f_c(x, \rho_{ci} + \rho_{cj}) \right. \\ \left. + \psi_{22c}^{(i,j)} f_c(x, \rho_{ci} - \rho_{cj}) \} \right] \\ + \left[\sum_k \gamma_{ck} b_{ck} (-\Gamma_o \gamma_{ck}) f(x, \rho_{ck}) \right] \left[\sum_i \gamma_{ci}^{(2)} b_{ci}^{(2)} g_c(x, \rho_{ci}^{(2)}) \right. \\ \left. + \sum_{i,j} \{ \psi_{21c}^{(i,j)} g_c(x, \rho_{ci} + \rho_{cj}) \right. \\ \left. + \psi_{22c}^{(i,j)} g_c(x, \rho_{ci} - \rho_{cj}) \} \right] \\ = \sum_{i,k} \{ c_{ik+}^{(2)} g_c(x, \rho_{ck} + \rho_{ci}^{(2)}) + c_{ik-}^{(2)} g_c(x, \rho_{ck} - \rho_{ci}^{(2)}) \} \\ + \sum_{i,j,k} \{ d_{ijk+}^{(2)} g_c(x, \rho_{ck} + \rho_{ci} + \rho_{cj}) + d_{ijk-}^{(2)} g_c(x, \rho_{ck} - \rho_{ci} - \rho_{cj}) \} \\ + \sum_{i,j,k} \{ e_{ijk+}^{(2)} g_c(x, \rho_{ck} + \rho_{ci} - \rho_{cj}) + e_{ijk-}^{(2)} g_c(x, \rho_{ck} - \rho_{ci} + \rho_{cj}) \}$$

where

$$(V.6b) \quad c_{ik\pm}^{(2)} = \frac{1}{2} (\rho_{ck} \pm \rho_{ci}^{(2)}) \left\{ \pm \frac{1}{\rho_{ci}^{(2)}} + \frac{1}{2\rho_{ck}} \right\} \Gamma_o \gamma_{ck}^2 \gamma_{ci}^{(2)} b_{ck} b_{ci}^{(2)},$$

$$(V.6c) \quad d_{ijk\pm}^{(2)} = \frac{1}{2}(\rho_{ck}^{\pm[\rho_{ci}+\rho_{cj}]}) \left[\mp \frac{1}{\rho_{ci}+\rho_{cj}} - \frac{1}{2\rho_{ck}} \right] \Gamma_o \gamma_{ck}^2 \psi_{21c}^{(i,j)} b_{ck} ,$$

$$(V.6d) \quad e_{ijk\pm}^{(2)} = \frac{1}{2}(\rho_{ck}^{\pm[\rho_{ci}-\rho_{cj}]}) \left[\mp \frac{1}{\rho_{ci}-\rho_{cj}} - \frac{1}{2\rho_{ck}} \right] \Gamma_o \gamma_{ck}^2 \psi_{22c}^{(i,j)} b_{ck} ,$$

$$(\quad = 0, i = j) .$$

The last term vanishes when $i = j$ since $\psi_{22c}^{(i,j)} = 0$. In the dry air

$$(V.7a) \quad J_{32d}(x) = \sum_{i,k} c_{ikd}^{(2)} g_d(x, \rho_{dk} + \rho_{di}^{(1)}) + \sum_{i,j,k} d_{ijkd}^{(1)} g_d(x, \rho_{dk} + \rho_{di} + \rho_{dj})$$

$$(V.7b) \quad c_{ikd}^{(2)} = -(\rho_{dk} + \rho_{di}^{(2)}) \left\{ \frac{1}{\rho_{di}^{(2)}} + \frac{1}{2\rho_{dk}} \right\} \Gamma_o \gamma_{dk}^2 \psi_{di}^{(2)} b_{dk} b_{di}^{(2)}$$

$$(V.7c) \quad d_{ijkd}^{(2)} = (\rho_{dk} + \rho_{di} + \rho_{dj}) \left\{ -\frac{1}{\rho_{di} + \rho_{dj}} - \frac{1}{2\rho_{dk}} \right\} \Gamma_o \gamma_{dk}^2 \psi_{21d}^{(i,j)} b_{dk} .$$

The advection term reduces in the cloudy air to

$$(V.8a) \quad J_{33c}(x) = - \left[\sum_k \gamma_{ck} b_{ck} f_c(x, \rho_{ck}) \right] \left[\sum_i b_{ci}^{(2)} f_c(x, \rho_{ci}^{(2)}) \right. \\ \left. + \sum_{i,j} \{ B_{21c}^{(i,j)} f_c(x, \rho_{ci} + \rho_{cj}) \right. \\ \left. + B_{22c}^{(i,j)} f_c(x, \rho_{ci} - \rho_{cj}) \} \right] \\ - \frac{1}{2} \left[\sum_k \gamma_{ck} b_{ck} g_c(x, \rho_{ck}) \right] \left[\sum_i b_{ci}^{(2)} \rho_{ci}^{(2)2} g_c(x, \rho_{ci}^{(2)}) \right. \\ \left. + \sum_{i,j} \{ B_{21c}^{(i,j)} (\rho_{ci} + \rho_{cj})^2 g_c(x, \rho_{ci} + \rho_{cj}) \right. \\ \left. + B_{22c}^{(i,j)} (\rho_{ci} - \rho_{cj})^2 g_c(x, \rho_{ci} - \rho_{cj}) \} \right]$$

$$\begin{aligned}
&= \sum_{i,k} \gamma_{ck} b_{ck} b_{ci}^{(2)} [-f_c(x, \rho_{ck}) f_c(x, \rho_{ci}^{(2)}) \\
&\quad - \frac{1}{2} \rho_{ci}^{(2)2} g_c(x, \rho_{ck}) g_c(x, \rho_{ci}^{(2)})] \\
&+ \sum_{i,j,k} \gamma_{ck} b_{ck} B_{21c}^{(i,j)} [-f_c(x, \rho_{ck}) f_c(x, \rho_{ci+\rho_{cj}}) \\
&\quad - \frac{1}{2} (\rho_{ci+\rho_{cj}})^2 g_c(x, \rho_{ck}) g_c(x, \rho_{ci+\rho_{cj}})] \\
&+ \sum_{i,j,k} \gamma_{ck} b_{ck} B_{22c}^{(i,j)} [-f_c(x, \rho_{ck}) f_c(x, \rho_{ci-\rho_{cj}}) \\
&\quad - \frac{1}{2} (\rho_{ci-\rho_{cj}})^2 g_c(x, \rho_{ck}) g_c(x, \rho_{ci-\rho_{cj}})] \\
&= \sum_{i,k} \{c_{ik+}^{(3)} f_c(x, \rho_{ck+\rho_{ci}^{(2)}}) + c_{ik-}^{(3)} f_c(x, \rho_{ck-\rho_{ci}^{(2)}})\} \\
&+ \sum_{i,j,k} \{d_{ijk+}^{(3)} f_c(x, \rho_{ck+\rho_{ci+\rho_{cj}}}) + d_{ijk-}^{(3)} f_c(x, \rho_{ck-\rho_{ci-\rho_{cj}}})\} \\
&+ \sum_{i,j,k} \{e_{ijk+}^{(3)} f_c(x, \rho_{ck+\rho_{ci-\rho_{cj}}}) + e_{ijk-}^{(3)} f_c(x, \rho_{ck-\rho_{ci+\rho_{cj}}})\},
\end{aligned}$$

where

$$(V.8b) \quad c_{ik\pm}^{(3)} = -\frac{1}{2} \left(1 \pm \frac{\rho_{ci}^{(2)}}{2\rho_{ck}}\right) \gamma_{ck} b_{ck} b_{ci}^{(2)},$$

$$(V.8c) \quad d_{ijk\pm}^{(3)} = -\frac{1}{2} \left(1 \pm \frac{\rho_{ci+\rho_{cj}}}{2\rho_{ck}}\right) \gamma_{ck} b_{ck} B_{21c}^{(i,j)},$$

$$(V.8d) \quad e_{ijk\pm}^{(3)} = -\frac{1}{2} \left(1 \pm \frac{\rho_{ci-\rho_{cj}}}{2\rho_{ck}}\right) \gamma_{ck} b_{ck} B_{22c}^{(i,j)} \quad (\text{even if } i = j).$$

In the dry air,

$$(V.9a) \quad J_{33d}(x) = \sum_{i,k} c_{ikd}^{(3)} f_d(x, \rho_{dk} + \rho_{di}^{(2)}) + \sum_{i,j,k} d_{ijkd}^{(3)} f_d(x, \rho_{dk} + \rho_{di} + \rho_{dj})$$

$$(V.9b) \quad c_{ikd}^{(3)} = -(1 + \frac{\rho_{di}^{(2)}}{2\rho_{dk}}) \gamma_{dk} b_{dk} b_{di}^{(2)}$$

$$(V.9c) \quad d_{ijkd}^{(3)} = -(1 + \frac{\rho_{di} + \rho_{dj}}{2\rho_{dk}}) \gamma_{dk} b_{dk} B_{21d}^{(i,j)}$$

Lastly,

$$\begin{aligned} (V.10a) \quad J_{34c}(x) &= \frac{1}{2} \left[\sum_k b_{ck} f_c(x, \rho_{ck}) \right] \left[\sum_i \gamma_{ci}^{(2)} b_{ci}^{(2)} f_c(x, \rho_{ci}^{(2)}) \right. \\ &\quad \left. + \sum_{i,j} \{ \psi_{21c}^{(i,j)} f_c(x, \rho_{ci} + \rho_{cj}) + \psi_{22c}^{(i,j)} f_c(x, \rho_{ci} - \rho_{cj}) \} \right] \\ &\quad + \left[\sum_k b_{ck} \rho_{ck}^2 g(x, \rho_{ck}) \right] \left[\sum_i \rho_{ci}^{(2)} b_{ci} g(x, \rho_{ci}^{(2)}) \right. \\ &\quad \left. + \sum_{i,j} \{ \psi_{21c}^{(i,j)} g_c(x, \rho_{ci} + \rho_{cj}) + \psi_{22c}^{(i,j)} g_c(x, \rho_{ci} - \rho_{cj}) \} \right] \\ &= \sum_{i,k} \{ c_{ik+}^{(4)} f_c(x, \rho_{ck} + \rho_{ci}^{(2)}) + c_{ik-}^{(4)} f_c(x, \rho_{ck} - \rho_{ci}^{(2)}) \} \\ &\quad + \sum_{i,j,k} \{ d_{ijk+}^{(4)} f_c(x, \rho_{ck} + \rho_{ci} + \rho_{cj}) + d_{ijk-}^{(4)} f_c(x, \rho_{ck} - \rho_{ci} - \rho_{cj}) \} \\ &\quad + \sum_{i,j,k} \{ e_{ijk+}^{(4)} f_c(x, \rho_{ck} + \rho_{ci} - \rho_{cj}) + e_{ijk-}^{(4)} f_c(x, \rho_{ck} - \rho_{ci} + \rho_{cj}) \} \end{aligned}$$

where

$$(V.10b) \quad c_{ik\pm}^{(4)} = \frac{1}{2} \left(\frac{1}{2} \pm \frac{\rho_{ck}}{\rho_{ci}^{(2)}} \right) \gamma_{ci}^{(2)} b_{ci}^{(2)} b_{ck}$$

$$(V.10c) \quad d_{ijk\pm}^{(4)} = \frac{1}{2} \left(\frac{1}{2} \pm \frac{\rho_{ck}}{\rho_{ci} + \rho_{cj}} \right) \psi_{21c}^{(i,j)} b_{ck}$$

$$(V.10d) \quad e_{ijk\pm}^{(4)} = \frac{1}{2} \left(\frac{1}{2} \pm \frac{\rho_{ck}}{\rho_{ci} - \rho_{cj}} \right) \psi_{22c}^{(i,j)} b_{ck} \quad (= 0, i = j) .$$

The last term vanishes when $i = j$ since $\psi_{22c}^{(i,i)} = 0$. In the dry air,

$$(V.11a) \quad J_{34d} = \sum_{i,k} c_{ikd}^{(4)} f_d(\rho_{dk} + \rho_{di}^{(2)}) + \sum_{i,j,k} d_{ijkd}^{(4)} f_d(\rho_{dk} + \rho_{di} + \rho_{dj})$$

$$(V.11b) \quad c_{ikd}^{(4)} = \left(\frac{1}{2} + \frac{\rho_{dk}}{\rho_{di}^{(2)}} \right) \gamma_{di}^{(2)} b_{di}^{(2)} b_{dk}$$

$$(V.11c) \quad d_{ijkd}^{(4)} = \left(\frac{1}{2} + \frac{\rho_{dk}}{\rho_{di} + \rho_{dj}} \right) \psi_{22d}^{(i,j)} b_{dk}$$

Using appendix IV I can find inhomogeneous solutions to (4.3.17) which produce the inhomogeneous terms \hat{R}_1 and \hat{R}_2 , now that they are written as sums of characteristic functions:

$$(V.12) \quad \psi_3^{(n)}(x, \tau) = \psi_3^{(n)}(x - x_j) A_j^3 .$$

For each term in the double sums in the Jacobian, I replace

$$(V.13a) \quad R_1 \leftarrow c_{ik\pm}^{(1)} + c_{ik\pm}^{(2)}$$

$$(V.13b) \quad R_2 \leftarrow c_{ik\pm}^{(3)} + c_{ik\pm}^{(4)}$$

to find the inhomogeneous solution generated by that term in the cloudy air, and similarly for the triple sums. The result is

$$\begin{aligned}
(V.14) \quad \psi_{3c}^{(n)}(x) &= \sum_{i,k} \{ \hat{c}_{ik+}^{(1)} Q_1 g_c(x, \rho_{ck} + \rho_{ci}^{(2)}) + \hat{c}_{ik-}^{(1)} Q_1 g_c(x, \rho_{ck} - \rho_{ci}^{(2)}) \\
&+ \sum_{i,j,k} Q_1 \{ \hat{d}_{ijk+}^{(1)} g_c(x, \rho_{ck} + \rho_{ci} + \rho_{cj}) + \hat{d}_{ijk-}^{(1)} g_c(x, \rho_{ck} - \rho_{ci} - \rho_{cj}) \} \\
&+ \sum_{i,j,k} Q_1 \{ \hat{e}_{ijk+}^{(1)} g_c(x, \rho_{ck} + \rho_{ci} - \rho_{cj}) + \hat{e}_{ijk-}^{(1)} g_c(x, \rho_{ck} - \rho_{ci} + \rho_{cj}) \}
\end{aligned}$$

$B_{3c}^{(n)}(x)$ can be written in the same form if superscripts (1) are replaced by (1) and "g" is replaced by f. Q_1 is an operator defined in (IV.3e) and $\hat{c}_{ik\pm}^{(1,2)}$ are the m_1 and m_2 defined in (IV.3c,d) for the choice of R 's above, and likewise for the other coefficients. These remarks apply in the dry air also, where $\psi_3^{(n)}(x)$ has the simpler form

$$(V.15) \quad \psi_{3d}^{(n)}(x) = \sum_{i,k} \hat{c}_{ikd}^{(1)} Q_1 g_d(x, \rho_{dk} + \rho_{di}^{(2)}) + \sum_{i,j,k} Q_1 \hat{d}_{ijkd}^{(1)} g_d(x, \rho_{dk} + \rho_{di} + \rho_{dj}).$$

Terms due to Slow Variations

From (4.3.19),

$$(V.16a) \quad \hat{R}_{12} = A_{j\tau} \nabla_1^2 \psi_1(x) - A_{jx} A_{j\tau} \nabla_1^2 \psi_{1x}$$

$$(V.16b) \quad \hat{R}_{22} = A_{j\tau} B_{\ell 1}(x) - A_{jx} A_{j\tau} B_{\ell 1x}.$$

In the cloudy air,

$$(V.17a) \quad \nabla_1^2 \psi_1 = \sum_k \epsilon_{ck} g_c(x, \rho_{ck}),$$

$$(V.17b) \quad B_{\ell 1} = \sum_k b_{ck} f_c(x, \rho_{ck}) ,$$

$$(V.17c) \quad \varepsilon_{ck} = -\Gamma_o \gamma_{ck}^2 b_{ck} .$$

Replacing "c" by "d", the same holds in the dry air.

Inhomogeneous solutions are found precisely as described in the previous section by replacing $R_1 \leftarrow \varepsilon_{ck}$ and $R_2 \leftarrow b_{ck}$ for each k . Using the carat notation again,

$$(V.18a) \quad \check{\psi}_3^{(t)}(x, \tau) = A_{j\tau} \check{\psi}_3^{(t)}(x) - A_{jx} \check{\psi}_3^{(x)}(x) ,$$

$$(V.18b) \quad \check{\psi}_{3c}^{(t)}(x) = \sum_k \hat{\varepsilon}_{ck}^{(1)} Q_1 g_c(x, \rho_{ck}) ,$$

$$(V.18c) \quad B_{3c}^{(t)}(x) = \sum_k \hat{\varepsilon}_{ck}^{(2)} Q_1 f_c(x, \rho_{ck}) ,$$

$$(V.18d) \quad \check{\psi}_{3c}^{(x)}(x) = d\check{\psi}_{3c}^{(t)}/dx ; \quad \check{B}_{3c}^{(x)} = (d/dx)\check{B}_{3c}^{(t)} ,$$

and similarly in the dry air (the superscripts are "t" for time-dependent, "x" for x-translation).

Terms due to Supercriticality

From (4.3.20), since

$$(V.19a) \quad N_c^2 - N_{co}^2 = \mu ,$$

$$(V.19b) \quad N_d^2 = N_{do}^2 ,$$

$$(V.19c) \quad \Gamma = N_c^2 + N_d^2 = \Gamma_o + \mu ,$$

$$(V.19d) \quad \hat{R}_{13} = -(N_{do}^2 / \Gamma_o) A_j B_{1x}(x)$$

$$(V.20b) \quad \hat{R}_{23} = -A_j \psi_{1x}(x) .$$

In the cloudy air

$$(V.21a) \quad -(N_{do}^2 / \Gamma_o) B_{1x}(x-x_j) = \sum_k \sigma_{ck} g(x, \rho_{ck}) ,$$

$$(V.21b) \quad \psi_{1x}(x-x_j) = \sum_k \gamma_{ck} b_{ck} f(x, \rho_{ck}) ,$$

$$(V.21c) \quad \sigma_{ck} = -(N_{do}^2 / \Gamma_o) b_{ck} \rho_{ck}^2$$

and likewise in the dry air with "c" and "d" interchanged except in N_{do} . With $R_1 \leftarrow \sigma_{ck}$ and $R_2 \leftarrow \gamma_{ck} b_{ck}$ for each k, a solution is found from appendix IV again:

$$(V.22a) \quad \psi_3^{(g)}(x, \tau) = A_j \psi_3^{(3)}(x-x_j)$$

$$(V.22b) \quad \psi_{3c}^{(g)}(x) = \sum_k Q_1 \hat{\sigma}_{ck}^{(1)} f_c(x, \rho_{ck})$$

$$(V.22c) \quad B_{3c}^{(g)}(\mathbf{x}) = \sum_k Q_{1c} \hat{\sigma}_{ck}^{(2)} f_c(\mathbf{x}, \rho_{ck}) ,$$

and similarly in the dry air (superscript "g" is for growth-inducing).

Terms due to Mean Field Interactions

From appendix II,

$$(V.23) \quad \tilde{\psi}_{m2} = -\theta_X \left[\sum_{n \text{ odd}} \hat{s}_{1n} \sin nz \right] .$$

From (4.3.21), since $\tilde{\psi}_{m2}$ is not a function of the short horizontal scale x

$$(V.24) \quad \begin{aligned} \hat{R}_{14} &= -A_j \theta_X \left[\psi_{1x} \overbrace{\sin z \psi_{m2zzz}} - \nabla_1^2 \psi_{1x} \overbrace{\sin z \psi_{m3z}} \right] \\ &= -A_j \theta_X \sum_{n \text{ odd}} \left[-n^3 \psi_{1x} - n \nabla_1^2 \psi_{1x} \right] \hat{s}_{1n} \overbrace{\sin z \cos nz} \\ &= 0 , \end{aligned}$$

so this inhomogeneity is illusory.

The Boundary Conditions at Large x

To take care of the exponential growth mandated by the boundary conditions (4.3.22), I recall that the asymptotic form of $\psi_1(\mathbf{x})$ for large $|x|$ is dominated by its slowest decaying characteristic function,

$$\begin{aligned}
 \text{(V.25)} \quad \psi_1(x) &\sim \gamma_{d1} b_{d1} g_d(x, \rho_{d1}) \\
 &= \gamma_{d1} b_{d1} \exp[-\rho_d(|x| - a_o/2)] .
 \end{aligned}$$

Thus

$$\begin{aligned}
 \text{(V.26a)} \quad \hat{\psi}_3 &\sim A_{j+1} \gamma_{d1} b_{d1} \cdot \mu^{-1} \exp(\rho_{d1}[x - x_{j+1} + \frac{1}{2}a_o]) \\
 &\sim \Pi \zeta_j A_{j+1} g_d(x - x_j, -\rho_{d1}), \quad x_j \ll x \ll x_{j+1}
 \end{aligned}$$

and similarly,

$$\text{(V.26b)} \quad \hat{\psi}_3 \sim \Pi \zeta_{j-1} A_{j-1} g_d(x - x_j, -\rho_{d1}), \quad x_j \ll x \ll x_{j-1}$$

where

$$\text{(V.26c)} \quad \Pi = b_{d1} \exp(\rho_{d1} a_o)$$

$$\text{(V.26d)} \quad \zeta_j = \mu^{-1} \exp[-\rho_{d1}(x_{j+1} - x_j)] .$$

These boundary conditions can be satisfied by a homogeneous solution

$$\text{(V.27a)} \quad \check{\psi}_3^{(e)}(x - x_j) \{A_{j+1} \zeta_j + A_{j-1} \zeta_{j-1}\} + \check{\psi}_3^{(o)}(x - x_j) \{A_{j+1} \zeta_j - A_{j-1} \zeta_{j-1}\};$$

$$\text{(V.27b)} \quad \check{\psi}_3^{(e)}(x) = \begin{cases} \frac{1}{2} \Pi g_d(x, -\rho_{d1}) & \text{both right and left of the cloud} \\ 0 & \text{inside the cloud} \end{cases} .$$

$$(V.27c) \quad \check{\psi}_3^{(o)}(x) = \begin{cases} \frac{1}{2}\Pi g_d(x, -\rho_{d1}) & \text{right of the cloud} \\ -\frac{1}{2}\Pi g_d(x, -\rho_{d1}) & \text{left of the cloud} \\ 0 & \text{inside the cloud} \end{cases} .$$

A complete inhomogeneous solution is the sum of all of these solutions

$$(V.28) \quad \check{\psi}_3(x, \tau) = \check{\psi}_3^{(n)}(x-x_j)A_j^3 + \check{\psi}_3^{(t)}(x-x_j)A_{j\tau} + \check{\psi}_3^{(x)}(x-x_j)A_{jx_{j\tau}} \\ + \check{\psi}_3^{(g)}(x-x_j)A_j + \check{\psi}_3^{(e)}\{A_{j+1}\zeta_j + A_{j-1}\zeta_{j-1}\} \\ + \check{\psi}_3^{(o)}\{A_{j+1}\zeta_j - A_{j-1}\zeta_{j-1}\} ;$$

however, this solution does not satisfy the matching condition across the cloud boundaries. This solution is symmetric about the cloud center $x = x_j$ except for the terms proportional to $A_{jx_{j\tau}}$ and $A_{j+1}\zeta_j - A_{j-1}\zeta_{j-1}$ which are antisymmetric in their effects.

APPENDIX VI

Numerical Values of the Coefficients

Below are tabulated the critical value N_{co}^2 and cloudwidth a , and the four coefficients σ , η , d , and ω of the linear terms of the cloud evolution equations (4.4.1), for various N_d^2 . For $N_d^2 = 14.23$ these coefficients were independently estimated using a computer simulation of the linear initial value problem--the estimated values are recorded in parenthesis below the theoretically derived values and agree quite well.

N_d^2	N_{co}^2	a	σ	η	d	ω
5	12.513	3.8328	.0658	1.601	1.1599	14.194
10	13.512	3.7636	.0641	1.185	.6632	25.090
14.23	14.230	3.7177	.0627 (.063)	1.060 (1.05)	.5131 (.55)	36.088 (36.2)
20	15.083	3.6668	.0609	.975	.4079	53.487
40	17.402	3.5450	.0559	.876	.2674	132.712
60	19.184	3.4644	.0523	.847	.2135	237.630
80	20.670	3.4040	.0495	.835	.1835	365.223
100	21.964	3.3557	.0472	.830	.1633	513.528

APPENDIX VII

The Buoyancy Flux from a Uniform Field of Clouds

Since all clouds have the same spatial structure, each cloud produces a vertically averaged buoyancy flux H_1 , where H_1 is the flux from a neutral isolated "linear" cloud of unit amplitude

$$(VII.1a) \quad H_1 = \frac{1}{\pi} \int_0^{\pi} dx \sin^2 z \int_{-\infty}^{\infty} w_1(x) B_1(x) dx$$

$$(VII.1b) \quad w_1(x) = \begin{cases} \sum_{i=1}^3 \gamma_{ci} b_{ci} f(x, \rho_{ci}) & |x| < a_o/2 \\ \sum_{i=1}^3 \gamma_{di} b_{di} f(x, \rho_{di}) & |x| > a_o/2 \end{cases}$$

$$(VII.1c) \quad B_1(x) = \frac{1}{\Gamma_0} \begin{cases} N_{co}^2 \sum_{i=1}^3 b_{ci} f(x, \rho_{ci}) & |x| < a_o/2 \\ -N_d^2 \sum_{i=1}^3 b_{di} f(x, \rho_{di}) & |x| > a_o/2 \end{cases}$$

Thus the average buoyancy flux H from a field of clouds spaced a distance λ apart is

$$(VII.2) \quad H = \frac{a^2(\lambda)}{\lambda} H_1,$$

where $a(\lambda) = A(\eta(\lambda))$, the equilibrium cloud amplitude, is the solution of

$$(VII.3) \quad f(A) = 2\eta(\lambda)A .$$

The maximum buoyancy flux occurs when

$$0 = \frac{dH}{d\lambda}(\lambda_{\max}) = \left\{ -\frac{A^2}{\lambda_{\max}^2} + \frac{2AA_{\eta} \cdot \eta(-\rho_{d1})}{\lambda_{\max}} \right\}_{H_1}$$

$$(VII.4) \quad 2\eta A_{\eta} + \frac{A}{\rho_{d1} \lambda_{\max}} = 0$$

since $\eta(\lambda) \propto \exp\{-\rho_{d1}\lambda\}$. But $\lambda_{\max} = O(\log 1/\mu) \gg 1$, so

$$2\eta A_{\eta} + A > 2\eta A_{\eta} + \frac{A}{\rho_{d1} \lambda_{\max}} = 0 ;$$

$$(VII.5) \quad \lambda_c < \lambda_{\max}$$

Since η must be small for (VII.3) to hold, $A \approx A(\eta \rightarrow 0) = A_0$ and $A_{\eta} = A_{\eta}(\eta \rightarrow 0) = A_{\eta 0}$, while $\rho_{d1} \lambda_{\max} \sim \log(\mu^{-1})$. Solving for η ,

$$\eta = \frac{A_0}{2(-A_{\eta 0}) \log(\mu^{-1})}$$

$$(VII.6) \quad \rho_{d1} \lambda_{\max} = \log(\mu^{-1}) + \log\{\log(\mu^{-1})\} + O(1)$$

Thus λ_{\max} lies asymptotically closer to λ_c than $2\lambda_c$, and is in the stable band

$$(VII.7) \quad \lambda_c < \lambda_{\max} < 2\lambda_c \quad \mu \ll 1 .$$

REFERENCES

- Abramowitz, M. and I. A. Stegun, 1964: Handbook of Mathematical Functions. National Bureau of Standards, New York, 1046pp.
- Agee, E. M. and K. E. Dowell, 1974: Observational Studies of Mesoscale Cellular Convection. *J. Appl. Met.*, 13, 46-53.
- Agee, E. M. and F. E. Lomax, 1978: Structure of the Mixed Layer and Inversion Layer Associated with Patterns of Mesoscale Cellular Convection During AMTEX 1975. *J.A.S.*, 35, 2281-2301.
- Asai, T. and I. Nakasuji, 1977: On the Preferred Mode of Cumulus Convection in a Conditionally Unstable Atmosphere. *J. Met. Soc. Japan*, 55, 151-167.
- Asai, T. and I. Nakasuji, 1982: A Further Study of the Preferred Mode of Cumulus Convection in a Conditionally Unstable Atmosphere. *J. Met. Soc. Japan*, 60, 425-431.
- Bjerknes, J., 1938: Saturated-Adiabatic Ascent of Air Through Dry-Adiabatically Descending Environment. *Q.J.R.M.S.*, 64, 325-330.
- Chandrasekhar, S., 1961: Hydrodynamic and Hydromagnetic Stability. Oxford Univ. Press, Lond, 652pp.
- Cho, H. R., 1978: Some Statistical Properties of a Shallow Homogeneous Cloud Field. *J.A.S.*, 35, 125-138.
- van Delden, A. and J. Oerlemans, 1982: Grouping of Clouds in a Numerical Convection Model. *Beitr. Phys. Atmosph.*, 55, 239-252.
- Emanuel, K. A., 1981: A Similarity Theory for Unsaturated Downdrafts within Clouds. *J.A.S.*, 38, 1541-1557.
- Fiedler, B., 1984: The Mesoscale Stability of Entrainment into Cloud-Topped Mixed Layers. *J.A.S.*, 41, 92-101.
- Fiedler, B., 1984: Is Mesoscale Cellular Convection Really Convection? Submitted to *Tellus*.
- Haque, S. M. A., 1952: The Initiation of Cyclonic Circulation in a Vertically Unstable Airmass. *Q.J.R.M.S.*, 78, 394-406.

- Hill, G. E., 1974: Factors Controlling the Size and Spacing of Cumulus Clouds as Revealed by Numerical Experiments. *J.A.S.*, 31, 646-673.
- Kitade, T., 1972: On the Convection in a Conditionally Unstable Atmosphere with Mean Vertical Motion. *J. Met. Soc. Japan*, 50, 243-258.
- Kuo, H. L., 1961: Convection in a Conditionally Unstable Atmosphere. *Tellus*, 13, 441-459.
- Kuo, H. L., 1963: Perturbations of Plane Couette Flow in Stratified Fluid and the Origin of Cloud Streets. *Phys. Fluids*, 6, 195-211.
- Kuo, H. L., 1965: Further Studies of the Properties of Cellular Convection in a Conditionally Unstable Atmosphere. *Tellus*, 17, 413-433.
- Lilly, D. K., 1960: On the Theory of Disturbances in a Conditionally Unstable Atmosphere. *Mon. Weath. Rev.*, 88, 1-17.
- Lindzen, R. S., 1974: Wave-CISK in the Tropics. *J.A.S.*, 31, 156-179.
- Lopez, R. E., 1976: Radar Characteristics of the Cloud Populations of Tropical Disturbances in the Northwest Atlantic. *Mon. Weath. Rev.*, 104, 268-283.
- Malkus, J. S. and H. Riehl, 1964: Cloud Structuring and Distribution over the Tropical Pacific Ocean. Univ. of Calif. Press, Berkeley, 229pp.
- Murray, F. W., 1970: Numerical Models of a Tropical Cumulus Cloud with Bilateral and Axial Symmetry. *Mon. Weath. Rev.*, 98, 14-28.
- Ogura, Y., 1963: The Evolution of a Moist Convective Element in a Shallow, Conditionally Unstable Atmosphere: A Numerical Calculation. *J.A.S.*, 20, 407-424.
- Plank, V. G., 1969: The Size Distribution of Cumulus Clouds in Representative Florida Populations. *J. Appl. Met.*, 8, 46-67.
- Ralston, A. and P. Rabinowitz, 1978: A First Course in Numerical Analysis. McGraw-Hill, New York, 556pp.
- Randall, D. A. and G. J. Huffman, 1980: A Stochastic Model of Cumulus Clumping. *J.A.S.*, 37, 2068-2078.
- Rothermel, J. and E. M. Agee, 1980: Aircraft Investigation of Mesoscale Cellular Convection during AMTEX 75. *J.A.S.*, 37, 1027-1040.
- Soong, S. T. and Y. Ogura, 1973: A Comparison Between Axisymmetric and Slab-Symmetric Cumulus Convection. *J.A.S.*, 30, 879-893.

- Shirer, H. N., 1980: Bifurcation and Stability in a Model of Moist Convection in a Shearing Environment. *J.A.S.*, 37, 1586-1602.
- Shirer, H. N., 1982: Toward a Unified Theory of Atmospheric Convective Instability. In *Cloud Dynamics*, E. M. Agee and T. Asai, eds. D. Reidel, Dordrecht, 163-177.
- Shirer, H. N. and Dutton, J., 1979: The Branching Hierarchy of Multiple Solutions in a Model of Moist Convection. *J.A.S.*, 36, 1705-1721.
- Spiegel, E. A. and G. Veronis, 1960: On the Boussinesq Approximation for a Compressible Fluid. *Astrophys. J.*, 131, 442-447.
- Squires, P., 1958: Penetrative Downdraughts in Cumuli. *Tellus*, 10, 381-389.
- Yamasaki, M., 1972: Small Amplitude Convection in a Conditionally Unstable Stratification. *J. Met. Soc. Japan*, 50, 465-481.
- Yamasaki, M., 1974: Finite Amplitude Convection in a Conditionally Unstable Stratification. *J. Met. Soc. Japan*, 52, 365-379.
- Yau, M. K. and R. Michaud, 1982: Numerical Simulations of a Cumulus Ensemble in Three Dimensions. *J.A.S.*, 39, 1062-1079.